8-2011

Adaptive Discontinuous Galerkin Finite Element Methods for a Diffuse Interface Model of Biological Growth

Andreas C Aristotelous
aaristot@utk.edu

To the Graduate Council:

I am submitting herewith a dissertation written by Andreas C Aristotelous entitled "Adaptive Discontinuous Galerkin Finite Element Methods for a Diffuse Interface Model of Biological Growth." I have examined the final electronic copy of this dissertation for form and content and recommend that it be accepted in partial fulfillment of the requirements for the degree of Doctor of Philosophy, with a major in Mathematics.

Ohannes A. Karakashian, Major Professor

We have read this dissertation and recommend its acceptance:

Steven M. Wise, Xiaobing H. Feng, Gao Yanfei

Accepted for the Council:

Carolyn R. Hodges

Vice Provost and Dean of the Graduate School

(Original signatures are on file with official student records.)

To the Graduate Council:

I am submitting herewith a dissertation written by Andreas Aristotelous entitled "Adaptive Discontinuous Galerkin Finite Element Methods for a Diffuse Interface Model of Biological Growth." I have examined the final paper copy of this dissertation for form and content and recommend that it be accepted in partial fulfillment of the requirements for the degree of Doctor of Philosophy, with a major in Mathematics.

O. A. Karakashian, Major Professor

We have read this dissertation
and recommend its acceptance:

Steven M. Wise

Xiaobing H. Feng

Gao Yanfei

Accepted for the Council:

Carolyn R. Hodges

Vice Provost and Dean of the Graduate School

To the Graduate Council:
I am submitting herewith a dissertation written by Andreas Aristotelous entitled "Adaptive Discontinuous Galerkin Finite Element Methods for a Diffuse Interface Model of Biological Growth." I have examined the final electronic copy of this dissertation for form and content and recommend that it be accepted in partial fulfillment of the requirements for the degree of Doctor of Philosophy, with a major in Mathematics.

O. A. Karakashian, Major Professor

We have read this dissertation
and recommend its acceptance:

Steven M. Wise

Xiaobing H. Feng

Gao Yanfei

Accepted for the Council:

Carolyn R. Hodges

Vice Provost and Dean of the Graduate School

(Original signatures are on file with official student records.)

Adaptive Discontinuous Galerkin Finite Element Methods for a Diffuse Interface Model of Biological Growth

A Dissertation

Presented for the

Doctor of Philosophy

Degree

The University of Tennessee, Knoxville

Andreas Aristotelous

August 2011

I dedicate this Dissertation to my parents Costas, and Kyriaki Aristotelous and to my brothers Nicolas and Georgios Aristotelous whose continuous support in my quest for knowledge gives me strength to move forward and realize my dreams.

Acknowledgements

I would like to thank both of my advisors, Professors Ohannes Karakashian and Steven Wise, for their expert guidance. Without their support and willingness to help, the completion of this dissertation would not be possible.

I would like to thank my Dissertation Committee, Dr. Xiaobing Feng and Dr. Gao Yanfei, for their time.

Finally, I would like to thank my family and my girlfriend for their support, encouragement, love and faith in my abilities.

"Education is the best provision for old age."

Aristotle, from Diogenes Laertius, Lives of Eminent Philosophers

Greek critic, philosopher, physicist, & zoologist (384 BC - 322 BC)

Abstract

This PhD dissertation concentrates on the development and application of adaptive Discontinuous Galerkin Finite Element (DG-FE) methods for the numerical solution of a Cahn-Hilliard-type diffuse interface model for biological growth. Models of this type have become popular for studying cancerous tumor progression *in vivo*. The work in this dissertation advances the state-of-the-art in the following ways: To our knowledge the work here contains the first primitive-variable, completely discontinuous numerical implementations of a 2D scheme for the Cahn-Hilliard equation as well as a diffuse interface model of cancer growth. We provide numerical evidence that the schemes above are convergent, with the optimal order. The efficiency of the numerical algorithms depends largely on the implementation of fast solvers for the systems of equations resulting from the DG-FE discretizations. We have developed such capabilities based on multigrid and sparse direct solver techniques. We demonstrate proof-of-concept regarding the implementation of a practical spatially adaptive meshing algorithm for the numerical schemes just mentioned and the effective use of a very simple, but powerful, marking strategy based on an inverse estimate. We demonstrate proof-of-concept for a novel simplified diffuse interface model of tumor growth. This model is essentially the Cahn-Hilliard equation with an added source term that is specialized for the context of cancerous tumor progression. We devise and analyze a mixed DG-FE scheme of convex splitting (CS) type for the Cahn-Hilliard equation in any space dimension. Specifically, we prove that our scheme is unconditionally energy stable and unconditionally uniquely

solvable. Likewise, we devise and analyze a CS, mixed DG-FE scheme for our diffuse interface cancer model. This scheme is energy stable for any (positive) time step size and for any (positive) space step size that is sufficiently small.

Contents

List of Tables

List of Figures

List of Algorithms

Chapter 1

Introduction

1.1 Background

In this dissertation we are primarily interested in the development of accurate, efficient, and adaptive discontinuous Galerkin (DG) finite element (FE) methods for a 2D diffuse interface model of biological growth. While our model will be applicable to various types of species proliferation (in the biological context), we are specifically interested in the problem of cancerous tumor progression. The model is based on a Cahn-Hilliard-type framework. We therefore spend a significant amount of space in the thesis developing numerical schemes and solution strategies for the classical Cahn-Hilliard equation using DG methods. This work will form a foundation for the more complicated diffuse interface growth model.

DG-FE methods have advantages compared to the finite difference and continuous Galerkin (CG) finite element methods. Most of the following points are detailed in [27, 32], but they merit repeating. (i) DG-FE methods can easily handle inhomogeneous boundary conditions, curved boundaries, and complex domains. (ii) They allow the use of very flexible meshes, even those that have hanging nodes . (iii) Because of the last fact there is less mesh propagation (if any at all) due to localized refinement (cf. Fig. 1.1). (iv) The mass matrices are block diagonal, making them trivial to

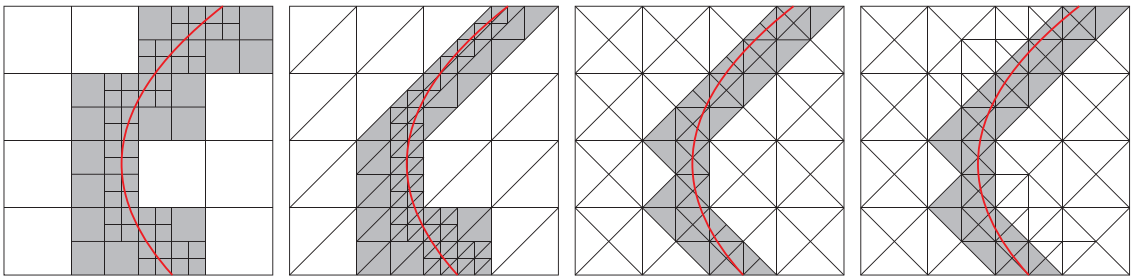

Figure 1.1: *Local refinement of various meshes.*

assemble from local element matrices. The stiffness matrices are block structured and easier to handle than those in the CG-FE setting (cf. Fig 1.2). (v) Many inter-

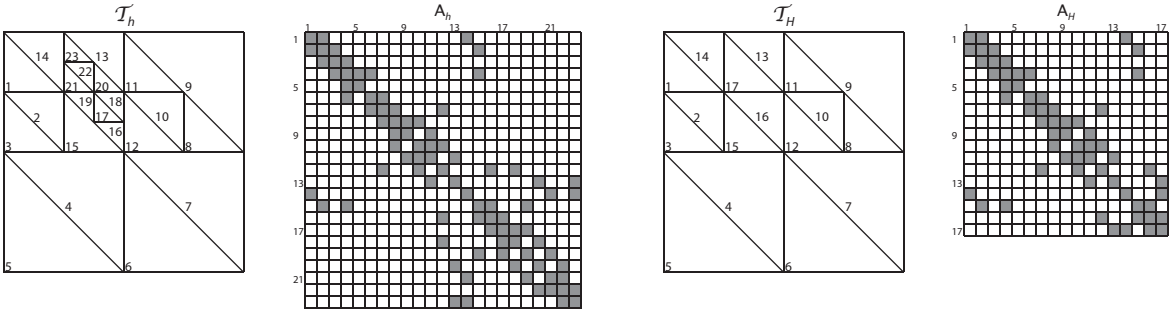

Figure 1.2: *Block structure of a stiffness matrix, A_h, on a locally refined mesh, $\mathcal{T}_h$, obtained from a coarse mesh, $\mathcal{T}_H$, with a corresponding stiffness matrix, A_H.*

mesh operations, such as projections from a locally refined mesh to a coarse mesh, are entirely local, which turns out to be important for implementing multi-level solvers. (vi) DG-FE methods are especially well-suited to *h-p* adaptivity, where in p adaptivity different polynomial spaces can be used on different elements. (vii) DG-FE methods allow for easy treatment of both advection and diffusion dominated problems within a common, suitable framework. (viii) DG-FE methods are naturally parallelizable because of the local nature of element contributions to the global algebraic equations. We take full advantage of some of these features in the present work, especially points (ii) – (vi).

Relatively few papers introducing and/or analyzing DG-FE methods for the Cahn-Hilliard equation have been published. Here we review those that are most well

known. The scheme proposed by Wells *et al.* [40] is a primitive variable form, C^0 DG-FE scheme, whereas the ones we examine here are totally discontinuous. We consider both primitive-variable and mixed type schemes herein. The scheme of Feng and Karakashian [27] is a primitive variable SIP DG-FE scheme. They prove convergence of their scheme, even in the context of mesh modification. The DG-FE scheme for the CH equation proposed in [42] is of LDG type, meaning (essentially) that there are variables for the primitive variable and each of its three spatial derivatives. While this type of treatment leads to large indefinite systems, it is perhaps an easier framework in which to devise "energy" stable schemes than the primitive variable-variable framework. On the other, in the mixed methods we introduce later, we are also able to devise energy stable schemes, but with only two variable instead of four. The work of Kay, Styles, and Süli [32] is concerned with the introduction and analysis of a mixed DG-FE scheme for the Cahn-Hilliard equation with an added, known convection term. They prove that their scheme is conditionally energy stable and conditionally solvable. They also establish optimal order *a priori* error estimates that guarantee convergence of their schemes. However, unlike the paper by Feng and Karakashian [27], Kay, Styles, and Süli do not consider mesh modification during approximation.

Diffuse interface modeling of moving boundary problems in materials science and fluid dynamics has a long history. On the other hand, the use of this framework in the context of biological modeling is somewhat recent. To our knowledge, the earliest paper in this context is one by Cohen and Murray [17], which appeared in 1981. They essentially reintroduced the Cahn-Hilliard equation in the setting of ecological population dynamics and added a source term to it, to model the growth of the population. Their principal motivation was that the usual (second-order) Fickian diffusion model, which is usually presumed in ecological equations, is too restrictive in many cases. They gave the example of populations that exhibit "negative diffusion," in other words, these populations can tend to aggregate. The Cahn-Hilliard diffusion

operator – or as they refer to it, the Ginzburg-Landau diffusion operator – is general enough to describe backward diffusion and Fickian diffusion as special cases.

Cohen and Murray performed a nonlinear stability analysis in the case that a logistic source term is added to the Cahn-Hilliard equation. In this sense, the equation that they analyzed is a generalized Fisher equation. Lara-Ochoa and Montalvo-Robles [37], a paper from 1983, used a Cahn-Hilliard-type equation to model aggregation of mobile cells, a process that is usually described via backward diffusion. More recently, Khain and Sander [34] analyze a 1D Cahn-Hilliard-like equation that includes a logistic growth term to model the motion of cells during wound healing. Wise *et al.* [41, 18] introduced Cahn-Hilliard type models in the context of cancerous tumor growth. The primary reason for using the Cahn-Hilliard framework in this setting was to obtain an accurate description of cell-cell adhesion. In many cancers, though not all, the tumor cells stick to other tumor cells. The model equations in [41, 18] are rather complicated, including as many as seven variables. Their source terms are essentially comprised of a term that accounts for cell mitosis, *i.e.*, growth, and terms that account for cell apoptosis and necrosis, *i.e.*, cell death. One of our motivations in this work is to introduce a simplified version of the models studied in [41, 18] which achieves comparable results and, additionally, to construct a robust and accurate approximation scheme based on the DG-FE framework described above.

1.2 Principle Contributions

The following represent our primary contributions in this dissertation.

1. To our knowledge the work here contains the first primitive-variable, completely discontinuous (*i.e.*, non-C^0) numerical implementation of a 2D scheme for the Cahn-Hilliard equation. Specifically, this work represents a partial completion of that began by Feng and Karakashian [27], where they presented and analyzed the scheme used herein.

2. This work also presents the first primitive-variable, completely discontinuous numerical implementation of a 2D scheme for a diffuse interface model of cancer growth.

3. We provide numerical evidence that the schemes above are convergent, with the optimal order, as the time and space step sizes are reduced toward zero.

4. We demonstrate proof-of-concept regarding the implementation of a practical spatially adaptive meshing algorithm for the numerical schemes just mentioned. Specifically, we show significant computational savings can be achieved using a 2D spatially adaptive mesh for the Cahn-Hilliard equation and our cancer model rather than using a uniform, static mesh. We also demonstrate the effective use of a very simple, but powerful, marking strategy based on an inverse estimate. In some of our tests, this error indicator performs significantly better than those based on *a posteriori* error estimates.

5. We demonstrate proof-of-concept for a novel simplified diffuse interface model of tumor growth. This model is essentially the Cahn-Hilliard equation with an added source term that is specialized for the context of cancerous tumor progression. Specifically, the source term included a logistic-like growth term, modeling cell mitosis at the tumor-healthy tissue interface, and a linear death term, describing the (lumped) processes of tumor cell necrosis and apoptosis.

6. The efficiency of the numerical algorithms depends largely on the implementation of fast solvers for the systems of equations resulting from the DG-FE discretizations. We have developed such capabilities based on *multigrid* and *sparse direct solver* techniques.

7. We devise and analyze a mixed DG-FE scheme of convex splitting (CS) type for the Cahn-Hilliard equation in any space dimension. Specifically, we prove that our scheme is unconditionally energy stable – with respect to a broken analog of the usual continuous Cahn-Hilliard (Ginzburg-Landau) free energy –

and unconditionally uniquely solvable. The first of these two properties holds, as long as the mesh is not time dynamic.

8. Likewise, we devise and analyze a CS, mixed DG-FE scheme for our diffuse interface cancer model. This scheme is energy stable for any (positive) time step size and for any (positive) space step size that is sufficiently small. The question of solvability, even at the PDE level, remains open.

1.3 Dissertation Organization

The work in this dissertation is organized in the following manner. In chapter 2 we motivate and introduce the main models under consideration in our work. In chapter 3 we present some basic results regarding the application of the symmetric interior penalty (SIP) DG-FE method on elliptic problems of second and fourth order. We make use of these results in our work done in the later chapters. In chapter 4 we present our results for a primitive variable formulation of the Cahn-Hilliard equation and the simplified tumor growth model. We describe the algorithms that we have used to implement our adaptive DG-FE code. We provide numerical experiments and we discuss our results. In chapter 5 we develop and analyze mixed DG-FE schemes that are energy stable under some appropriate energy functional, which we define therein. Finally in chapter 6 we finish our discussion with some concluding remarks and future plans.

Chapter 2

A Diffuse Interface Model For Biological Growth

2.1 Introduction

In this chapter we introduce a simplified model for biological growth. Though we will be primarily interested in this model in the context of cancerous tumor progression, it is practical for more general types of biological growth, and we will briefly describe some of the other possible applications. The model is based on a diffuse interface description of the boundary between the growing tissue (the tumoral tissue) and the host tissue. Since the model is essentially comprised of the classical Cahn-Hilliard equation with a nonlinear source term, we begin with a review of the Cahn-Hilliard equation (without source terms), especially as it is used in the context of biological populations. The earliest reference for diffuse interface modeling in the realm of biological population growth is the paper by Cohen and Murray [17], and we will refer to this paper often. The later papers [37, 34] are also relevant. For diffuse interface models in the context of cancerous tumor growth, the papers by Wise *et al.* [41, 18] should be consulted.

2.2 The Cahn-Hilliard (Ginzburg Landau) Energy

Let $\Omega \subset R^d$, $d = 1, 2, 3$, be a bounded domain, and suppose $u : \Omega \to R$ is a state variable, or, in other words, an indicator function. In the biological context, u could describe the population of a certain "species", say species A, where $u(\mathbf{x}) = 0$ indicates no species A is present at $\mathbf{x} \in \Omega$, and $u(\mathbf{x}) = 1$ indicates that species A is at the carrying capacity (*i.e.*, at 100% capacity) of the environment at $\mathbf{x}$. In the materials science context, u is usually the chemical concentration of one of the components of a binary alloy occupying the region Ω. Strictly speaking, in either of these contexts, states for which $u \leq 0$ are nonphysical. Such values will be mathematically realizable in the present modeling framework, and we will interpret them to mean essentially $u = 0$, *i.e.*, 'no population A present.' We will use the term species in both the biological and materials science contexts, as this is standard terminology in either field.

Herein we will only consider binary populations. In other words, only two species or population types are present in Ω. To this end, let $u_B : \Omega \to R$ be another state variable, which indicates the population of species B. The same meaning will be attached to the values of the state variable, u_B, as are attached to u. We make the following close packing assumption (approximation):

$$u_B = 1 - u \ . \tag{2.1}$$

Thus, when $u(\mathbf{x}) = 0$, $u_B(\mathbf{x}) = 1$, meaning species B is at its environmental carrying capacity at $\mathbf{x}$. And when, $u(\mathbf{x}) = 1$, $u_B(\mathbf{x}) = 0$, meaning there are no members of species B at position $\mathbf{x}$. This approximation implies, trivially, that the sum of the two populations is at the carrying capacity of the environment:

$$u(\mathbf{x}) + u_B(\mathbf{x}) = 1 \quad \mathbf{x} \in \Omega \ . \tag{2.2}$$

In words, every possible (usable) space is filled by some constituent of one of the two species; consequently it is also called a 'no voids,' or 'no gaps' approximation. It is a very good approximation in many crystalline binary alloys, where atomic species occupy fixed sites of a coherent lattice (cf. [15]). In the biological context, it may in some situations be a rather poor approximation. However, in the case of tissue growth *in vivo*, where we will concentrate our study, this can be a quite plausible model assumption (cf. [41]). The primary importance of (2.1) is that we only have to describe the dynamics of u, since u_B is related in an elementary way to the former.

Now, consider the following system energy (cf. [15, 17]):

$$E(u) := (F(u), 1)_{L^2(\Omega)} + \frac{\epsilon^2}{2}(\nabla u, \nabla u)_{L^2(\Omega)} \ , \tag{2.3}$$

where $F : R \to R$ is an energy density and $\epsilon \geq 0$. Here, we will work in unit-less variables, for simplicity. The idea is that given any state of the system, which is described completely by the (sufficiently regular) state variable u, we can calculate a unit-less energy of the system. The first part of the energy is called the chemical energy, or homogeneous energy. The second part of the energy is called the gradient energy. In the materials science context, the energy (2.3) is related to a *bona fide* energy, namely, the Helmholtz free energy (cf. [15]). In the biological context, the meaning of the energy is less clear, though Cohen and Murray [17] give some justification for its use.

For simplicity, we assume that the chemical energy density F is a quartic double-well potential, *i.e*,

$$F(u) = \frac{1}{4}u^2(1-u)^2 \ . \tag{2.4}$$

Other polynomial and logarithmic chemical energies are also commonly used. A plot of the quartic energy is given in Fig. 2.1. With respect to this energy density, the system has two lowest energy states, specifically, $u = 0$ (no species A, 100% species B) and $u = 1$ (no species B, 100% species A). In other words, the chemical energy 'prefers' a system which is decomposed into pure phases. If $\epsilon = 0$ it is trivial to

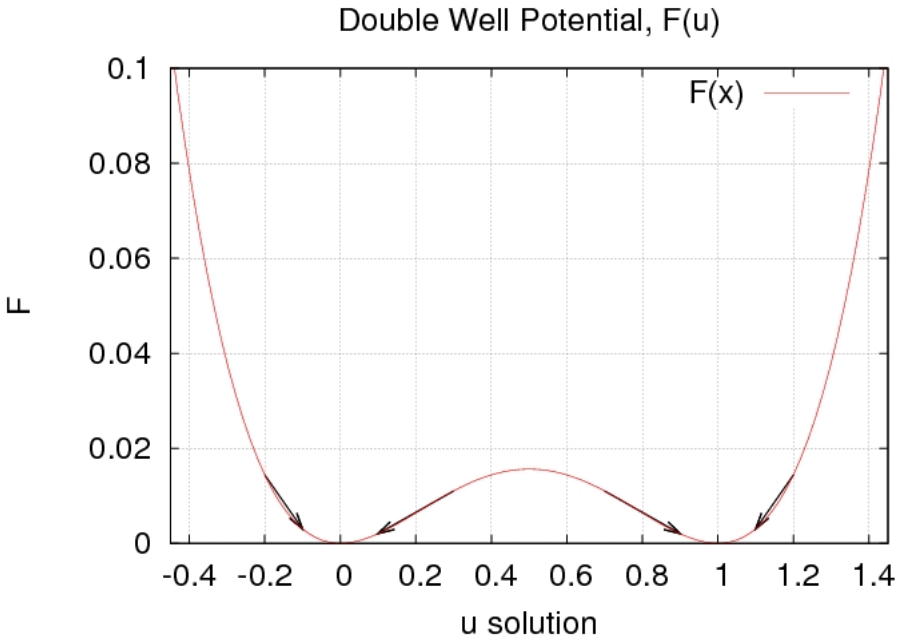

Figure 2.1: *Double well potential* (2.4)

.

construct minimizers of (2.3). Let Ω be the disjoint union of the (measurable) sets Ω_0, $\Omega_1 \subseteq \Omega$, with $u|_{\Omega_i} \equiv i$, $i = 0, 1$. Then $E(u) = 0$, and since, $E \geq 0$, u is a (non-unique) minimizer. In the biological context, such an arrangement would represent perfectly segregated populations. We can also view such a property as an effective self adhesion, because constituents of like species prefer to adhere one to another. Thus in the biological context we will call F an *adhesion potential* (cf. [18], [41]).

If $\epsilon > 0$, the situation is much more interesting. Let us consider the 1D case, *i.e.*, $\Omega = (-\infty, \infty)$. The energy is in this case is

$$E(u) := \int_{-\infty}^{\infty} \left\{ F(u) + \frac{\epsilon^2}{2} \left(\frac{du}{dx} \right)^2 \right\} dx \ . \tag{2.5}$$

The variation of the energy, often called the chemical potential in the materials science context, is

$$\delta_u E(u) = f(u) - \epsilon^2 \frac{d^2 u}{dx^2}, \tag{2.6}$$

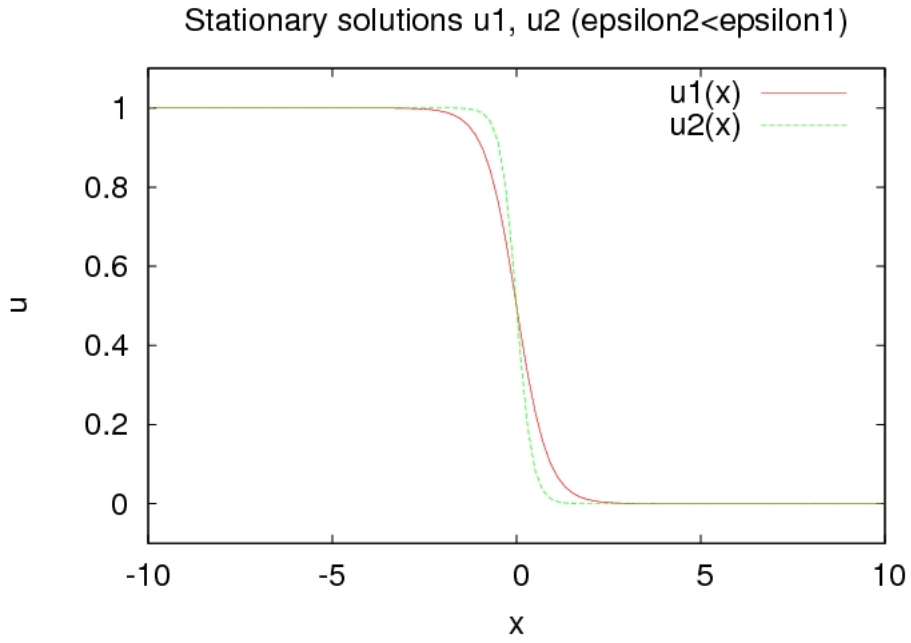

Figure 2.2: *Minimizers of energy* (2.5)*, where* $u_i = s(\,\cdot\,, 0, \epsilon_i)$*,* $i = 1, 2$*, with* $\epsilon_2 < \epsilon_1$*.*

where $f(u) = F'(u)$. Formally, minimizers of the 1D energy (2.5) satisfy $\delta_u E = 0$. It can be shown by a simple calculation that the hyperbolic tangent,

$$s(x, c, \epsilon) := \frac{1}{2}\left(1 - \tanh\left(\frac{\pm x - c}{2\sqrt{2}\epsilon}\right)\right), \tag{2.7}$$

satisfies

$$\delta_u E\left(s(\,\cdot\,, c, \epsilon)\right) \equiv 0 \quad \forall c \in R. \tag{2.8}$$

So, while critical points are clearly not unique – in fact $u \equiv 0$, $u \equiv 1$, and $u \equiv 1/2$ are also critical points – we at least see that nontrivial extrema exist and can have a simple hyperbolic tangent structure. It can be shown, with some additional assumptions that the hyperbolic tangent solutions (2.7) above are unique minimizers up to translation.

Define $u_i = s(\,\cdot\,, 0, \epsilon_i)$, $i = 1, 2$. We plot u_1 and u_2 in Fig. 2.2, where $0 < \epsilon_2 < \epsilon_1$. The indicator function u is approximately 1 or 0 sufficiently far away from $x = 0$. Near $x = 0$, the solution has a boundary layer, where the values transition rapidly from 1 to 0. Note that smaller ϵ results in a more narrow interfacial region (or a

'sharper' interface). Formally, we can consider the limit of vanishing gradient energy. Clearly, u approaches a step function in this limit as $\epsilon \searrow 0$.

2.3 The Cahn-Hilliard Equation

We again return to the general case, where $\Omega \subset R^d$, $d = 1, 2, 3$. Now, suppose that indicator function u has time dependence in addition to space dependence, $u : \Omega \times [0, \infty) \to R$. We need a boundary condition for the system. The natural boundary condition is

$$\partial_n u(\mathbf{x}, t) := n \cdot \nabla u(\mathbf{x}, t) = 0 \quad \mathbf{x} \in \partial\Omega \ , \quad t \geq 0 \ , \tag{2.9}$$

where n is the outward unit normal vector on $\partial\Omega$. This is also called a local thermodynamic equilibrium boundary condition in the materials science context, and it is in many cases appropriate when the system is in isolation (cf. [15], [21]). (This boundary condition controls the contact angle formed when the diffuse interface touches the boundary $\partial\Omega$.)

We will assume that the system is isolated, meaning that populations and energy do not flux across the boundary $\partial\Omega$. Thus, without any internal population sources inside Ω the populations of species A should remain constant in time. Moreover, as we pointed out earlier, the total energy (2.3) should decrease in time, that is, high energy states should settle into lower energy states over time. To this end, we choose the conserved dynamics

$$\partial_t u + \nabla \cdot \mathbf{J} = 0 \qquad \mathbf{x} \in \Omega \ , \quad t > 0 \ , \tag{2.10}$$

$$\mathbf{n} \cdot \mathbf{J} = 0 \qquad \mathbf{x} \in \partial\Omega \ , \quad t > 0 \ , \tag{2.11}$$

where $\mathbf{J}$ is the mass flux. This law automatically implies that $d_t \int_\Omega u(\mathbf{x}, t)\, d\mathbf{x} = 0$. We use the constitutive assumption

$$\mathbf{J} = -\nabla\mu \ , \tag{2.12}$$

where μ is the chemical potential defined as the functional (Frechét) derivative of the energy:

$$\mu =: \delta_u E = F'(u) - \epsilon^2 \triangle u \ . \tag{2.13}$$

This choice implies that

$$\begin{aligned} d_t E(u) &= \int_\Omega \delta_u E \, \partial_t u \, d\mathbf{x} \\ &= \int_\Omega \mu \triangle \mu \, d\mathbf{x} \\ &= \int_{\partial\Omega} \mu \, \partial_n \mu \, d\mathbf{s} - \int_\Omega \nabla\mu \cdot \nabla\mu \, d\mathbf{x} \\ &= -\|\nabla\mu\|_{L^2}^2 \leq 0 \ . \end{aligned} \tag{2.14}$$

In other words, the energy E is non-increasing in time.

Collecting our model components (2.10), (2.12), (2.13), we arrive at the Cahn-Hilliard equation

$$\partial_t u = \triangle \left(F'(u) - \epsilon^2 \triangle u \right) \ , \tag{2.15}$$

with the local thermodynamic equilibrium (2.9) and no-flux (2.11) boundary conditions

$$\partial_n u = \partial_n \mu = 0 \ . \tag{2.16}$$

To summarize the properties of the solutions, the total mass is conserved in time, $d_t \int_\Omega u(\mathbf{x}, t) \, d\mathbf{x} = 0$, and the total energy decreases in time $d_t E(u) \leq 0$.

Given some initial value for u, suppose that the system evolves so as to decrease the energy (2.3). If the chemical energy density, F, alone were the controlling mechanism in the dynamics of the system, one might expect that the system would evolve toward step functions. However, the second piece of the energy (2.3), the gradient energy, acts against such a situation, because it penalizes large values of the gradient of u. This complex interplay between the chemical and gradient energies is an important feature of Cahn-Hilliard equation (2.15). It was introduced in [15], [23] as a model for spinodal decomposition, a process whereby a well-mixed binary fluid (or binary

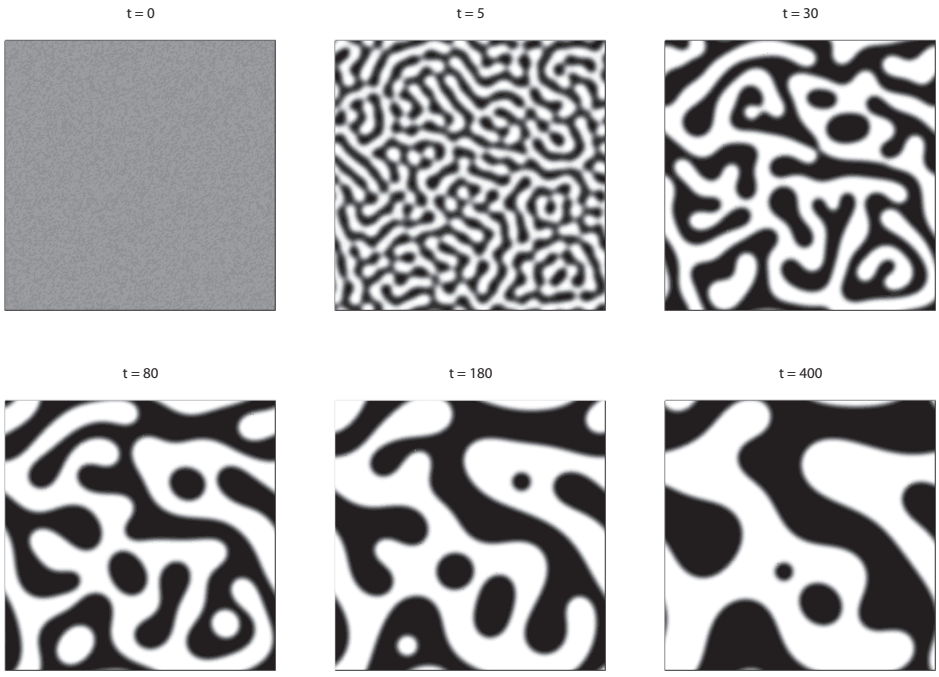

Figure 2.3: *A simulation of spinodal decomposition using the Cahn-Hilliard equation (2.15). Black represents $u = 0$ and white represents $u = 1$. The average composition is $\bar{u} = 0.5$.*

alloy) spontaneously separates into regions where the material is approximately pure in each component. Let $0 < \bar{u} < 1$ be a constant, and suppose ζ is a (sufficiently regular) mean-zero function of small amplitude, *i.e*, $\int_\Omega \zeta \, d\mathbf{x} = 0$ and $|\zeta(\mathbf{x})| \leq A \ll 1$, for all $\mathbf{x} \in \Omega$. We consider initial data of the form

$$u(\mathbf{x}, 0) =: u_0(\mathbf{x}) = \bar{u} + \zeta(\mathbf{x}) \quad \mathbf{x} \in \Omega \, . \tag{2.17}$$

If $\bar{u} \in \{u \in R \mid F''(u) \leq 0\}$, called the chemical spinodal region, then the solution can evolve as depicted in Fig. 2.3. Initially a very fine-scale structure, comprised of alternating layers of (nearly) pure phase regions, emerges. Afterwards, certain of these pure phase regions grow, and some shrink, a process known as coarsening. Coarsening occurs on a very slow time scale. The whole phenomenon, rapid phase separation followed by slow coarsening is what materials scientists call spinodal decomposition. Note that after the phases are well separated, the one-dimensional

profile of the indicator function u perpendicular to the diffuse phase boundaries is nearly a hyperbolic tangent, especially later in time. Due to the work done in [2], this statement can be reinterpreted in a rigorous framework, but we shall not pursue this here.

The *classical Cahn-Hilliard* equation (2.15) has been studied extensively. Various papers have been written to answer questions such as *existence* and *uniqueness* of solutions (cf. [23]). For the physical background, derivation, and discussion of the Cahn-Hilliard equation and related equations, we refer to [15], [23], [21], [22] and the references therein.

Cahn-Hilliard type equations are used to *describe a variety of phenomena* in material science, in industrial applications, in physics and recently in *biology*. Of interest to us is the use of Cahn-Hilliard type equations to *model cell cell adhesion* and *cell diffusion* (cf. [37], [17]).

2.4 Cahn-Hilliard Equation with Logistic Growth

As we have pointed out earlier, the use of the Cahn-Hilliard equation as a biological model is rather recent, going back the paper by Cohen and Murray [17] published in 1981. In it they analyzed a model comprised of the Cahn-Hilliard equation with an added logistic growth term. In one space dimension, *i.e.*, $\Omega = (-\infty, \infty)$, the problem is

$$
\begin{aligned}
u_t &= (f(u) - \epsilon^2 u_{xx})_{xx} + L(u), && \text{(2.18a)}\\
& f(u) = F'(u) = u\left(u - \frac{1}{2}\right)(u-1), && \text{(2.18b)}\\
& L(u) = \lambda_g u(1-u), && \text{(2.18c)}\\
& \lim_{x\to-\infty} u(x) = 1, && \text{(2.18d)}\\
& \lim_{x\to+\infty} u(x) = 0, && \text{(2.18e)}
\end{aligned}
$$

where $\lambda_g \in R$. It is easy to show that this problem has traveling wave solutions of the form

$$u(x,t) = s(x, \lambda_g\sqrt{2}\epsilon t, \epsilon), \tag{2.19}$$

where $s(x, c, \epsilon)$ is the stationary solution defined in (2.7). Note that the speed of the traveling wave is dependent on the growth parameter, λ_g, as expected, and also on the interfacial width parameter ϵ. By plotting the solution (2.19) and the logistic growth $L(u)$ term with respect to x in Figure 2.4, we can observe that the source term acts at the center of the diffuse interface. This resembles the way that many biological populations grow, that is, by obtaining nutrients at the interface with other populations. See for example the papers [17]. Khain and Sander [34] investigate a similar model to that above in the context of wound healing. Note that in structure this model is closely related to the Fisher equation, except that the diffusion is of Cahn-Hilliard type, rather than Fickian.

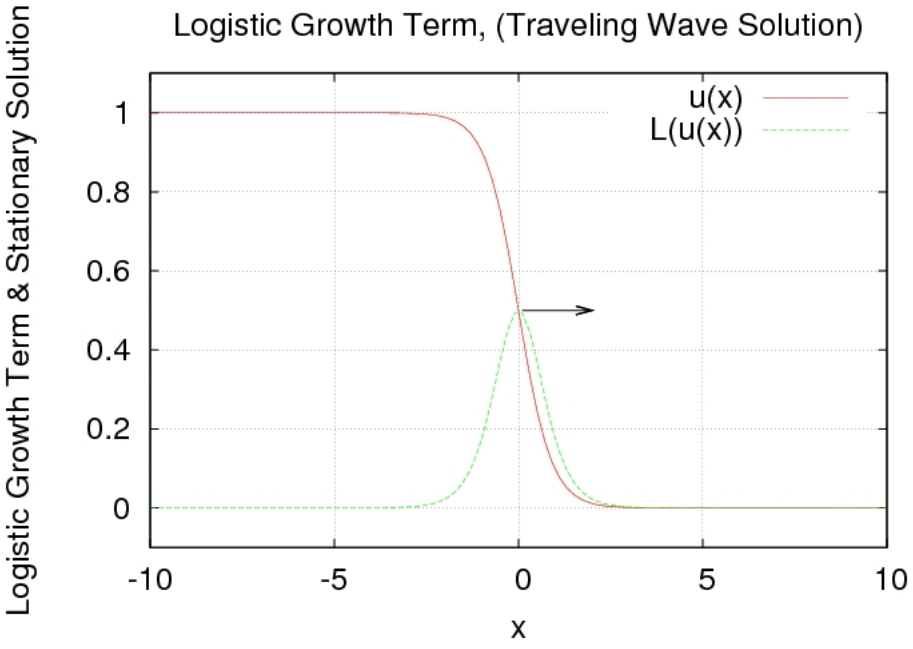

Figure 2.4: *Traveling wave solution* (2.19).

Therefore from the above observations we are ready to introduce our tumor model using a Chan-Hilliard equation as a basis.

2.5 The Cancer Model

The following simplified cancer model serves as the main topic of this research.

$$\begin{aligned}
\partial_t u &= \nabla \cdot (D\nabla\mu) + \lambda_g u^2(1-u)^2 - \lambda_d u, \quad \text{in} \quad \Omega_T, && \text{(2.20a)}\\
\mu &= f(u) - \epsilon^2\nabla^2 u, && \text{(2.20b)}\\
f(u) &= F'(u) = u\left(u - \frac{1}{2}\right)(u-1), && \text{(2.20c)}\\
\partial_n u &= 0, \quad \partial_n \mu = 0, \quad \text{on} \quad \partial\Omega_T := \partial\Omega \times [0,T], && \text{(2.20d)}\\
u &= u_0, \quad \text{on} \quad \Omega \times \{0\}, && \text{(2.20e)}
\end{aligned}$$

where here λ_g and λ_d are positive constants and $\Omega_T := \Omega \times (0,T]$. Here u is the density of tumor cells. $u \approx 1$ represents tumorous tissue, while $u \approx 0$ represents healthy tissue. Also μ is called the chemical potential (2.13), F is the double well potential described above in (2.4) and $D > 0$ is called the *mobility* or diffusion coefficient. In our study we choose D to be positive constant but in reality it can be chosen to be a function that for example can account for the different diffusive properties of cancerous cells through the *gray* and *white* matter of the brain.

The homogeneous Neumann boundary conditions (2.20d) mean that the net flux of mass through the boundary is zero, and thus the total mass of the system is conserved *i.e.* the mass of the cancerous cells, u, plus the mass of the healthy cells, u_B, is constant, $u + u_B = 1$. In this case we assume that while the cancer grows it replaces the healthy tissue in our computational domain Ω.

The model is inspired by work done in [18] and is essentially the Cahn-Hilliard equation (2.15) with the addition of a non linear source term, $S(u) := \lambda_g u^2(1-u)^2 - \lambda_d u$, which is composed of a hyper-logistic *growth* term and a linear *death* term. In the context of viewing equation (2.20a) as a PDE describing tumor growth we make

the following sense about the nonlinear source term, S. The source term has the effect that the tumor growth happens along the interfacial region between the healthy cells and the tumorous cells. This is due to the hyper-logistic part in the source term, which mimics the true behavior of cancerous tumors (cf. [18], [41]). The linear *death* component in the source term peeks in the interior of the tumor (due to the fact that the growth term is minimum there) and this phenomenon simulates the effect of *necrosis* which is more clearly observed in malignant or more aggressive tumors, that grow rapidly, and create large interior domains where the cancer cells become nutrient starved and die (cf. [18]). In our model simulations this is depicted with an observable "sinking" of the solution in the interior of a large enough tumorous region. (See Figure 2.5). In Fig. 2.6 we provide some sample computational snapshots, N,

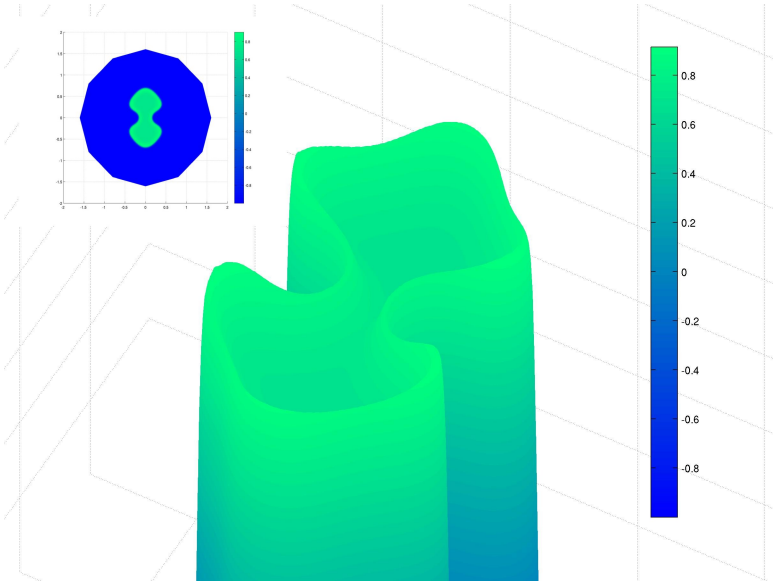

Figure 2.5: *A 3D zoom of a 2D contour solution profile snapshot, depicted in the inset, generated by using model (2.20a)–(2.20e). We observe that the cancerous cells are "sinking" in the interior of the green tumorous region, simulating the phenomenon of necrosis.*

using the tumor model (2.20a)–(2.20e) with an appropriate choice of parameters. In Fig. 2.6b – 2.6d we show a "less aggressive" tumor; and in Fig. 2.6e – 2.6g we show a "more aggressive" tumor.

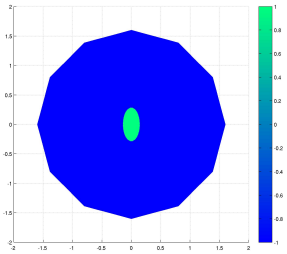

(a) Initial profile $N = 0$

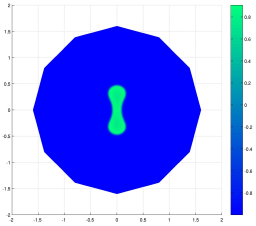

(b) Less Aggressive $N = 5500$

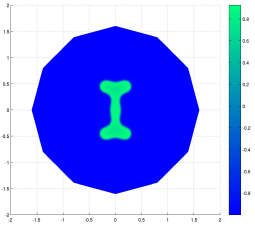

(c) Less Aggressive $N = 11000$

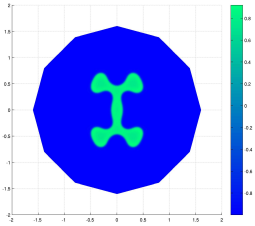

(d) Less Aggressive $N = 16500$

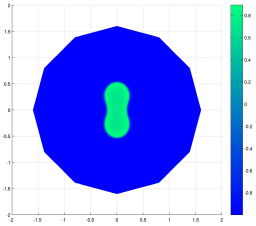

(e) More Aggressive $N = 5500$

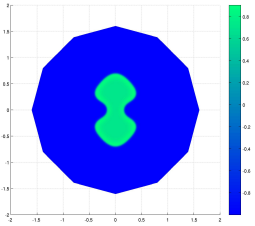

(f) More Aggressive $N = 11000$

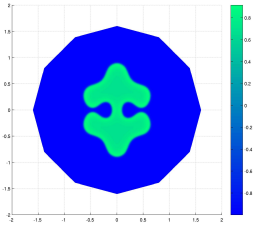

(g) More Aggressive $N = 16500$

Figure 2.6: *Time snapshots, N, from the simulation of tumor growth using model (2.20a)–(2.20e). Green indicates a high density of tumor cells ($u \approx 1$), while blue indicates a high density of healthy tissue cells ($u \approx 0$). The growth parameter for the "Less Aggressive" tumor, (b) – (d), is $\lambda_g = 70$ and the one for the "More Aggressive" tumor, (e) – (g), is $\lambda_g = 75$. The other parameters are the same for both simulations: $D = 1$, $\epsilon = 0.009$, and $\lambda_d = 23$. The plot in (a) corresponds to the initial profile.*

2.6 PDE Energy of the Cancer Model

Next we show that the model (2.20a)–(2.20e) can be interpreted as a gradient flow of some energy. This is more easily done if we change from homogeneous Neumann

boundary conditions, *i.e.*, (2.20d), to homogeneous Dirichlet boundary conditions:

$$u = \mu = 0 \quad \text{on} \quad \partial\Omega_T. \tag{2.21}$$

In particular, in this section we consider the following model: (**PM1)**

$$\begin{aligned}
\partial_t u &= \triangle\bar{\mu}, \quad \text{in} \quad \Omega_T, && \text{(2.22a)}\\
\bar{\mu} &:= f(u) - \epsilon^2\triangle u + w, \quad \text{in} \quad \Omega_T, && \text{(2.22b)}\\
-\triangle w &= g'(u), \quad \text{in} \quad \Omega_T, && \text{(2.22c)}\\
u = \mu = w &= 0, \quad \text{on} \quad \partial\Omega_T, && \text{(2.22d)}\\
u &= u_0, \quad \text{on} \quad \Omega \times \{0\}, && \text{(2.22e)}
\end{aligned}$$

where $u, \bar{\mu}, w \in H_0^1(\Omega)$ (cf. [1]). Here $-g' := \lambda_g u^2(1-u)^2 - \lambda_d u$ is the function corresponding to the non linear growth and linear death source term, S, in (2.20a). It is easy to see that this model reduces to (2.20a) – (2.20e), when the homogeneous Dirichlet boundary conditions (2.21) are replaced with the homogeneous Neumann boundary conditions (2.20d). We now will show that solutions to (2.22a) – (2.22e), *i.e.*, problem **PM1**, dissipate an energy.

Before we do so we define the following H^{-1} inner product where H^{-1} is the continuous dual space of H_0^1 (cf. [1]):

Definition 2.6.1. Let $f,\ g \in H^{-1}$. Then,

$$(f, g)_{H^{-1}} := (\nabla\Psi_f, \nabla\Psi_g), \tag{2.23}$$

where $(\cdot,\cdot)$ is the L^2 inner product on Ω and $\Psi_f,\ \Psi_g$ unique and satisfy,

$$\begin{aligned}
-\triangle\Psi_f &= f, \qquad -\triangle\Psi_g = g, \ \text{in } \Omega,\\
\Psi_f &= 0, \qquad \Psi_g = 0, \ \text{on } \partial\Omega.
\end{aligned}$$

We observe that for $f,\ g \in L^2$ and by multiplying by a test function $u \in H_0^1$ and integrating once by parts we have that,

$$\begin{aligned} \exists! \Psi_f \in H_0^1 :\ (\nabla \Psi_f, \nabla v) &= (f, v), \quad \forall\ v \in H_0^1. \\ \exists! \Psi_g \in H_0^1 :\ (\nabla \Psi_g, \nabla v) &= (g, v), \quad \forall\ v \in H_0^1. \end{aligned}$$

Hence we have,

$$(f, g)_{H^{-1}} := (\nabla \Psi_f, \nabla \Psi_g) = (\Psi_f, g) = (f, \Psi_g). \tag{2.24}$$

Now we are ready to introduce the energy functional corresponding to formulation (**PM1)**.

Definition 2.6.2. Let $u \in H_0^1(\Omega)$. We define the energy functional E at the PDE level as,

$$E(u) = (F(u), 1) + \frac{\epsilon^2}{2}(\nabla u, \nabla u) + (g(u), 1)_{H^{-1}}. \tag{2.25}$$

It is worth mentioning that sufficiently regular solutions of (**PM1)** dissipate the previous energy at the rate

$$\frac{d}{dt} E(u) = -(\nabla \bar{\mu}, \nabla \bar{\mu}) \leq\ 0.$$

In order to see this we take the derivative of E with respect to time and using (2.24) we have,

$$\begin{aligned} \partial_t E(u) &= (f(u), u_t) + \epsilon^2 (\nabla u, \nabla u_t) + (g'(u), u_t)_{H^{-1}} \\ &= (f(u), u_t) + \epsilon^2 (\nabla u, \nabla u_t) + (w, u_t). \end{aligned} \tag{2.26}$$

Setting $v = u_t$ and multiplying the second equation of **(PM1)** by it and integrating once by parts we have,

$$\begin{aligned}(\bar{\mu}, u_t) &= (f(u), u_t) + \epsilon^2(\nabla u, \nabla u_t) + (w, u_t), \\ &= (f(u), u_t) + \epsilon^2(\nabla u, \nabla u_t) + (g'(u), u_t)_{H^{-1}}.\end{aligned}$$

Taking $v = \bar{\mu}$ and multiplying the first equation of **(PM1)** by it we also have,

$$(\bar{\mu}, u_t) = -(\nabla\bar{\mu}, \nabla\bar{\mu}).$$

Thus by combining the two relations above and (2.26) we have the following energy law at the PDE level for **(PM1)**,

$$\frac{d}{dt}E = (f(u), u_t) + \epsilon^2(\nabla u, \nabla u_t) + (g'(u), u_t)_{H^{-1}} = -(\nabla\bar{\mu}, \nabla\bar{\mu}). \tag{2.27}$$

One goal of this research is the development, when possible, of fully discrete schemes that preserve the energy dissipation nature of the corresponding continuous problem. We will show that, in particular, the dissipation (2.27) can be preserved at the numerical level in chapter 5.

Chapter 3

SIP-DG Method for Second and Fourth Order Elliptic Problems

3.1 Introduction

Our numerical schemes for the Cahn-Hilliard equation and cancer model are based intimately on the spatial discretizations of second and fourth order elliptic problems. We will use discontinuous Galerkin here. To this end, we describe the DG formulations for these two type of problems together with pertinent results coming from the literature encompassing a variety of issues including solvability and a-priori estimates. It is worth mentioning that one of the attractive features of the SIP-DG is that it produces symmetric block structured positive definite matrices which enable us to use the preconditioned Conjugate Gradient method as a solver. This is done in the case of the primitive variable formulation of our models described in chapter 4.

3.2 Notation and Preliminaries

Let R^d, $d = 1, 2, 3$, be the set of real numbers in one, two, and three dimensions and $p \in [1, \infty]$ and $m \in [1, \infty)$. Throughout this dissertation, we adopt the standard

norm and inner product notation on the L^p spaces and the Sobolev spaces H^m. (cf. [1]). In particular, for a regular domain D, $\|\cdot\|_D$ and $(\cdot,\cdot)_D$ will denote the standard norm and inner product on $L^2(D)$ (we shall use $(\cdot,\cdot) := (\cdot,\cdot)_\Omega$, $\|\cdot\| := \|\cdot\|_\Omega$), and $\|\cdot\|_{m,D}$ will denote the norm on $H^m(D)$. Also, $|\cdot|_{m,D}$ will denote the seminorm of derivatives of order m. We shall also use $|\cdot|_{\partial D}$ and $\langle\cdot,\cdot\rangle_{\partial D}$ to denote the usual L^2 norm and integral respectively on ∂D.

Let $\mathcal{T}_h = \{K\}$ be a family of star-like partitions (triangulations) of the domain Ω parametrized by $0 < h < 1$ and $h = \max_{K\in\mathcal{T}_h} h_K$, where h_K denotes the diameter of $K \in \mathcal{T}_h$. We assume that $\mathcal{T}_h$ satisfies the following assumptions:

(i) The elements (cells) of $\mathcal{T}_h$ satisfy the minimal angle condition

(ii) $\mathcal{T}_h$ is locally quasi-uniform. That is if two cells K and K' are adjacent (the $(n-1)$-dimensional measure of $\partial K \cap \partial K'$ is positive), then $h_K \approx h_{K'}$.

The weak formulations as well as the approximations themselves involve functions that are discontinuous across interelement boundaries. This motivates the use of so-called "broken" Sobolev spaces

$$H^m(\mathcal{T}_h) := \Pi_{K\in\mathcal{T}_h} H^m(K) = \{v \in L^2(\Omega) \mid v|_K \in H^m(K)\}$$

In particular, the "energy space" for second order problems will be $E_h := H^2(\mathcal{T}_h)$, and the corresponding one for fourth order problems $E_h := H^4(\mathcal{T}_h)$. Also we will make use of the following quotient space $E_h/R := \{v \in E_h |\ (v,1) = 0\}$, whose members have zero average over the domain Ω. It is worth mentioning that the members of the aforementioned spaces are not functions in the proper sense since they can be multivalued on the interelement boundaries; so we must apply care in dealing with quantities such as traces.

A feature of the discontinuous Galerkin method is that the edges/faces of the partition $\mathcal{T}_h$ play an important role in the formulation of the methods as well as their

analysis. We define

$$\begin{aligned}\mathcal{E}^I &:= \text{ set of all interior edges/faces of } \mathcal{T}_h,\\ \mathcal{E}^B &:= \text{ set of all boundary edges/faces of } \mathcal{T}_h,\\ \mathcal{E} &:= \mathcal{E}^I \cup \mathcal{E}^B = \text{ set of all edges/faces of } \mathcal{T}_h.\end{aligned}$$

For $e \in \mathcal{E}^I$, we have $e = \partial K^+ \cap \partial K^-$ for some $K^+, K^- \in \mathcal{T}_h$. For $v \in E_h$ we define the jump $[v]$ of v on e as $[v]\,|_e = v^+|_e - v^-|_e$ where v^+ and v^- denote the restrictions of v to K^+ and K^- respectively. For $e \in \mathcal{E}^B$, we set $[v]|_e = v|_e$. We also let ∂_n denote the normal derivative operator in the direction outward from K^+. For $e \in \mathcal{E}^I$ we define $[\partial_n v]\,|_e := [\nabla v]\,|_e \cdot n^+$ and for $e \in \mathcal{E}^B$ we set $[\partial_n v]\,|_e = \partial_n v|_e = \nabla v|_e \cdot n$, where n^+ is the outward unit normal to K^+. For $e \in \mathcal{E}$, h_e will denote the length of e for $d = 2$, or the diameter of e for $d \geq 3$. It follows from the local quasiuniformity assumption that $h_e \approx h_{K^+} \approx h_{K^-}$. This fact is used repeatedly in this dissertation. For $e \in \mathcal{E}^I$ we define the *average* of v on e to be $\{v\}|_e := \frac{1}{2}\big(v^+|_e + v^-|_e\big)$. If $e \in \mathcal{E}^B$, set $\{v\}|_e = v|_e$. For $e \in \mathcal{E}^I$ we define $\{\partial_n v\}|_e := \{\nabla v\}|_e \cdot n^+$ and for $e \in \mathcal{E}^B$ we set $\{\partial_n v\}|_e = \partial_n v|_e = \nabla u|_e \cdot n$.

The following trace inequalities are well known (cf. [16]).

Lemma 3.0.1. *There exists a positive constant C, which is independent of h, such that for any $K \in \mathcal{T}_h$, if $\phi \in H^1(K)$, then*

$$|\phi|^2_{\partial K} \leq C(h_K^{-1}||\phi||^2_K + ||\phi||_K|\phi|_{1,K}) \tag{3.1}$$

which easily implies,

$$|\phi|^2_{\partial K} \leq C\big(\, h_K^{-1}\|\,\phi\,\|^2_K + h_K\|\,\nabla\phi\,\|^2_K\,\big), \tag{3.2}$$

where h_K is the diameter of K.

For any $K \in \mathcal{T}_h$ and integer $q \geq -1$, let $P_q(K)$ denote the set of all polynomials of degree q on K, (we let $P_{-1} = \{0\}$).
The discontinuous finite element space V_h is defined by $V_h := \mathcal{P}_q(\mathcal{T}_h)$ where,

$$\mathcal{P}_q(\mathcal{T}_h) := \prod_{K \in \mathcal{T}_h} P_q(K) = \{v|_K \in P_q(K) \mid v \in L^2(\Omega)\}.$$

Clearly, $V_h \subset E_h \subset L^2(\Omega)$. But $V_h \not\subset H^2(\Omega)$. In fact, $V_h \not\subset H^1(\Omega)$. We also define similarly as with the E_h case the following quotient space,
$V^h/R := \{v|_K \in \mathcal{P}_q(K) \mid v \in L^2(\Omega),\ (v,1) = 0\}$.
In practice as basis for V^h we shall use local basis functions $v_{K,j}$ corresponding to local Lagrangian nodes, $x_{K,j}$, $K \in \mathcal{T}_h,\ j = 1, \ldots, m(q)$, where $m(q)$ is the total number of local degrees of freedom. The support of $v_{K,j}$ is the cell K and is extended by zero outside of K. The functions $v_{K,j}$ satisfy

$$v_{K,j}(x_{K',i}) = \delta_{K,K'}\delta_{i,j},\ K, K' \in \mathcal{T}_h,\ i, j = 1, \ldots, m(q).$$

For practical reasons we define a local to global numbering order such that $v_\nu|_K := v_{K,i}$ and $v_\nu|'_K := 0$ for $i \in \{1, \ldots m(q)\}$, on each element K where ν is the global number index corresponding to the local pair (K, i).

In our work we make use of inverse inequalities that hold on spaces of polynomial functions (cf. [11]).

Lemma 3.0.2. *There exists a constant c depending only on the minimum angle of K and q such that*

$$|\chi|_{j,K} \leq c h_K^{i-j} |\chi|_{i,K}, \quad \forall \chi \in P_q(K),\ 0 \leq i \leq j \leq q. \tag{3.3}$$

An immediate consequence of the trace and the inverse inequalities for polynomials are the following trace inequalities. For $e = \mathcal{E}^I$ and $v \in V_h$ there hold

$$|\{v\}|_e^2 \leq Ch_e^{-1}\Big(\|v\|_{K^+}^2 + \|v\|_{K^-}^2\Big), \tag{3.4}$$

$$|\{\partial_n v\}|_e^2 \leq Ch_e^{-3}\Big(\|v\|_{K^+}^2 + \|v\|_{K^-}^2\Big). \tag{3.5}$$

For $e \in \mathcal{E}^B$, the above inequalities hold without K^-.

The spaces V_h possess good approximation properties due to the fact that the approximations can be localized to individual elements. Indeed from a result of Scott-Dupont (cf. [11] and also [7]) we have

Lemma 3.0.3. *For $K \in \mathcal{T}_h$ let $\phi \in H^m(K)$, $m \geq 0$. Then for each q with $-1 \leq q \leq m-1$, there exists $\chi \in P_q(K)$ such that*

$$|\phi - \chi|_{j,K} \leq Ch_K^{q+1-j}|\phi|_{q+1,K}, \quad 0 \leq j \leq q+1, \tag{3.6}$$

where C is independent of $h_K,\ \phi,\ q$.

In our work we make use of the L^2-projection operator $\Pi_h : L^2(\Omega) \to V^h$. For $\phi \in L^2(\Omega)$ we denote by $\Pi_h\phi$ the L^2-projection of ϕ on V^h:

$$\Pi_h\phi \in V^h, \quad (\Pi_K\phi, v)_K = (\phi, v)_K, \ \forall\ v \in V^h \tag{3.7}$$

where $\Pi_K := \Pi_h|_K$. The following approximation properties of this operator are well known and can be found in [11].

Lemma 3.0.4. *Approximation properties of the operator Π_h:*
For $\psi \in H^{q+1}(K)$, $q \geq 0$, there exists $\Pi_K\psi \in P_q(K)$ and a constant c independent of h, K, and ψ, such that,

$$|\Pi_K\psi - \psi|_{j,K} \leq ch_K^{q+1-j}|\psi|_{q+1,K},\ j = 0, \cdots, q+1 \tag{3.8}$$

We will also make use of the usual nodal based Lagrangian interpolation operators $I_K : C(\overline{K}) \to P_q(K)$. The approximation properties of this operator are well known and can be found in [16].

Lemma 3.0.5. *For $K \in \mathcal{T}_h$, let $\phi \in H^s(K) \cap C(\overline{K})$, with $2 \leq q+1 \leq s$. Then*

$$|\phi - I_K\phi|_{j,K} \leq C\, h_K^{q+1-j} |\phi|_{q+1,K}, \quad 0 \leq j \leq q+1. \tag{3.9}$$

Furthermore, if $\phi \in W^{2,\infty}$, then

$$|\phi - I_K\phi|_{L^\infty(K)} \leq c h_K^2 |\phi|_{W^{2,\infty}(K)}. \tag{3.10}$$

3.3 SIP-DG for the Second Order Elliptic Problem

We first consider the model Poisson's equation with Dirichlet boundary conditions.

$$\begin{aligned} -\triangle u &= f, \quad \text{in } \Omega \\ u &= g_D, \quad \text{on } \partial\Omega \end{aligned} \tag{3.11}$$

This formulation, described below, gives rise to the bilinear form needed in the DG mixed formulation of the tumor model explained in chapter 5.

3.3.1 Derivation of the SIP-DG Formulation

Here we provide for the convenience of the reader the derivation of the SIP-DG formulation of Poisson's equation. Assume $u \in H^2(\Omega)$. Multiplying the equation in (3.11) by a test function $v \in E_h = H^2(\mathcal{T}_h)$ and integrating by parts we have,

$$\begin{aligned} -(\triangle u, v) &= -\sum_{K\in\mathcal{T}_h} (\triangle u, v)_K \\ &= \sum_{K\in\mathcal{T}_h} (\nabla u, \nabla v)_K - \sum_{K\in\mathcal{T}_h} \langle \partial_n u, v\rangle_{\partial K} \end{aligned}$$

Now by rewriting the sum over the triangle boundary integrals as a sum over the edges we have,

$$\begin{aligned} -(\triangle u, v) &= \sum_{K\in\mathcal{T}_h}(\nabla u, \nabla v)_K - \sum_{e\in\mathcal{E}^I}(\langle \nabla u^+ \cdot n^+, v^+\rangle_e + \langle \nabla u^- \cdot n^-, v^-\rangle_e) \\ &- \sum_{e\in\mathcal{E}^B}\langle \nabla u^+ \cdot n^+, v^+\rangle_e, \\ \text{(since } n^- = -n^+) \quad &= \sum_{K\in\mathcal{T}_h}(\nabla u, \nabla v)_K - \sum_{e\in\mathcal{E}^I}(\langle \nabla u^+ \cdot n^+, v^+\rangle_e - \langle \nabla u^- \cdot n^+, v^-\rangle_e), \\ &- \sum_{e\in\mathcal{E}^B}\langle \nabla u^+ \cdot n^+, v^+\rangle_e. \end{aligned} \tag{3.12}$$

Recalling Arnold's formula (cf. [5]),

$$a^+b^+ - a^-b^- = \{a\}[b] + \{b\}[a] \tag{3.13}$$

we rewrite the interior edge integrals as,

$$\int_e (\nabla u^+ v^+ - \nabla u^- v^-)\cdot n^+ ds = \int_e \{\nabla u\}\cdot n^+[v] + \{v\}[\nabla u]\cdot n^+ ds. \tag{3.14}$$

Note. Since $u \in H^2(\Omega)$ the terms $[\nabla u]$ is zero. Thus (3.14) becomes,

$$\int_e (\nabla u^+ v^+ - \nabla u^- v^-)\cdot n^+ ds = \int_e \{\nabla u\}\cdot n^+[v] ds \tag{3.15}$$

Thus using (3.15) in (3.12) we have,

$$\begin{aligned} -(\triangle u, v) &= \sum_{K\in\mathcal{T}_h} (\nabla u, \nabla v)_K - \sum_{e\in\mathcal{E}^I} \langle \{\partial_n u\}, [v]\rangle_e \\ &- \sum_{e\in\mathcal{E}^B} \langle \nabla u \cdot n, v\rangle_e \\ &= \sum_{K\in\mathcal{T}_h} (\nabla u, \nabla v)_K - \sum_{e\in\mathcal{E}} \langle \{\partial_n u\}, [v]\rangle_e \end{aligned} \tag{3.16}$$

Remark. We observe that the right hand side of (3.16) is non symmetric. However we can symmetrize it by subtracting artificially $\langle [u], \{\partial_n v\}\rangle_e$. Observe that for interior edges, since $u \in H^2(\Omega)$, we have $[u]|_e = 0$ and thus the symmetric term $\langle [u], \{\partial_n v\}\rangle_e$ is zero. For boundary edges, the value of u is g_D which is known. Thus we must subtract from the right hand side the symmetric term corresponding to boundary edges in order for our formulation to be consistent. Also we introduce the penalty term $\gamma h_e^{-1}\langle [u], [v]\rangle_e$ that allows us to have control over the jumps of the function by choosing $\gamma > 0$ accordingly. Again as before, we need to add to the right hand side the non-zero portion of the penalty term corresponding to the boundary edges. These are known quantities.

Hence after adding the new terms on (3.16) for the function $u \in H^2(\Omega)$ we obtain the following bilinear form $\alpha_h^D(\cdot,\cdot)$ on $E_h \times E_h$,

$$\begin{aligned} \alpha_h^D(u,v) &:= \sum_{K\in\mathcal{T}_h} (\nabla u, \nabla v)_K \\ &- \sum_{e\in\mathcal{E}} (\langle \{\partial_n u\}, [v]\rangle_e + \langle [u], \{\partial_n v\}\rangle_e \\ &- \gamma h_e^{-1}\langle [u], [v]\rangle_e), \text{ for } v \in E_h \text{ and } \gamma > 0 \end{aligned} \tag{3.17}$$

It follows easily from the construction outlined above that for $u \in H^2(\Omega)$

$$\alpha_h^D(u,v) = -(\triangle u, v) - \sum_{e \in \mathcal{E}^B} \langle \partial_n v - \gamma h_e^{-1} v, u \rangle_e, \ \forall\ v \in E_h. \tag{3.18}$$

This shows that $\alpha_h^D(\cdot,\cdot)$ is consistent with the PDE of (3.11). Therefore, we define the discontinuous weak formulation of (3.11) by seeking $u \in E_h$ satisfying,

$$\alpha_h^D(u,v) = F(v) := (f,v) - \sum_{e \in \mathcal{E}^B} \langle \partial_n v - \gamma h_e^{-1} v, g_D \rangle_e, \ \forall\ v \in E_h, \tag{3.19}$$

and thus we use (3.19) to define the following SIP-DG formulation:

$$\text{find } u_h \in V^h \text{ such that,} \qquad \alpha_h^D(u_h, v) = F(v), \ \forall\ v \in V^h. \tag{3.20}$$

In order to show any theoretical results such as solvability and convergence of our SIP-DG formulation (3.20) we will need an appropriate norm on the energy space as well as on the discontinuous finite element space. The bilinear form given by (3.17) motivates the use of the following norm on E_h (cf. [30]),

$$|||v|||_D^2 \ := \ \Big(\sum_{K \in \mathcal{T}_h} ||\nabla v||_k^2 + \sum_{e \in \mathcal{E}} (\frac{1}{h_e} |[v]|_e^2 + h_e |\{\nabla v\}|_e^2). \tag{3.21}$$

The following lemma establishes the continuity of the bilinear form in E_h and the coercivity of the bilinear form on V^h (cf. [5] and [30] and references therein) and therefore establishes the solvability of the SIP-DG formulation (3.20).

Lemma 3.3.1.1. *Let $|||\cdot|||_D$ defined as in (3.21) then we have the following.*
i) The $|||\cdot|||_D$ is a norm on V^h.
ii) $|\alpha_h(u,v)| \leq (1+\gamma)|||u|||_D \ |||v|||_D$, $\forall\ u, v \in E_h$

iii) $\exists \gamma_0 > 0$ *and* $c_a > 0$ *such that for* $\gamma \geq \gamma_0$,
$\alpha_h(u,u) \geq c_a |||u|||_D^2, \ \forall \ u \in V^h$

It can be shown that the following error estimates hold (cf. [7]).

Theorem 3.1. *Let* u *and* u_h *be the solutions of* (3.11) *and* (3.20)*, respectively, and suppose that* $u \in H^{q+1}(\Omega) \cap H_0^1(\Omega)$ *with* $q \geq 1$*. Then there exists a positive constant* c*, which is independent of* h *and* u*, such that*

$$|||u - u_h|||_D \leq c \left(\sum_{K \in \mathcal{T}_h} h_K^{2q} |u|_{q+1,K}^2 \right)^{1/2}, \tag{3.22}$$

$$\|u - u_h\| \leq c h^{q+1} |u|_{q+1,\Omega}. \tag{3.23}$$

Also for our research we will need to know the bilinear form corresponding to the Poisson's equation with pure Neumann boundary conditions. This bilinear form arises in the mixed formulation of the Cahn Hilliard equation in chapter 5. In order to obtain the bilinear form for this case we work similarly as for the Dirichlet case but we omit from the bilinear the contributions from the boundary edges, since these quantities are known and can be moved to the right hand side. Also we do not add penalty for boundary edges in the bilinear form since the value of the function u is not known on $\partial\Omega$. Hence we arrive at the following bilinear form, $a_h(\cdot,\cdot)$ on $E_h \times E_h$, corresponding to pure Neumann boundary conditions,

$$\begin{aligned} \alpha_h(u,v) \ &:= \ \sum_{K \in \mathcal{T}_h} (\nabla u, \nabla v)_K \\ &- \ \sum_{e \in \mathcal{E}^I} (\langle \{\partial_n u\}, [v] \rangle_e + \langle [u], \{\partial_n v\} \rangle_e - \gamma h_e^{-1} \langle [u], [v] \rangle_e). \end{aligned} \tag{3.24}$$

It follows similarly with the Dirichlet case, the following consistency result, for $u \in H^2(\Omega)$,

$$\alpha_h(u,v) = -(\triangle u, v) + \sum_{e \in \mathcal{E}^B} \langle v, \partial_n u \rangle_e, \ \forall \ v \in E_h. \tag{3.25}$$

The bilinear form given by (3.24) motivates the following seminorm on E_h (cf. [32]),

$$|||v|||^2 \;:=\; \sum_{K\in\mathcal{T}_h} ||\nabla v||_k^2 + \sum_{e\in\mathcal{E}^I} \Big(2\frac{\gamma}{h_e}|[v]|_e^2 + \frac{h_e}{\gamma}|\{\nabla v\}|_e^2\Big). \tag{3.26}$$

Lemma 3.3.1.2. *Let $|||\cdot|||$ defined as in (3.24) then we have the following.*
i) The $|||\cdot|||$ seminorm is a norm on E_h/R.
ii) $|\alpha_h(u,v)| \le (1+\gamma)|||u|||\ |||v|||$, $\forall\ u,v \in E_h$
iii) $\exists \gamma_0 > 0$ and $c_a > 0$ such that for $\gamma \ge \gamma_0$,
$\alpha_h(u,u) \ge c_a|||u|||^2,\ \forall\ u \in V^h$

Note. When u = *constant* we have that the third part of Lemma 3.3.1.2 is automatically satisfied since the left part and the right part of the inequality are both zero.

Now we continue this subsection by listing some results that we will need in chapter 5.

In our analysis of the mixed formulation of the Cahn-Hilliard equation we will make use of the following norm equivalence which easily follows from part *ii*) and *iii*) of Lemma 3.3.1.2. For $v \in V^h$ there are positive constants c_1 and c_2 independent of h such that,

$$c_1|||v|||_\alpha \le |||v||| \le c_2|||v|||_\alpha \tag{3.27}$$

where, $|||v|||_\alpha^2 := \alpha_h(v,v)$.
Next we describe the *discrete Laplacian* as follows (cf. [32]).

Lemma 3.3.1.3. *For $w \in V^h$ there exists $\triangle_h w \in V^h/R$ such that,*

$$(-\triangle_h w, v) = \alpha_h(w,v),\ \forall v \in V^h \tag{3.28}$$

Proof. The existence and uniqueness of $\triangle_h w$ is guaranteed by the Riesz representation theorem on $\langle V^h/R, (\cdot,\cdot)\rangle$. That is, we fix $w \in V^h$ and note that $v \in V^h/R \to$

$\alpha_h(w,v) \in R$ is a bounded linear functional on the Hilbert space $\langle V^h/R, (\cdot,\cdot)\rangle$ by the continuity of the bilinear form described in Lemma 3.3.1.2 and the equivalence of $|||\cdot|||$ with $||\cdot||$ in finite dimensional vector spaces. Thus $(-\triangle_h w, v) = \alpha_h(w,v),\ \forall v \in V^h/R$. Now by observing that $V^h = V^h/R \oplus \text{span}\{1\}$ and $\alpha_h(w,1) = 0$ the relation (3.28) follows. □

Also the following broken version of *Agmon's inequality* will prove useful and its proof can be found in (cf. [32]).

Lemma 3.3.1.4.

$$||z - \fint_\Omega z||_{0,\infty} = ||\triangle_h z||^{1/2}||z||^{1/2},\ \forall z \in V^h \tag{3.29}$$

and

$$||z||_{0,\infty} = ||\triangle_h z||^{1/2}||z||^{1/2},\ \forall z \in V^h/R \tag{3.30}$$

Finally we will need the following *broken Friedrich's inequality* which its proof is presented in [13] and [32].

Lemma 3.3.1.5. *For $v \in E_h \cap V^h/R$ and $p \in [2,\infty)$ we have,*

$$||v||_{0,p} \leq c(p)|||v||| \tag{3.31}$$

where $||\cdot||_{0,p}$ is the L^p norm on Ω.

3.4 SIP-DG for the Biharmonic Equation

The SIP-DG method for the biharmonic problem was first studied in [6]. In this section we will present some classical results for the biharmonic equation that can be found or easily derived from work done in [6], [36], [25], [27] and others.
We first examine the following biharmonic equation with essential boundary conditions.

$$\begin{aligned} \triangle^2 u &= f, \quad \text{in } \Omega \\ \frac{\partial u}{\partial n} &= g_N, \quad \text{on } \partial\Omega \\ u &= g_D, \quad \text{on } \partial\Omega \end{aligned} \tag{3.32}$$

Where $f \in L^2$, $g_D \in H^{\frac{7}{2}}$, $g_N \in H^{\frac{5}{2}}$ are such that a **PDE solution** exists in $H^4(\Omega)$ and Ω is a convex polygon (cf. [29]).

3.4.1 Derivation of the SIP-DG Formulation

Let $u \in H^4(\Omega) \subset E_h = H^4(\mathcal{T}_h)$ such that u satisfies (3.32) and $v \in E_h$ a test function, then by multiplying the biharmonic equation by v and integrating twice by parts we have,

$$\begin{aligned} (\triangle^2 u, v) &= \sum_{K\in\mathcal{T}_h} (\triangle^2 u, v)_K \\ &= -\sum_{K\in\mathcal{T}_h} (\nabla(\triangle u), \nabla v)_K + \sum_{K\in\mathcal{T}_h} \langle \partial_n \triangle u, v\rangle_{\partial K} \\ &= \sum_{K\in\mathcal{T}_h} (\triangle u, \triangle v)_K + \sum_{K\in\mathcal{T}_h} (\langle \partial_n \triangle u, v\rangle_{\partial K} - \langle \triangle u, \partial_n v\rangle_{\partial K}) \end{aligned}$$

Now by rewriting the sum over the triangle boundary integrals as a sum over the edges we have,

$$\begin{aligned} (\triangle^2 u, v) &= \sum_{K\in\mathcal{T}_h} (\triangle u, \triangle v)_K + \sum_{e\in\mathcal{E}^I} (\langle \nabla\triangle u^+ \cdot n^+, v^+\rangle_e + \langle \nabla\triangle u^- \cdot n^-, v^-\rangle_e \\ &- \langle \triangle u^+, \nabla v^+ \cdot n^+\rangle_e - \langle \triangle u^-, \nabla v^- \cdot n^-\rangle_e) \\ &+ \sum_{e\in\mathcal{E}^B} (\langle \nabla\triangle u^+ \cdot n^+, v^+\rangle_e - \langle \triangle u^+, \nabla v^+ \cdot n^+\rangle_e) \end{aligned}$$

For interior edges $n^- = -n^+$ and for boundary edges $n^+, u^+, v^+ = n, u, v$ thus we have,

$$\begin{aligned}(\triangle^2 u, v) &= \sum_{K\in\mathcal{T}_h}(\triangle u, \triangle v)_K + \sum_{e\in\mathcal{E}^I}(\langle\nabla\triangle u^+\cdot n^+, v^+\rangle_e - \langle\nabla\triangle u^-\cdot n^+, v^-\rangle_e \\ &- (\langle\triangle u^+, \nabla v^+\cdot n^+\rangle_e - \langle\triangle u^-, \nabla v^-\cdot n^+\rangle_e)), \text{ since} \\ &+ \sum_{e\in\mathcal{E}^B}(\langle\partial_n\triangle u, v\rangle_e - \langle\triangle u, \partial_n v, \rangle_e),\end{aligned} \tag{3.33}$$

Now we rewrite the interior edge terms above and apply Arnold's formula (3.13) on them,

$$\begin{aligned}\int_e(\nabla\triangle u^+v^+ - \nabla\triangle u^-v^-)\cdot n^+ ds &= \int_e\{\nabla\triangle u\}\cdot n^+[v] + \{v\}[\nabla\triangle u]\cdot n^+ ds \\ \int_e(\nabla v^+\triangle u^+ - \nabla v^-\triangle u^-)\cdot n^+ ds &= \int_e\{\nabla v\}\cdot n^+[\triangle u] + \{\triangle u\}[\nabla v]\cdot n^+ ds\end{aligned} \tag{3.34}$$

Note. Since $u \in H^4(\Omega)$ the terms $[\nabla\triangle u]$ and $[\triangle u]$ are zero. Thus (3.34) becomes,

$$\begin{aligned}\int_e(\nabla\triangle u^+v^+ - \nabla\triangle u^-v^-)\cdot n^+ ds &= \int_e\{\partial_n\triangle u\}[v]ds \\ \int_e(\nabla v^+\triangle u^+ - \nabla v^-\triangle u^-)\cdot n^+ ds &= \int_e\{\triangle u\}[\partial_n v]ds\end{aligned} \tag{3.35}$$

Thus from using (3.35) in (3.33) we have,

$$\begin{aligned}(\triangle^2 u, v) &= \sum_{K\in\mathcal{T}_h}(\triangle u, \triangle v)_K + \sum_{e\in\mathcal{E}^I}(\langle\{\partial_n\triangle u\},[v]\rangle_e - \langle\{\triangle u\},[\partial_n v]\rangle_e)\\ &+ \sum_{e\in\mathcal{E}^B}(\langle\partial_n\triangle u, v\rangle_e - \langle\triangle u, \partial_n v\rangle_e)\\ &= \sum_{K\in\mathcal{T}_h}(\triangle u, \triangle v)_K + \sum_{e\in\mathcal{E}}(\langle\{\partial_n\triangle u\},[v]\rangle_e - \langle\{\triangle u\},[\partial_n v]\rangle_e) \quad (3.36)\end{aligned}$$

Remark. We observe that the right hand side of (3.36) is not symmetric thus we add and subtract respectively $\langle\{\partial_n\triangle v\},[u]\rangle_e$ and $\langle\{\triangle v\},[\partial_n u]\rangle_e$ artificially in order to symmetrize the bilinear form. Observe that, since $u \in H^4(\Omega)$, for interior edges we have $[u]|_e = 0$, $[\partial_n u]|_e = 0$ and thus the symmetric terms are zero. For boundary edges, the value of $u = g_D$, and $\partial_n u = g_N$ thus we must subtract from the right hand side the symmetric terms corresponding to boundary edges in order for our formulation to remain consistent. Also we introduce the penalty terms $\gamma h_e^{-3}\langle[u],[v]\rangle_e$ and $\gamma h_e^{-1}\langle[\partial_n v],[\partial_n u]\rangle_e$ that allow us to have control over the jumps of the function and the normal derivative by choosing $\gamma > 0$ accordingly. Again as before we need to add to the right hand side the non-zero portion of the penalty terms corresponding to the boundary edges.

Hence after adding the new terms on both sides of (3.36) for the function $u \in H^4(\Omega)$ we obtain the following bilinear form $\beta_h^E(\cdot,\cdot)$ on $E_h \times E_h$,

$$\begin{aligned}\beta_h^E(u,v) &:= \sum_{K\in\mathcal{T}_h}(\triangle u, \triangle v)_K + \sum_{e\in\mathcal{E}}(\langle\{\partial_n\triangle u\},[v]\rangle_e + \langle[u],\{\partial_n\triangle v\}\rangle_e\\ &- \langle\{\triangle u\},[\partial_n v]\rangle_e - \langle[\partial_n u],\{\triangle v\}\rangle_e\\ &+ \gamma h_e^{-1}\langle[\partial_n u],[\partial_n v]\rangle_e + \gamma h_e^{-3}\langle[u],[v]\rangle_e),\ \forall\ u,v\in E_h, \quad (3.37)\end{aligned}$$

where $\gamma > 0$. It follows easily from the construction outlined above that for $u \in H^4(\Omega)$

$$\beta_h^E(u,v) = (\triangle^2 u, v) + \sum_{e\in\mathcal{E}^B}(\langle\partial_n\triangle v + \gamma h_e^{-3} v, u\rangle_e - \langle\triangle v - \gamma h_e^{-1}\partial_n v, \partial_n u\rangle_e),\ \forall\ v\in E_h.$$

This shows that $\beta_h^E(\cdot,\cdot)$ is consistent with the PDE of (3.32). Therefore, we define the discontinuous weak formulation of (3.32) by seeking $u \in E_h$ satisfying,

$$\beta_h^E(u,v) = F(v) := (f,v) + \sum_{e\in\mathcal{E}^B} (\langle \partial_n \triangle v + \gamma h_e^{-3} v, g_D\rangle_e - \langle \triangle v - \gamma h_e^{-1}\partial_n v, g_N\rangle_e),\ \forall\, v \in E_h. \tag{3.38}$$

and thus we use (3.38) to define the following SIP-DG formulation.
Find $u_h \in V^h$ such that,

$$\beta_h^E(u_h,v) = F(v),\ \forall\ v \in V^h. \tag{3.39}$$

The bilinear form given by (3.37) motivates the use of the following norm on E_h,

$$\begin{aligned} ||u||_{2,h} \ &:= \ \Big(\sum_{K\in\mathcal{T}_h} ||\triangle u||_K^2 + \sum_{e\in\mathcal{E}} (h_e^{-3}|[u]|_e^2 + h_e^{-1}|[\partial_n u]|_e^2 \\ &+ \ h_e|\{\triangle u\}|_e^2 + h_e^3|\{\partial\triangle u\}|_e^2)\Big)^{1/2}. \end{aligned} \tag{3.40}$$

The following lemma establishes the continuity of the bilinear form in E_h and the coercivity of the bilinear form in V^h (cf. [6], [36], [25] and references therein) and therefore establishes the solvability of the SIP-DG formulation (3.39).

Lemma 3.4.1.1. *Let $||\cdot||_{2,h}$ defined as in (3.37) then we have the following.*
i) The $||\cdot||_{2,h}$ is a norm on E_h and V^h.
ii) $|\beta_h^E(u,v)| \le (1+\gamma)||u||_{2,h}\ ||v||_{2,h},\ \forall\ u,v \in E_h$
iii) $\exists \gamma_0 > 0$ and $c_b > 0$ such that for $\gamma \ge \gamma_0$,
$\beta_h^E(u,u) \ge c_b||u||_{2,h}^2,\ \forall\ u \in V^h$

Now we consider the following biharmonic equation with natural boundary conditions.

$$\begin{aligned} \triangle^2 u &= f, \quad \text{in } \Omega \\ \frac{\partial u}{\partial n} &= g_N, \quad \text{on } \partial\Omega \\ \frac{\partial \triangle u}{\partial n} &= h_N, \quad \text{on } \partial\Omega \end{aligned} \tag{3.41}$$

This formulation serves as a basis for the development of the SIP-DG discretizations of our primitive variable formulations for our Cahn-Hilliard models in chapter 4.

Now working in an entirely similar way as for the formulation (3.32) and paying attention to the different boundary conditions, and also keeping in mind that we do not know the value of u on the boundary, we arrive at the following bilinear form described in [27].

$$\begin{aligned} \beta_h(u,v) \;:=\; & \sum_{k\in\mathcal{T}_h} (\triangle v, \triangle u)_k + \sum_{e\in\mathcal{E}^I} (\langle\{\partial_n \triangle u\}, [v]\rangle_e + < \{\partial_n \triangle v\}, [u] >_e \\ & - \langle\{\triangle u\}, [\partial_n v]\rangle_e - \langle\{\triangle v\}, [\partial_n u]\rangle_e \\ & + \gamma h_e^{-1} \langle [\partial_n v], [\partial_n u]\rangle_e + \gamma h_e^{-3} \langle [u], [v]\rangle_e) \\ & - \sum_{e\in\mathcal{E}^B} (\langle \triangle u, \partial_n v\rangle_e + \langle \triangle v, \partial_n u\rangle_e - \gamma h_e^{-1} \langle \partial_n v, \partial_n u\rangle_e), \;\; \forall\; u, v \in E_h, \end{aligned} \tag{3.42}$$

where $\gamma > 0$. The above bilinear form is not coercive anymore in V^h. For a detailed explanation see ([27]). In an analogous way as before we can see that for $u \in H^4(\Omega)$ the bilinear form is consistent with the PDE in (3.41) in the sense that,

$$\beta_h(u,v) = (\triangle^2 u, v) - \sum_{e\in\mathcal{E}^B} (\langle v, \partial_n \triangle u\rangle_e + \langle \triangle v - \gamma h_e^{-1} \partial_n v, \partial_n u\rangle_e), \;\; \forall\; v \in E_h. \tag{3.43}$$

and thus we can define the following weak formulation of (3.41) by seeking $u \in E_h$ satisfying,

$$\beta_h(u,v) = F(v) := (f,v) - \sum_{e\in\mathcal{E}^B}(\langle v, h_N\rangle_e + \langle \triangle v - \gamma h_e^{-1}\partial_n v, g_N\rangle_e),\ \forall\ v \in E_h. \quad (3.44)$$

and thus we use (3.44) to define the following SIP-DG formulation:

$$\text{find } u_h \in V^h \text{ such that,} \qquad \beta_h(u_h,v) = F(v),\ \forall\ v \in V^h. \quad (3.45)$$

The bilinear form given by (3.42) induces the following seminorm on E_h,

$$\begin{aligned} |||u|||_{2,h} &:= \Big(\sum_{k\in\mathcal{T}_h}||\triangle u||_k^2 + \sum_{e\in\mathcal{E}^I}(h_e^{-3}|[u]|_e^2 + h_e^3|\{\partial\triangle u\}|_e^2) \\ &+ \sum_{e\in\mathcal{E}}(h_e|\{\triangle u\}|_e^2 + h_e^{-1}|[\partial_n u]|_e^2)\Big)^{1/2}. \end{aligned} \quad (3.46)$$

The following lemma establishes the continuity of the bilinear in E_h and the coercivity of the bilinear in V^h/R.

Lemma 3.4.1.2. *Let $|||\cdot|||_{2,h}$ defined as in (3.46) then we have the following.*
i) The $|||\cdot|||_{2,h}$ seminorm is a norm on the quotient spaces E_h/R and thus also on V^h/R.
ii) $|\beta_h(u,v)| \le (1+\gamma)|||u|||_{2,h}|||v|||_{2,h}$, $\forall\ u,v \in E_h$
iii) $\exists\gamma_0 > 0$ and $c_b > 0$ such that for $\gamma \ge \gamma_0$,
$\beta_h(u_h,u_h) \ge c_b|||u_h|||_{2,h}^2$, $\forall\ u_h \in V^h$

3.4.2 A-priori Error Estimates

In [6], Baker obtained optimal a-priori error estimates for (3.32) in the energy norm as well as negative norms under the assumption that $u \in H^s(\Omega)$, $s \ge 4$ and $q \ge 3$. Estimates for the case $q = 2$ can also be obtained except that the rate for the L^2-norm

of the error is suboptimal. In their paper [27] the authors obtained similar results for the BVP (3.41). For completeness we mention the following Theorem 3.2 taken from their paper that summarizes the a-priori estimates for BVP (3.41).

It follows easily from the approximation properties (3.6) that for $v \in H^s(\mathcal{T}_h)$, $s \geq 4$ and $r = q + 1$,

$$\|\phi - \chi\|_{2,h} \leq \begin{cases} C|h^{r-2}\phi|_{H^r(\mathcal{T}_h)} & 4 \leq r \leq s, \\ C|h\phi|_{H^3(\mathcal{T}_h)} + |h^2\phi|_{H^4(\mathcal{T}_h)} & r = 3, \end{cases} \tag{3.47}$$

where $|h^j v|_{H^\ell(\mathcal{T}_h)} := \Big(\sum_{K \in \mathcal{T}_h} h_K^{2j} |v|_{\ell,K}^2 \Big)^{1/2}$.

Theorem 3.2. *Assume that the solution u of the BVP (3.41) is in $H^3(\Omega) \cap H^s(\mathcal{T}_h)$, $s \geq 4$ and let $u_h \in V_h$ be given by (3.45). Then,*

(i) For $4 \leq r \leq s$, there holds

$$\| u - u_h \|_{2,h} \leq \; c|h^{r-2}u|_{H^r(\mathcal{T}_h)}. \tag{3.48}$$

If in addition $\int_\Omega u_h \, dx = \int_\Omega u \, dx$, then

$$\|u - u_h\| \leq \; ch^2|h^{r-2}u|_{H^r(\mathcal{T}_h)}. \tag{3.49}$$

For $K \in \mathcal{T}_h$ and musince $u \in H^4(\Omega)$lti-index α, $1 \leq |\alpha| \leq r$, we have

$$\|D^\alpha(u - u_h)\|_K \leq \; ch_K^{r-|\alpha|}|u|_{H^r(K)} + ch_K^{-|\alpha|}\|u - u_h\|_K. \tag{3.50}$$

(ii) Similarly, for $r = 3$, there holds

$$\| u - u_h \|_{2,h} \leq \ c|hu|_{H^3(\mathcal{T}_h)} + c|h^2 u|_{H^4(\mathcal{T}_h)}. \tag{3.51}$$

If in addition $\int_\Omega u_h \, dx = \int_\Omega u \, dx$, *then*

$$\|u - u_h\| \leq \ ch\Big(|hu|_{H^3(\mathcal{T}_h)} + |h^2 u|_{H^4(\mathcal{T}_h)}\Big). \tag{3.52}$$

For $K \in \mathcal{T}_h$ *and multi-index* α, $1 \leq |\alpha| \leq 3$, *we have*

$$\|D^\alpha (u - u_h)\|_K \leq \ ch_K^{3-|\alpha|} |u|_{H^r(K)} + ch_K^{-|\alpha|} \|u - u_h\|_K. \tag{3.53}$$

3.5 A-posteriori Estimates and Adaptive Methods

Since the solution of the Cahn-Hilliard model's can be described as a moving wave with a sharp interface whereby away from this interface the solution either has value $u = 1$ or $u = 0$, it makes sense to use an adaptive scheme. The basic adaptive cycle for stationary problems is given by,

1. Compute the solution u_H on mesh $\mathcal{T}_H$;
2. Estimate the error in u_H;
3. If error $<$ Tol, stop;
   else refine/coarsen and go to 1.;

which is described by algorithm 1 in much more detailed form.

We have used the aforementioned elliptic problems described above for second and fourth order as test problems in the development of our adaptive routines and multilevel solvers. Algorithms and routines that perform the *refinement* and *coarsening* have been developed in our work, and they have been tested successfully in an adaptive implementation for solving those elliptic problems.

In particular since in the classical adaptive cycle described in algorithm 1 we require an *a posteriori* error estimate we have made use of *a posteriori* error estimates found

in [30] for the second order BVP (3.11) and in [28] for the biharmonic case for the BVP (3.32). Also it is worth mentioning that for the BVP (3.11) the authors in [31] have proven convergence of the adaptive algorithm 1 for the SIP-DG formulation.

It is important to mention that in our case we have not pursued the development

Algorithm 1 Adaptive algorithm using the marking strategy found in [20].

Start with an initial coarse mesh $\mathcal{T}_h$;
for $aiter = 1, \cdots, max_{aiter}$ **do**
  Compute u_h on $\mathcal{T}_h$;
  Estimate the local error, Err_K, on each $K \in \mathcal{T}_h$;
  Calculate $TotalError = \sum_{K \in \mathcal{T}_h} Err_K$;
  if $Total\ Error < (Prescibed)\ Tolerance$ **then**
    $break$;
  else
    Arrange $K \in \mathcal{T}_h$ in descending order in a list $\mathcal{T}_{R,err_K}$, and in ascending order in a list $\mathcal{T}_{C,err_K}$ according to their Err_K;
    for $K \in \mathcal{T}_{R,err_K}$ **do**
      Insert K in $\mathcal{T}_{R,marked}$ list;
      if $\sum_{\mathcal{T}_{R,marked}} Err_K \leq \theta_R\ Total\ Error$ **then**
        $break$;
      end if
    end for
    if $\mathcal{T}_{R,marked} = NULL$ **then**
      $break$;
    else
      for $K \in \mathcal{T}_{C,err_K}$ **do**
        Insert K in $\mathcal{T}_{C,marked}$ list;
        if $\sum_{\mathcal{T}_{C,marked}} Err_K \geq \theta_C\ Total\ Error$ **then**
          $break$;
        end if
      end for
      Coarsen the triangles in $\mathcal{T}_{C,marked}$ and refine the triangles in $\mathcal{T}_{R,marked}$ to get an updated $\mathcal{T}_h$;
    end if
  end if
end for

of a posteriori error estimates for the adaptive implementation of our Cahn Hilliard models but we have used a new generic marking strategy introduced in [8] and [9] that uses the inverse inequality (3.3) to measure how large is the gradient of the finite

element solution, u_h. To be more specific we have set $i = 0$, $j = 1$, $\chi = u_h + const$ in (3.3) and noting that $\nabla(u_h + const) = \nabla u_h$, we have the following,

$$c_K := h_K \frac{||\nabla u_h||_K}{||u_h + const||_K} \leq c. \tag{3.54}$$

Note. Adding a constant function on u_h does not affect the sharpness of the estimate (3.3). The reason we have chosen to add a constant function on u_h is because with the right choice of that *constant* we can guarantee that the denominator in (3.54) stays away from zero hence avoiding the complications arising form the case where $||u_h||_K = 0$ and because of (3.3) consequently having $||\nabla u_h||_K = 0$, hence ending up with an undetermined form.

The idea behind the new marking strategy is based on the fact that if the quantity c_K is too close to c this implies that our solution u_h possesses a steeper gradient on that part of the domain Ω and thus in order to capture more accurately the solution we must have more information, thus we need to perform refinement. Also similarly if the value of the local variable c_K is much smaller than c then this means that our solution u_h is relatively flat on that part of the domain hence we do not need so much information in order to adequately capture the solution and thus we can coarsen.
We have used this marking strategy in the adaptive implementation of the elliptic problems (see algorithm 2) described in this chapter and compared our results with the ones coming from the use of algorithm 1 in order to tune the procedure and gain inside on how the strategy works.

Remark. There is no general rule on how to determine the percentages θ_R and θ_C a priori in algorithms 1 and 2. The choice has to be made after performing some experiments which help us tune up the procedure for a specific setup.

In our tests for the elliptic problems of this section we have observed that with the right tuning of the input parameters related to the inverse estimate marking strategy, for certain test problems, we can achieve results that are comparable or even better

Algorithm 2 Adaptive algorithm using inverse estimate marking strategy.

Start with an initial coarse mesh $\mathcal{T}_h$;
for $aiter = 1, \cdots, max_{aiter}$ **do**
  Compute u_h on $\mathcal{T}_h$;
  Estimate the local inverse constant, c_K, on each $K \in \mathcal{T}_h$;
  Arrange $K \in \mathcal{T}_h$ in descending order in a list $\mathcal{T}_{R,c_K}$ and in ascending order in a list $\mathcal{T}_{C,c_K}$ according to their c_K;
  for $K \in \mathcal{T}_{R,c_K}$ **do**
    if $c_k < \theta_R \; c$ **then**
      Insert K in $\mathcal{T}_{R,marked}$ list;
    else
      $break$;
    end if
  end for
  if $\mathcal{T}_{R,marked} = NULL$ **then**
    $break$;
  else
    for $K \in \mathcal{T}_{C,c_K}$ **do**
      if $c_k > \theta_C \; c$ **then**
        Insert K in $\mathcal{T}_{C,marked}$ list;
      else
        $break$;
      end if
    end for
    Coarsen the triangles in $\mathcal{T}_{C,marked}$ and refine the triangles in $\mathcal{T}_{R,marked}$ to get an updated $\mathcal{T}_h$;
  end if
end for

than the ones obtained when using a residual type a posteriori estimators like the ones mentioned earlier in this section (cf. Fig. 3.1).

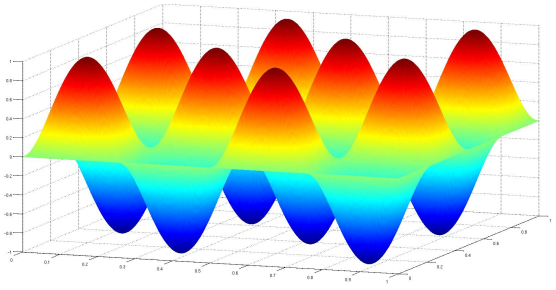

(a) Oscillatory Solution

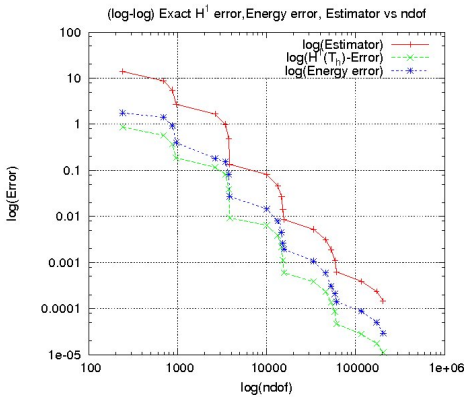

(b) Error Decrease

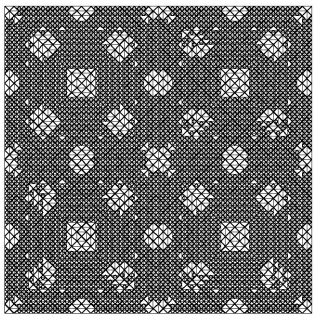

(c) Final Mesh

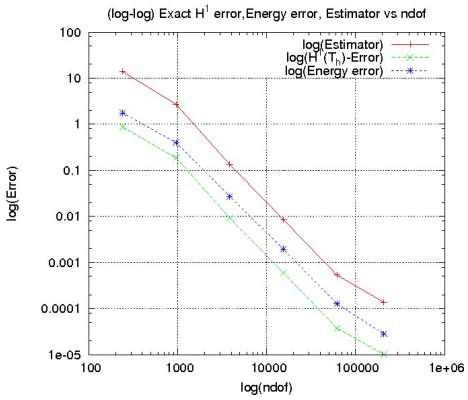

(d) Error Decrease

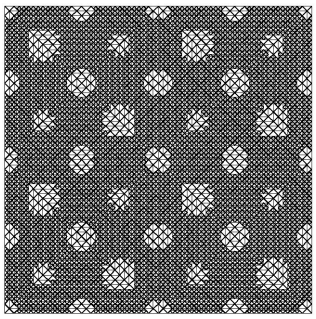

(e) Final Mesh

Figure 3.1: *Oscillatory test problem for Poisson's equation with exact solution given by* $u_e = \sin(4\pi x)\sin(4\pi y)$*, Fig. 3.1a. In figures 3.1b–3.1c we have the error reduction and the final mesh achieved after 20 adaptive iterations using Poisson's equation with Dirichlet boundary conditions. We have used the adaptive strategy described in Alg. 1 using the* a posteriori *error estimate developed in [30]. In figures 3.1d, 3.1e we have the error reduction plot and the final mesh for the same problem achieved after only 5 adaptive iterations using the marking strategy described in Alg. 2.*

Chapter 4

Primitive Variable Formulation and SIP-DG Implementation for our Cahn-Hilliard Models.

4.1 Introduction

Here we consider the primitive variable formulation **(Pv1)** of the tumor model equation (2.20a) with homogeneous Neumann boundary conditions.

$$
\begin{aligned}
u_t + \triangle(\epsilon\triangle u - \frac{1}{\epsilon}f(u)) &= S_\epsilon(u), \quad \text{in } \Omega_T, && \text{(4.1a)}\\
\frac{\partial u}{\partial n} &= 0, \quad \text{on } \partial\Omega_T, && \text{(4.1b)}\\
\frac{\partial \triangle u}{\partial n} &= 0, \quad \text{on } \partial\Omega_T, && \text{(4.1c)}\\
u &= u_0, \quad \text{on } \partial\Omega \times \{t = 0\}. && \text{(4.1d)}
\end{aligned}
$$

We have written our initial model as one equation with the only unknown to be the population density variable, u. To do this we have replaced the chemical potential, μ, in the PDE (2.20a) with its u expression, i.e. $\mu = f(u) - \epsilon^2\triangle u$. In the formulation **(Pv1)** we have also scaled the time variable so that t here, called the *fast time*,

represents $\frac{t}{\epsilon}$ in the original formulation (2.20a)–(2.20e) (cf. [27]). Also we utilized a simple affine transformation to shift the stable stationary solutions $u = -1$, $u = 1$ of (2.20a) to $u = 0$, $u = 1$. Under the aforementioned transformations the source term becomes $S_\epsilon(u) = \frac{1}{\epsilon}\lambda_g(1-u)^2(1+u)^2 - \frac{\frac{1}{\epsilon}\lambda_d(1+u)}{2}$ with $\lambda_d > 0$, $\lambda_g > 0$ constants, and also $f := H'$, $H(s) = \frac{1}{4}(s^2-1)^2$, is the transformed version of the double well potential $F(s)$ given by (2.4). We assume that a PDE solution exists in $L^2(0,T;H^4(\Omega))$ and Ω is a convex polygon. We have performed the above transformations for compatibility of our formulation with the one in (cf. [27]). For the latter reason we have chosen the use of pure Neumann boundary conditions instead of Dirichlet ones since by an easy switch (by setting $\lambda_g = 0$ and $\lambda_d = 0$) we can also solve the classical Cahn-Hilliard equation with fast time described in [27] and thus complete the implementational aspect of their work.

Another reason as to why we have formulated our IBVP in this way, is because it gives us the flexibility with the appropriate treatment of the non linear terms to create a method that uses a non linear multigrid setup called fast approximation (FAS), or a different method that results in an algebraic linear system that is symmetric and positive definite (SPD). This gives us the flexibility to tap into the vast literature of established fast iterative and direct solvers for SPD systems such as *preconditioned conjugate gradient* (PCG) and sparse versions of Cholesky factorization.

4.2 Derivation of the Weak Formulation and the Corresponding Spatial SIP-DG Formulation

Let $u \in L^2(0,T;H^4(\Omega)) \subset L^2(0,T;E_h))$, $E_h = H^4(\mathcal{T}_h)$, such that u satisfies **(Pv1)** and $v \in E_h$ a test function, then by multiplying the PDE equation in **(Pv1)** by v and integrating over Ω we have the following,

$$(u_t, v) + \epsilon(\triangle^2 u, v) - \frac{1}{\epsilon}(\triangle f(u), v) = (S_\epsilon(u), v), \quad \text{in } \Omega_T \tag{4.2}$$

We observe that the formulation **(Pv1)** has the same type of boundary conditions with the BVP (3.41) that we have studied in chapter 3 and thus using the consistency equation (3.43) with homogeneous boundary conditions we have for the second term in the left hand side above,

$$\epsilon(\triangle^2 u, v) = \epsilon\beta_h(u, v), \ \forall\ v \in E_h. \tag{4.3}$$

To finish the spatial discretization of **(Pv1)** we rewrite the non linear term, $(\triangle f(u), v)$, as follows (cf. [27]).

$$\begin{aligned} N_h(u,v) &:= \sum_{k\in\mathcal{T}_h} (-\triangle f(u), v)_k, \\ &= \sum_{k\in\mathcal{T}_h} \big((\nabla f(u), \nabla v)_K - \langle f'(u)\partial_n u, v\rangle_{\partial K}\big), \\ &= -\sum_{k\in\mathcal{T}_h} (f(u), \triangle v)_K + \sum_{k\in\mathcal{T}_h} \big(\langle f(u), \partial_n v\rangle_{\partial K} - \langle f'(u)\partial_n u, v\rangle_{\partial K}\big). \end{aligned}$$

Now as is common practice in DG formulations, we rewrite the sum over the cell boundary integrals, in the equation describing $N_h(\cdot,\cdot)$ above, as a sum over the cell edges,

$$\begin{aligned} N_h(u,v) &= -\sum_{k\in\mathcal{T}_h} (f(u), \triangle v)_K + \sum_{e\in\mathcal{E}} \big(\langle f(\{u\}), [\partial_n v]\rangle_e - \langle f'(\{u\})\{\partial_n u\}, [v]\rangle_e\big), \\ &= -\sum_{k\in\mathcal{T}_h} (f(u), \triangle v)_K + \sum_{e\in\mathcal{E}} \langle f(\{u\}), [\partial_n v]\rangle_e - \sum_{e\in\mathcal{E}^I} \langle f'(\{u\})\{\partial_n u\}, [v]\rangle_e \\ &- \sum_{e\in\mathcal{E}^B} \langle f'(\{u\})\partial_n u, v\rangle_e. \end{aligned}$$

Since we have homogeneous boundary conditions, $\partial_n u|_e = 0,\ e \in \mathcal{E}^B$, we can omit the last sum above, taken over the boundary edges. Therefore the non linear form

$N_h(\cdot,\cdot)$ is given by,

$$\begin{aligned} N_h(u,v) &= -\sum_{k\in\mathcal{T}_h}(f(u),\triangle v)_K \\ &+ \sum_{e\in\mathcal{E}}\langle f(\{u\}),[\partial_n v]\rangle_e - \sum_{e\in\mathcal{E}^I}\langle f'(\{u\})\{\partial_n u\},[v]\rangle_e,\ \forall\ v\in E_h. \end{aligned} \tag{4.4}$$

Hence from (4.4) and (4.3) we get the following weak formulation for **(Pv1)**. Find $u\in L^2(0,T;E_h)$ such that,

$$\begin{aligned} (u_t,v)+\epsilon\beta_h(u,v)+\frac{1}{\epsilon}N_h(u,v) &= F(u,v) := (S_\epsilon(u),v),\ \forall\ v\in E_h, \\ (u(\cdot,0),v) &= (u_0,v),\ \forall\ v\in E_h. \end{aligned} \tag{4.5}$$

Thus (4.5) implies the following semi-discrete or continuous in time SIP-DG formulation of **(Pv1)**. Find $u_h\in V_t^h := L^2(0,T;V^h)$ such that,

$$\begin{aligned} ((u_h)_t,v_h)+\epsilon\beta_h(u_h,v_h)+\frac{1}{\epsilon}N_h(u_h,v_h) &= F(u_h,v_h),\ \forall\ v_h\in V^h, \\ (u_h(\cdot,0),v)=(u_0,v) &= (\Pi_h u_0,v),\ \forall\ v\in V^h. \end{aligned} \tag{4.6}$$

4.3 Formulation of the Fully Discrete Adaptive Mesh SIP-DG Method for the Tumor Model

In order to formulate correctly the formulation 4.6 in a spatially adaptive fully discrete setting, we will need the following notation and some useful results that are natural extensions of the ones mentioned in section 3.2 of chapter 3 for elliptic problems.

4.3.1 Notation-results

Let $I_n := (t_{n-1}, t_n],\ n = 1, \ldots, n_{max}$ be a partition of $[0, T]$ and $k_n := t_n - t_{n-1}$. For each I_n, $n = 1, \ldots, n_{max}$, let $\mathcal{T}_h^n$ be a partition of Ω as defined in section 3.2 and let V_n^h denote the finite element space associated with the partition $\mathcal{T}_h^n$.

At certain times t_n the spatial mesh may be changed (possibly several times) via a process of refinement and coarsening based on the inverse inequality marking strategy discussed in section 3.5, Alg. 2. Let m be the integer that indicates in which time step the resulting mesh, $\mathcal{T}_{h'}^m$, belongs to. The algorithmic design and implementation was governed by the following conditions impose on the process $\mathcal{T}_h^{n-1} \rightarrow \mathcal{T}_{h'}^m$, where $m = n$ or $(n-1)$ in this case.

(**M1**) A cell (the *father*) in $\mathcal{T}_h^{n-1}$ marked for refinement is cut into a number of cells (the *sons*). In our two dimensional implementations a triangle is subdivided into four similar triangles.

(**M2**) A cell in $\mathcal{T}_h^{n-1}$ marked for coarsening is removed from the mesh only if the remaining sons of its father are all marked for coarsening. Then all sons are removed from the mesh.

(**M3**) The action described in (**M2**) is performed only if at least one cell of $\mathcal{T}_h^{n-1}$ is guaranteed to be refined in the manner described in (**M1**).

(**M4**) The actions described in the previous conditions (**M1**), (**M2**) and (**M3**) are performed only if the resulting updated mesh $\mathcal{T}_{h'}^m$, will maintain the at most one hanging node per edge condition (*i.e. a whole edge of a cell belonging to the updated mesh can have a non empty intersection with at most two edges belonging to (two) different cells of the updated mesh*).

Supposing that a new mesh $\mathcal{T}_{h'}^m$ has been obtained from $\mathcal{T}_h^{n-1}$ by the process of refinement/coarsening described above, we shall need an operator that serves as a natural embedding operator from spaces defined on $\mathcal{T}_h^{n-1}$ to those defined on $\mathcal{T}_{h'}^m$.

We define $\Pi^m : L^2(\mathcal{T}_h^{n-1}) \to L^2(\mathcal{T}_{h'}^m)$ as follows: Let $v \in L^2(\mathcal{T}_h^{n-1})$ and let $K \in \mathcal{T}_{h'}^m$; then the restriction $\Pi^m v|_K$ of $\Pi^m v$ to K is given by:

(1) If K also belongs to $\mathcal{T}_h^{n-1}$, then $\Pi^m v|_K = v|_K$.

(2) If K is the son of an element in $\mathcal{T}_h^{n-1}$, then $\Pi^m v|_K = I_K v$.

(3) If K is obtained by the merger of its sons that belonged to $\mathcal{T}_h^{n-1}$, then $\Pi^m v|_K = \Pi_K v$.

We first note that Π^m is defined as a local operator and we let Π_K^m denote the restriction of Π^m to K. Moreover, Π^m is the interpolation operator on the part of $\mathcal{T}_{h'}^m$ obtained from $\mathcal{T}_h^{n-1}$ by refinement, the identity operator on part of $\mathcal{T}_{h'}^m$ remained unchanged and the L^2 projection operator on the part of $\mathcal{T}_{h'}^m$ which has been obtained from $\mathcal{T}_h^{n-1}$ by coarsening.

The operator Π^m has good approximation properties. Indeed, it follows from (3.8), Lemma 3.0.5 and properties (1)-(3) above that,

$$|\phi - \Pi_K^m \phi|_{j,K} \leq c h_K^{q+1-j} |\phi|_{q+1,K} \quad \forall \phi \in H^s(\mathcal{T}_h^m),\ s \geq 0, \quad 0 \leq j \leq q+1 \leq s,$$

where $K \in \mathcal{T}_h^m$.

4.3.2 Fully Implicit Scheme

We choose the implicit Euler scheme for the time discretization of our SIP-DG formulation (4.6) in a *spatially adaptive* setting, using the inverse inequality marking strategy described in section 3.5. Also we make the assumption that k_n is the same on each time step. Our fully discrete formulation **(FDPv1)** is,
find $u_h^n \in V_n^h$, for $n = 1 \ldots n_{max}$, such that,

$$\left(\frac{u_{h,aiter}^n - \Pi^n u_h^{n-1}}{k_n}, v_h\right) + \epsilon \beta_h^n(u_{h,aiter}^n, v_h) + \frac{1}{\epsilon} N_h^n(u_{h,aiter}^n, v_h) = F^n(u_{h,aiter}^n, v_h),\ \forall\ v_h \in V_n^h,$$
$$\text{for} \quad aiter = 0, \ldots, J,\ 0 \leq J \leq aiter_{max},$$

where *aiter* is the adaptive iteration index,

$$u^n_{h,aiter=0} = \begin{cases} \Pi^n u^{n-1}_h, & n = 1, \\ 2\Pi^n u^{n-1}_h - (\Pi^n)(\Pi^{n-1}_h)u^{n-2}_h, & n \geq 2, \end{cases}$$

and

$$u^0_h = \Pi^0 u_0 := \Pi_h u_0.$$

4.3.3 Treatment of the Nonlinear Term

We have used two approaches in order to tackle the nonlinearity in our formulation **(FDPv1)**. First a linearization method and second a nonlinear approach by using non linear multigrid techniques. We next explain those methods.

First Approach

We employ an implicit-explicit iteration scheme in order to deal with the non linearity coming from N_h and F. The advantages of this approach is that it allows us to use a variety of linear system solvers tailored to a SPD system such as PCG and a sparse Cholesky factorization. Thus **(FDPv1)** becomes: **(LFDPv1)** find $u^n_h \in V^h_n$, for $n = 1 \dots n_{max}$, such that,

$$\begin{aligned} \Big(\frac{u^n_{h,aiter\,(l+1)} - \Pi^n u^{n-1}_h}{k_n}, v_h\Big) \quad &+ \quad \epsilon\beta^n_h(u^n_{h,aiter\,(l+1)}, v_h), \\ &+ \quad \frac{1}{\epsilon} N^n_h(u^n_{h,aiter\,(l)}, v_h) = F^n(u^n_{h,aiter\,(l)}, v_h),\ \forall\ v_h \in V^h_n, \\ \text{for} \quad & aiter = 0, \dots, J,\ 0 \leq J \leq aiter_{max}, \\ \text{and for} \quad & l = 0 \dots L-1,\ L \geq 1, \end{aligned}$$

where

$$u^n_{h,aiter=0\,(l=0)} = \begin{cases} \Pi^n u^{n-1}_h, & n = 1, \\ 2\Pi^n u^{n-1}_h - (\Pi^n)(\Pi^{n-1}_h)u^{n-2}_h, & n \geq 2, \end{cases}$$

and

$$u_h^0 = \Pi^0 u_0 = \Pi_h u_0.$$

We proceed now to perform the appropriate linearization and algebraic linear system formulation of **(LFDPv1)**. First we rewrite the first equation in **(LFDPv1)** by moving all the terms not containing $l+1$ to the right part of the equality. Thus we have,

$$\begin{aligned}(u^n_{h,aiter_{(l+1)}}, v_h) + \epsilon k_n \beta^n_h (u^n_{h,aiter_{(l+1)}}, v_h) &= (\Pi^n_h u^{n-1}_h, v_h) + k_n [F^n(u^n_{h,aiter_{(l)}}, v_h), \\ &- \frac{1}{\epsilon} N^n_h (u^n_{h,aiter_{(l)}}, v_h)].\end{aligned}$$

Let M^n_K be the total number of cells K in the mesh $\mathcal{T}^n_h$ then the total number of degrees of freedom in the mesh is $M := m(q) M^n_K$. We express the unknown function u^n_h as a linear combination of the local/global basis function by $u^n_h = \sum_{K\in\mathcal{T}_h} \sum_{j=0}^{m(q)-1} u^{(j)}_K v_{j,K} = \sum_{\nu=0}^{M-1} u^{(\nu)} v_\nu$, where $u^{(j)}_K = u^{(\nu)}$ are the unknown coefficients. By substituting u^n_h with its linear combination, choosing $v_h = v_\vartheta = v_{i,K'}$, for some $0 \le \vartheta \le M-1$, $0 \le i \le m(q)-1$, $K' \in \mathcal{T}^n_h$, and using the properties of the Lagrange basis functions described in section 3.2 in the above equation we have the following algebraic formulation of **(LFDPv1)**: **(LAPv1)** find $\vec{U}^n \in R^M$, for $n = 1 \dots n_{max}$, such that,

$$\begin{aligned}(G^n_{aiter} + \epsilon k_n S^n_{aiter}) \vec{U}^n_{aiter_{(l+1)}} &= G^n_{aiter} P^n \vec{U}^{n-1} + k_n \overrightarrow{NL}(u^n_{h,aiter_{(l)}}), \\ \text{for } \ aiter &= 0, \dots, J, \ 0 \le J \le aiter_{max}, \\ \text{and for } \ l &= 0 \dots L-1, \ L \ge 1,\end{aligned}$$

where

$$\vec{U}^n_{aiter=0_{(l=0)}} = \begin{cases} P^n \vec{U}^{n-1}, & n = 1, \\ 2P^n \vec{U}^{n-1} - (P^n)(P^{n-1}) \vec{U}^{n-2}, & n \ge 2, \end{cases}$$

and

$$\vec{U}^0 = \vec{U}_0.$$

In the formulation **(LAPv1)** we have for $\vartheta, \nu = 0, \cdots, M-1$, G^n: is the grammian matrix, $(G^n)_{\vartheta,\nu} := (v_\nu, v_\vartheta)$, S^n: is the stiffness matrix, $(S^n)_{\vartheta,\nu} := \beta_h^n(v_\nu, v_\vartheta)$, $\vec{U}$: is the coefficient vector, $(\vec{U})_\nu := u^{(\nu)}$, $\overrightarrow{NL}$: is the vector corresponding to the nonlinear terms, $(\overrightarrow{NL}(u_h^n))_\nu := F^n(u_h^n, v_\nu) - \frac{1}{\epsilon}N_h^n(u_h^n, v_\nu)$, $(P^n)^T$: is the matrix corresponding to the operator Π^n and $(\vec{U_0})_\nu := (u_0, v_\nu)$ is the initial condition vector.

We observe that the linear system matrix $G^n + \epsilon k_n S^n$ is SPD, since is the sum of the SPD matrix G^n and the semi-SPD matrix $\epsilon k_n S^n$, hence in solving the linear system **(LAPv1)** we have used PCG with linear V-cycle multigrid as a preconditioner, and a sparse version of Cholesky solver (cf. [19]). The implementation of the formulation in **(LFDPv1)** or **(LAPv1)** is described in algorithm 4.

Note. For the PCG linear system solver being described by algorithm 3 and used in algorithm 4 for the solution of the resulting linear systems, we have used as a preconditioner, M_{prec}, the linear version of the multigrid algorithm described and used as a solver in the context of the second approach to the non linearity presented next.

Second Approach

Since we have a non linear IBVP it makes sense to try to solve it by using a non linear scheme in order to deal with the non linearity coming from N_h and F. The advantages of this approach is that it allows us to use a non linear solver such as the well proven non linear multigrid method. For this approach we move the terms that contain the unknown function u_h^n and that is $\vec{U}^n$, to the left side of the equality in

Algorithm 3 PCG for solving $A\vec{V} = \vec{b}$, $\vec{V} \leftarrow PCG(\vec{V}^0)$

Require: Iteration matrix $A := G^n + \epsilon k_n S^n$, right hand side $\vec{b}$, initial guess $\vec{V}^0$;

$\vec{V} \leftarrow \vec{V}^{(0)}$;
$\vec{r} \leftarrow \vec{b} - A\vec{V}$;
for $1 \leq iter \leq iter_{max}$ **do**
  $\vec{z} \leftarrow (M_{prec})^{-1}\vec{r}$ (using linear multigrid);
  $\rho_1 = \vec{r} \cdot \vec{r}$, $\rho_{z1} = \vec{z} \cdot \vec{r}$, $err = (\rho_1/M)^2$;
  if $err < tolerance$ **then**
    $break$;
  end if
  if $iter = 1$ **then**
    $\vec{p} \leftarrow \vec{z}$
  else
    $\beta = \rho_{z1}/\rho_{z2}$, $\vec{p} = \beta\vec{p} + \vec{z}$;
  end if
  $\vec{q} \leftarrow A\vec{p}$, $d = \vec{p} \cdot \vec{q}$;
  if $d \neq 0$ **then**
    $\alpha = \rho_{z1}/d$;
  end if
  $\vec{V} \leftarrow \alpha\vec{p} + \vec{V}$, $\vec{r} \leftarrow \vec{r} - A\vec{q}$, $\rho_{z2} = \rho_{z1}$;
end for

Algorithm 4 Adaptive algorithm for the implementation of **(LAPv1)**.

Start with an initial coarse mesh $\mathcal{T}_h^0$;
for $aiter = 0, \ldots, max_{aiter}$ **do**
  $\vec{U}^0 \leftarrow \vec{U}_0$ on $\mathcal{T}_h^0$;
  Mark for refinement and generate refinement list $\mathcal{T}_R$ as in algorithm 2;
  if $\mathcal{T}_R = NULL$ **then**
    $break$;
  else
    Perform refinement as in algorithm 2 and update $\mathcal{T}_h^0$;
  end if
end for
for $n = 1, \ldots, n_{max}$ **do**
  if $n = 1$ **then**
    $\vec{U}^n_{(l=0)} \leftarrow P^n \vec{U}^{n-1}$;
  else
    $\vec{U}^n_{(l=0)} \leftarrow 2P^n \vec{U}^{n-1} - (P^n)(P^{n-1})\vec{U}^{n-2}$;
  end if
  for $l = 0, \ldots, L-1$ **do**
    $\vec{U}^n_{(l+1)} \leftarrow (G^n + \epsilon k_n S^n)^{-1}\Big(G^n P^n \vec{U}^{n-1} + k_n \overrightarrow{NL}(u^n_{h(l)})\Big)$;
  end for
  for $aiter = 1, \ldots, max_{aiter}$ **do**
    Mark for refinement/coarsening and generate $\mathcal{T}_{R,marked}$ as in algorithm 2;
    if $\mathcal{T}_{R,marked} = NULL$ **then**
      $break$;
    else
      Generate $\mathcal{T}_{C,marked}$ as in algorithm 2;
      Coarsen the triangles in $\mathcal{T}_{C,marked}$ and refine
      the triangles in $\mathcal{T}_{R,marked}$ to get an updated $\mathcal{T}_h^n$;
      for $l = 0, \ldots, L-1$ **do**
        $\vec{U}^n_{aiter_{(l+1)}} \leftarrow (G^n_{aiter} + \epsilon k_n S^n_{aiter})^{-1}\Big(G^n_{aiter} P^n \vec{U}^{n-1} + k_n \overrightarrow{NL}(\Pi^n u^n_{h,aiter_{(l)}})\Big)$;
      end for
    end if
  end for
end for

the first equation of the formulation **(FDPv1)**. Hence we have,

$$\begin{aligned}(u^n_{h,aiter}, v_h) &+ \epsilon k_n \beta^n_h (u^n_{h,aiter}, v_h) \\ &- k_n[F^n(u^n_{h,aiter}, v_h) - \frac{1}{\epsilon} N^n_h(u^n_{h,aiter}, v_h)] \\ &= (\Pi^n_h u^{n-1}_h, v_h).\end{aligned}$$

Now by working as before and by defining a nonlinear operator $Q : V^n_h \to R^M$ as

$$Q(u^n_h) := (G^n + \epsilon k_n S^n)\vec{U}^n - k_n \overrightarrow{NL}(u^n_h)$$

we can write the above equation and thus the second method for the solution of **(FDPv1)** in the following algebraic formulation: **(NLAPv1)** find $\vec{U}^n \in R^M$ such that,

$$\begin{aligned}Q(u^n_{h,aiter}) &= \vec{s}_h := G^n_{aiter} P^n \vec{U}^{n-1}, \\ \text{for} \quad aiter &= 0, \ldots, J, \ 0 \leq J \leq aiter_{max},\end{aligned}$$

where

$$\vec{U}^n_{aiter=0} = \begin{cases} P^n \vec{U}^{n-1}, & n = 1, \\ 2P^n \vec{U}^{n-1} - (P^n)(P^{n-1})\vec{U}^{n-2}, & n \geq 2, \end{cases}$$

and

$$\vec{U}^0 = \vec{U}_0.$$

The implementation of **(NLAPv1)** is given by the algorithm 5.

Algorithm 5 Adaptive algorithm for the implementation of **(NLAPv1)**.

Start with an initial coarse mesh $\mathcal{T}_h^0$;
for $aiter = 0, \ldots, max_{aiter}$ **do**
  $\vec{U}^0 \leftarrow \vec{U}_0$ on $\mathcal{T}_h^0$;
  Mark for refinement and generate refinement list $\mathcal{T}_R$ as in algorithm 2;
  if $\mathcal{T}_R = NULL$ **then**
    $break$;
  else
    Perform refinement as in algorithm 2 and update $\mathcal{T}_h^0$;
  end if
end for
for $n = 1, \ldots, n_{max}$ **do**
  if $n = 1$ **then**
    $\vec{U}^n \leftarrow P^n \vec{U}^{n-1}$;
  else
    $\vec{U}^n \leftarrow 2P^n \vec{U}^{n-1} - (P^n)(P^{n-1})\vec{U}^{n-2}$;
  end if
  $\vec{U}^n \leftarrow Q(u_h^n)^{-1}\Big(G^n P^n \vec{U}^{n-1}\Big)$;
  for $aiter = 1, \ldots, max_{aiter}$ **do**
    Mark for refinement/coarsening and generate $\mathcal{T}_{R,marked}$ as in algorithm 2;
    if $\mathcal{T}_{R,marked} = NULL$ **then**
      $break$;
    else
      Generate $\mathcal{T}_{C,marked}$ as in algorithm 2;
      Coarsen the triangles in $\mathcal{T}_{C,marked}$ and refine
      the triangles in $\mathcal{T}_{R,marked}$ to get an updated $\mathcal{T}_h^n$;
      $\vec{U}^n_{aiter} \leftarrow Q(\Pi^n u^n_{h,aiter})^{-1}\Big(G^n_{aiter} P^n \vec{U}^{n-1}_{aiter}\Big)$;
    end if
  end for
end for

As we mentioned already the solution of the resulting nonlinear system above, thus the inversion of the non linear operator Q, is performed by using a non linear multigrid solver.

The idea of using multigrid methods for the CH equation can be traced to [35], where they used a non-adaptive finite difference space discretization. Kay and Welford extended the idea to the mixed Continuous Galerkin FE setting in [33] with adaptivity. To our knowledge, no one has looked at such an algorithm in the DG-FE setting, and therefore, there are many open theoretical and practical questions.

Before we introduce the algorithms for the multigrid solver we define some preliminary ideas needed when describing multigrid. We assume that there is a preexisting hierarchical mesh $\mathcal{T}_h$ on which the solution is to be obtained. The hierarchical mesh occurs naturally in the context of adaptivity by considering the partition of the finest mesh $\mathcal{T}_h$ into a hierarchy of meshes that their union is equal to $\mathcal{T}_h$. We have used several ways to partition our mesh. Each way was proven useful in implementing our methods. To define some of these partitions first we need to introduce the idea of level. For a nonnegative integer l if a cell $K \in \mathcal{T}_h$ can be obtained by l regular refinements, as described in (**M1**), of its level zero ancestor cell $K_{ancestor}$, that is the one belonging to the initial mesh $\mathcal{T}_0 := \mathcal{T}_H$, then we say that the cell $K \in \mathcal{T}_h$ is of $level = l$. Analogously we say that a mesh $\mathcal{T}_h$ has level depth $l \geq 0$, if its highest $level$ cell is of level l. Hence we say that our finest mesh $\mathcal{T}_h$ can be denoted as $\mathcal{T}_{L_{max}}$, where L_{max} is the level of its highest level cell. Also another useful idea needed here is the idea of a leaf cell. We will call every cell $K \in \mathcal{T}_{L_{max}} (= \mathcal{T}_h)$ a leaf cell. It is useful to make the following correspondence between the leaf mesh $\mathcal{T}_h$ and the tree structure $\mathbb{T}$ which represents all the cells in $\mathcal{T}_h$ and additionally all of their previous levels ancestors. (i.e. for a specific leaf cell K its ancestors are all the cells that were used to create it by undergoing regular refinement, starting from its level zero ancestor). Therefore we can define the following hierarchy of meshes used in our multigrid algorithm, $\{\mathcal{T}_l\}_{l=0}^{l=L_{max}}$, where $\mathcal{T}_l := \{K \in \mathbb{T} |$ level $K = l,$ or level $K \leq l,$ and K is a leaf$\}$. It will suffice to

consider the two-grid algorithm first, as the extension to *multi*-grid can be obtained by recursion. We consider a coarse mesh $\mathcal{T}_0 = \mathcal{T}_H$ and a fine mesh $\mathcal{T}_{L_{max}=1} = \mathcal{T}_h$, where the fine mesh is obtained by (regular) refinement of certain triangles of the coarse mesh. We will adapt our notation established before so a subscript or superscript H, h will mean that the quantity under consideration is related to $\mathcal{T}_H$, $\mathcal{T}_h$ respectively. Subordinate to the triangulations are the respective DG-FE spaces V^H and V^h, where we have the nesting $V^H \subset V^h$. Now, we let $B_h = \{u_{h,i}\}_{i=1}^{M_h}$ be the (global) Lagrange nodal basis for V^h. Suppose B_H is defined similarly. Naturally, the basis functions corresponding to elements that are in both triangulations are identical. Since $V^H \subset V^h$, there are constants $p_{i,j}$ such that $u_{H,i} = \sum_{j=1}^{M_h} p_{i,j} u_{h,j}$, $1 \leq i \leq M_H$. We define the prolongation (or subspace embedding) matrix as $\mathsf{P} = \left[p_{i,j}\right]$. The restriction matrix is defined as $\mathsf{R} := \mathsf{P}^T$. One nice feature about the DG-FE setting is that these matrices can be defined entirely locally on each element, by restricting them to the local basis of each element. Lastly, we define $\hat{\mathsf{R}}$ to be the L^2 projection matrix relative to the bases B_h and B_H. Once again, $\hat{\mathsf{R}}$ is completely local to the respective elements.

The following two-grid method is an iterative solver based on the full approximation scheme (FAS) version of multigrid (cf. [39]).

Algorithm 6 FAS, two-grid V-cycle: $\vec{U}_h^{new} \leftarrow FAS(\vec{U}_h^{old})$

1: Pre-smoothing: $\vec{U}_h \leftarrow BCSS(\vec{U}_h^{old})$;
2: Residual: $\vec{r}_h \leftarrow \vec{s}_h - Q(u_h)$;
3: Coarse-level (full) approximation: $\vec{U}_H \leftarrow \hat{\mathsf{R}}\vec{U}_h$;
4: Coarse-level right-hand-side: $\vec{s}_H \leftarrow \mathsf{R}\vec{r}_h + Q\left(u_H\right)$;
5: Coarse-level update: $\vec{U}_H^{new} \leftarrow Q\left(u_H\right)^{-1}\left(\vec{s}_H\right)$;
6: Coarse-grid correction: $\vec{e}_H \leftarrow \vec{U}_H^{new} - \vec{U}_H$;
7: Fine-level update: $\hat{\vec{U}}_h \leftarrow \vec{U}_h + \mathsf{P}\vec{e}_H$;
8: Post-smoothing: $\vec{U}_h^{new} \leftarrow BCSS\left(\hat{\vec{U}}_h\right)$;

We extend this algorithm to make it truly "multi-grid" by replacing step 5 with a recursive application of the same algorithm. It is also worth mentioning that the

algorithm 6, for the case of linear $Q(u_h)$, is equivalent to the usual two-level linear multigrid algorithm which we have used to precondition our PCG solver in the context of the algorithm 4.

For the smoothing routine of the non linear multigrid solver described in algorithm 6, we have utilized a block Gauss-Seidel smoother (BGSS). To show how we have implemented the smoothing part we rewrite the nonlinear equation of the formulation **(NLAPv1)** as,

$$(G^n + \epsilon k_n S^n)\vec{U}^n_{(siter+1)} = G^n P^n \vec{U}^{n-1} + k_n \overrightarrow{NL}(u^n_{h,(siter)}), \tag{4.7}$$

where $siter = 0, \ldots, siter_{max} - 1$ are the smoothing iterations performed in this way only for the highest level mesh. Here $siter_{max}$ is the maximum number of smoothing iterations, $siter$, performed at L_{max}. In a way we can say that at the finest mesh $\mathcal{T}_h$ we are using the smoothing iterations $siter$ to perform an implicit explicit iteration within our smoother for the solution of the non linear equation (4.7).

Another important issue regarding the implementation of the smoothing strategy in algorithm 7 is the total number of smoothing iterations per level, $tot_{siter}(l)$. There are several papers written about the implementation of V-cycle (mostly linear version) for solution of systems resulting from the discretization of variational problems (cf. [14] and references there in). The issue here is that for fourth order formulations like in our case, the standard V-cycle with constant smoothing, i.e the same number of smoothing iterations are performed across all levels $l \in \{0, \ldots, L_{max}\}$, might produce solvers with unsatisfactory convergence [12, 10] rate and we observed that in our case might be even divergent. Hence we have implemented for our linear and non-linear multigrid algorithms the so called *variable* V-cycle [38, 10]. This is performed by increasing the total number of smoothing iterations, in lower levels. We have used $tot_{siter}(l) = (siter_{max})^{(L_{max}-l+1)}$, for $l = 1, \ldots, L_{max}$, to establish the appropriate number of smoothing iterations per level l. We present the smoothing procedure in the following algorithm.

Algorithm 7 BGSS, $\vec{V} \leftarrow BGSS(\vec{U}^{old}_{h,l})$

Require: $siter_{max}$, $level = l, \mathcal{T}_l, \vec{U}^{old}_{h,l}$;

Require: Iteration matrix $A_l := G^n_l + \epsilon k_n S^n_l$ and right hand side vector $\vec{b}_l$;

1: $\vec{V}^{(0)} \leftarrow \vec{U}^{old}_{h,l}$;
2: Smoothing cycles:
3: **for** $siter \leq tot_{siter}(l) - 1$ **do**
4: **for** $K \in \mathcal{T}_l$ **do**
5: $\vec{V}^{(siter+1)}_{K_i} \leftarrow A^{-1}_{K_i,K_i}\Big(\vec{b}_{K_i} - \sum_{j<i} A_{K_i,K_j}\vec{V}^{(siter)}_{K_j} - \sum_{j>i} A_{K_i,K_j}\vec{V}^{(siter+1)}_{K_j}\Big)$;
6: **end for**
7: Updating right hand side vector at max level:
8: **if** $l = L_{max}$ **then**
9: $v_{h,(siter+1)} \leftarrow \vec{V}^{(siter+1)}$;
10: $\vec{b} \leftarrow G^n P^n \vec{U}^{n-1} + k_n \overrightarrow{NL}(v_{h,(siter+1)})$;
11: **end if**
12: **end for**

Remark. In algorithm 7 we are updating the the vector $\vec{U}^{old}_{h,l}$ on a cell by cell basis, i.e $\vec{U}^{old}_{h,l}|_K$ is the portion of the unknown global vector corresponding to cell K. This is a very convenient feature of DG-FE methods and is due to the local nature of the the corresponding basis functions. In our algorithmic implementations we have tried to exploit this fact by treating all the quantities as being local.

4.4 Numerical Experiments

4.4.1 L^2-convergence

We have used cubic elements to establish the rate of convergence of our numerical schemes. Both the linearized version **(LAPv1)** and the non linear formulation **(NLAPv1)** gave the same L^2-error reduction for our test problem having exact solution, $u(x, y, t) = x^2(1. - x)^2y^2(1. - y)^2\cos(t)$. The results of our L^2-convergence test are summarized in the table 4.1. We have recorded the L^2-error against the uniform mesh step size parameter, h, obtained by subdividing the initial value of $h = 1/25$ for each subsequent run and setting the time step size Δt to be equal to h

and h^2 respectively (cf. table 4.1). By taking the base two logarithm of the ratio of two consecutive error values we are calculating the rate of convergence for each case (cf. table 4.1).

L^2-convergence Test on $\Omega_T = \Omega \times (0,T)$				
Test function: $u(x,y,t) = x^2(1.-x)^2y^2(1.-y)^2\cos(t)$;				
$T = 1.5$	$\Delta t = h^2$		$\Delta t = h$	
h	$\|\|u(\cdot,T) - u_h\|\|_\Omega$	rate	$\|\|u(\cdot,T) - u_h\|\|_\Omega$	rate
1/4	2.159576×10^{-05}	$--$	7.861590×10^{-05}	$--$
1/8	5.491616×10^{-06}	1.97545	4.206323×10^{-05}	0.90226
1/16	1.357806×10^{-06}	2.01595	2.157278×10^{-05}	0.96335
1/32	4.275466×10^{-07}	2.05151	1.083228×10^{-05}	0.99388
1/64	8.081954×10^{-08}	2.01892	5.412341×10^{-06}	1.00101

Table 4.1: *L^2-convergence test using cubic, $q = 3$, elements. The final time is $T = 1.5$, and the refinement paths are taken to be $\Delta t = h^2$ and $\Delta t = h$ respectively, where Δt is the constant time step. The other parameters are $\epsilon = 1.0, D = 1.0, \lambda_g = 1.0, \lambda_d = 1.0$; $\Omega = (0,1)^2$. The global error at T is expected to be $O(\Delta t) + O(h^{q-1})$, $q \geq 3$, and this is confirmed.*

The results of our experiments also are confirmed in Fig. 4.1a and Fig. 4.1b, where we plot in a log-log graph the logarithm of the L^2-error, for the two cases described before, together with a known function of slope one and two respectively against the logarithm of h. In these graphs we confirm again that the rate of convergence of our method is of order $O(\Delta t) + O(h^{q-1})$, $q \geq 3$. In the case of Cahn-Hilliard equation this result verifies the convergence rate proved by Feng and Karakashian in [27].

4.4.2 Adaptive Spinodal Decomposition Simulation

Spinodal decomposition is the procedure where we have separation of a mixture of two, or more, components into regions composed almost purely on each component. This phenomenon occurs when a high-temperature mixture of two, or more, alloys is

rapidly cooled. We model the separation of a binary mixture by switching off the non linear source term $S(u)$ in our model, *i.e.* setting λ_d and λ_g to be zero. Let $0 < \bar{u} < 1$ be a constant, and suppose ζ is a (sufficiently regular) mean-zero function of small amplitude, *i.e*, $\int_\Omega \zeta \, d\mathbf{x} = 0$ and $|\zeta(\mathbf{x})| \leq A \ll 1$, for all $\mathbf{x} \in \Omega$. We consider initial data of the form

$$u(\mathbf{x}, 0) =: u_0(\mathbf{x}) = \bar{u} + \zeta(\mathbf{x}) \quad \mathbf{x} \in \Omega \ ,$$

(cf. Fig. 4.3a). If $\bar{u} \in \{u \in R \mid F''(u) \leq 0\}$, called the chemical spinodal region, then the solution can evolve as depicted in Fig. 4.3.

Initially a very fine-scale structure, comprised of alternating layers of (nearly) pure phase regions, emerges Fig. 4.3b. Afterwards, certain of these pure phase regions grow, and some shrink, a process known as coarsening Fig. 4.3c–4.3f. Coarsening occurs on a very slow time scale. The whole phenomenon, rapid phase separation followed by slow coarsening is what materials scientists call spinodal decomposition and it will continue until the interface(s) develop a constant curvature.

In our spinodal decomposition simulation described in figure 4.3 we have superposed the solution with its corresponding adaptive mesh to demonstrate that the latter follows the evolution of the former. This becomes more apparent in Fig. 4.4a where we have superposed the final time solution Fig. 4.4b with its accompanied level six mesh Fig. 4.4c.

Note. We make sense of the final mesh being a six level mesh, by labeling as level one the initial adaptive mesh containing only twenty eight cells shown in figure 4.2.

We observe that just by looking at the adaptive mesh we can see the exact same shape of the corresponding solution. Also after superposing both of them (mesh and solution) we see that the mesh is refined more along the interface and is more coarse in regions that the solution is more flat. This is what we expect to happen in an adaptive setting and thus our algorithms perform as intended.

4.4.3 Adaptive Cancer Simulation

We perform the cancer simulation starting with an ellipse as an initial condition, Fig. 4.5a. The reason we have chosen an ellipse is just because we want to have a symmetric distribution of non constant curvature along its initial interfacial region. We first resolve the initial condition adaptively starting from the initial mesh shown in figure 4.2. This will have the effect of creating solution profiles closely resembling a cancerous tumor progression. On the other hand a choice of a circle for instance would create solutions that are expanding circles since the initial circular profile of the solution has constant curvature along the interface.

We observe that the choice of our growth and death coefficients has the effect of creating a cancerous tumor progression that possesses relatively thin interior regions. We remind the reader about the correlation of the growth and death parameter mentioned in Sec. 2.5.

As in the Cahn-Hilliard simulation, described previously, in our cancer model simulation – shown in figure 4.5 – we have superposed the solution with its corresponding adaptive mesh to demonstrate that the latter follows the evolution of the former. This becomes more apparent in Fig. 4.6a where we have superposed the final time solution Fig. 4.6b with its accompanied mesh Fig. 4.6c. We observe as before that just by looking at the adaptive mesh we can see the exact same shape of the corresponding solution. Also after we superpose both of them (mesh and solution) we see that the mesh is refined more along the interface and it is more coarse inside regions that the solution is more flat. Thus as with the spinodal decomposition case our adaptive routines perform as intended.

Finally for the cancer model simulation, which some selected time snapshots appear in figure 4.5, we have also plotted the number of leaf cells present in the adaptive mesh for a number of time steps (cf. Fig. 4.7). In this figure we observe substantial computational savings, since in order to achieve the same resolution with our six level adaptive mesh, by just using a fixed uniform mesh without adaptivity, we

must use exactly twenty eight thousand, six hundred and seventy two cells during the entire run of thirty five thousand and so time steps. Something that is very wasteful, because as we can observe from figure 4.7 the number of cells needed for our adaptive simulation is much smaller. Specifically the number of cells increases linearly from an initial number of around five hundred to a number of around five thousand cells close to the twentieth thousandth time step. Afterwards, due to our coarsening strategy the mesh gets coarsened and the number of cells drops to less than three thousand. From that point and on it slowly "climbs" again (linearly) to its final value of little more than seven thousand cells at the end of the simulation, generating a final mesh of level depth six.

4.4.4 Solver Test

To perform our timing test for comparison of our solvers, Sparse-Cholesky, FAS-multigrid and PCG, we use spinodal decomposition as a test case. We time the runs of the spinodal decomposition simulation, using our three solvers on three different constant uniform meshes (cf. Fig. 4.9). Those meshes are created by uniformly refining the initial triangulations (cf. Fig. 4.8) of the three test domains, $(0, 0.5)^2$, $(0, 1)^2$ and $(0, 2)^2$.

The dimensions of a cell belonging to anyone of the final test meshes in Fig. 4.9 are the same. Hence the only difference between the test meshes is the number of cells they contain, and their domain size. We have done this in order to keep the time test "fair", by having the same h and Δt dependence on the error for each mesh case. For the timing test of the Sparse-Cholesky and PCG solvers, we use the linearized formulation **(LAPv1)** and for the time test of the FAS-multigrid, we use the non linear formulation **(NLAPv1)**. For each case (*i.e.*, corresponding to each test mesh) we perform three runs, (for our spinodal decomposition test problem) paying attention to avoid "warming" of the cache (*i.e.* a phenomenon that occurs when running the same algorithm consecutively, resulting in speeding up and thus affecting the true

computational time), and taking the average of the three resulting computational times. The initial and final profile of the spinodal decomposition simulation for each case can be seen in Fig. 4.10 and the results of our test are presented in table 4.2.

Solver Timing Test Operating System (OS): FEDORA 14 (Laughlin) Kernel: Linux 2.6.35.13-92.f14.x86 64 Hardware: Processor: Intel(R) Core(TM)2 Duo CPU T9800 @2.93GHz Memory: 8GiB			
Spinodal Decomposition using quartic, $q = 4$, basis functions Parameters: $D = 1$, $\epsilon = 0.015$, $t_0 = 0$, $T = 0.005$, $n_{max} = 10000$, $\lambda_g = \lambda_d = 0$			
	Sparse Cholesky	Nonlinear Multigrid (FAS)	PCG
mesh 1 (512 cells) level depth 4:	1min 58.001sec	1min 35.393sec	1min 31.423sec
mesh 2 (2048 cells) level depth 5:	9min 24.116sec	7min 44.360sec	7min 23.718sec
mesh 3 (8192 cells) level depth 6:	45min 43.886sec	33min 45.438sec	31min 56.567sec

Table 4.2: *Solver timing test for comparison of our solvers, (direct solver) Sparse-Cholesky, (iterative solver) FAS-multigrid and (iterative solver) PCG. Here we have used the following parameters for our test case:* $D = 1$, $\epsilon = 0.015$, $t_0 = 0$, $T = 0.005$, $n_{max} = 10000$, $\lambda_g = \lambda_d = 0$

We observe that as the number of cells increases the iterative solvers, PCG and FAS-multigrid, perform better (*i.e.* faster) than the direct solver, Sparse-Cholesky. Also we must observe that the fastest solver in our test is, PCG, which we expected to be, but with not so much difference from our non linear multigrid solver.

Note. We want to mention here that for both of our iterative solvers, we have used the same $siter_{max} = 3$. That is, the same number of post and pre-smoothing iterations,

per smoothing step, are performed at maximum level and thus at any lower level following the variable V-cycle idea described before.

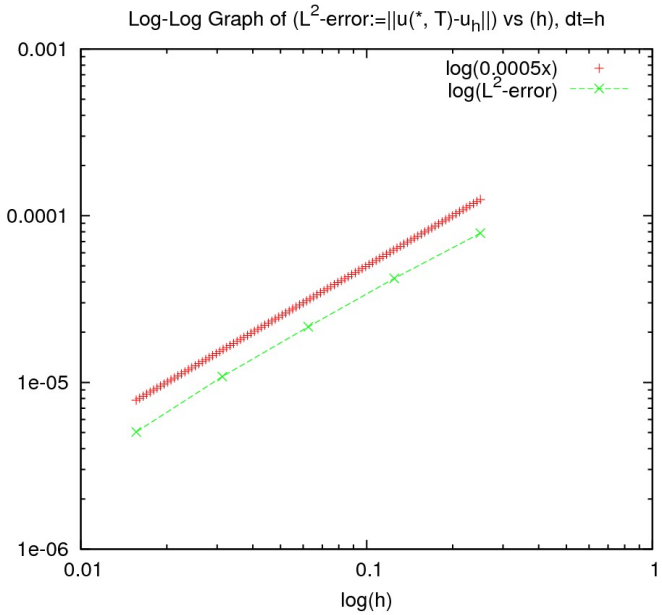

(a) L^2-error using $\Delta t = h$

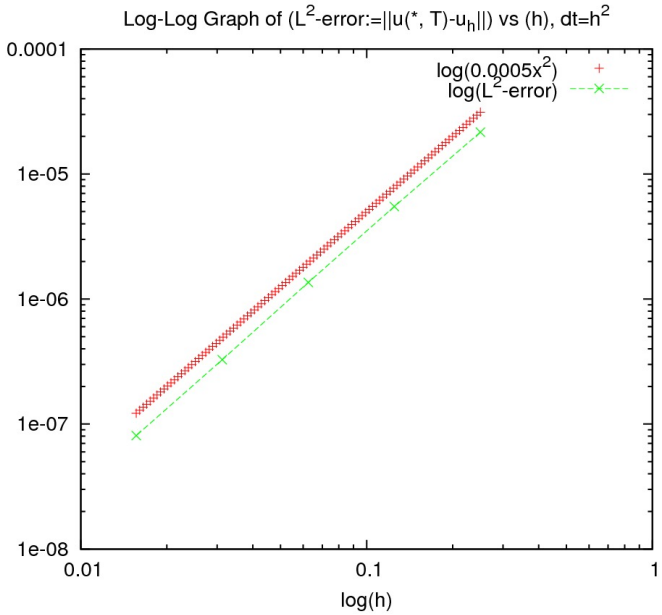

(b) L^2-error using $\Delta t = h^2$

Figure 4.1: *L^2-error convergence test plots using Table 4.1. In Fig. 4.1a, Fig. 4.1b we plot the logarithm of the L^2-error and a slope one, slope two, respectively logarithmic curve versus $log(h)$, where h is the uniform mesh spatial step size. We observe by comparing our error plots with the two known slope curves, that the log-log error plot has slope one whenever $\Delta t = h$ and slope two whenever $\Delta t = h^2$. This confirms that our method* **(FDPv1)** *is of first order as expected.*

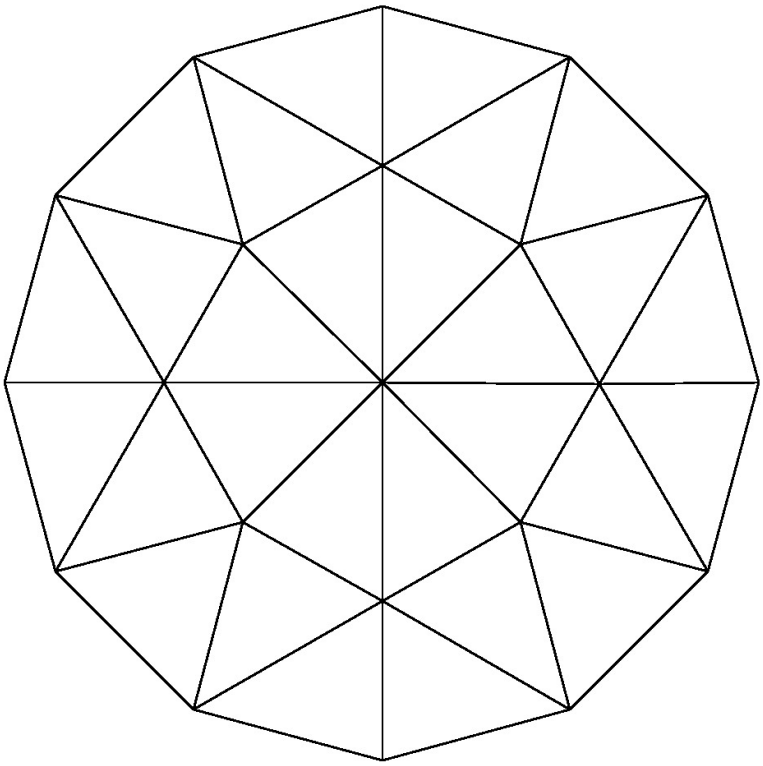

Figure 4.2: *Initial mesh used to generate the adaptive multilevel meshes for the simulations of spinodal decomposition and cancer growth.*

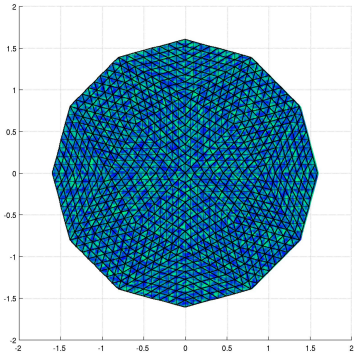

(a) N=0

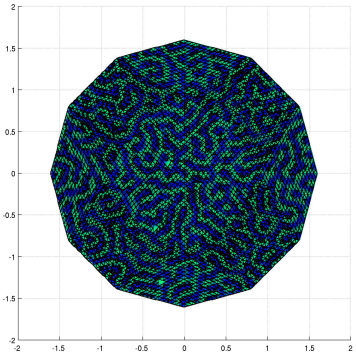

(b) N=500

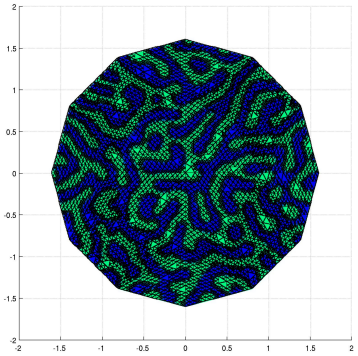

(c) N=3500

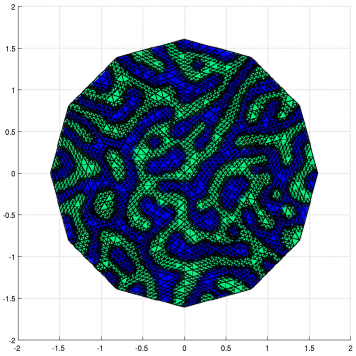

(d) N=7500

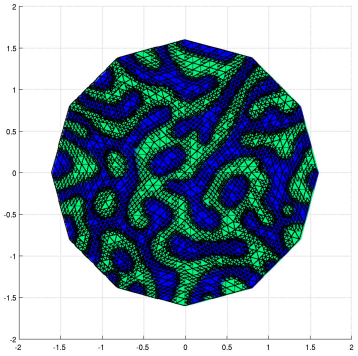

(e) N=11500

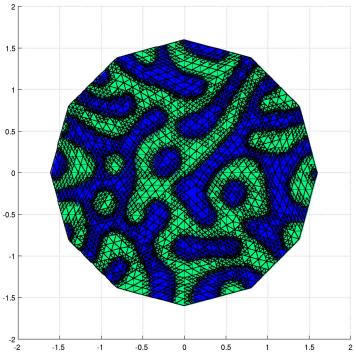

(f) N=22500

Figure 4.3: *Adaptive simulation snapshots with superposed corresponding adaptive mesh from the simulation of spinodal decomposition using model* **(Pv1)** *with* $t_0 = 0$, $T = 0.15$, $n_{max} = 22500$, $\epsilon = 0.015$, $D = 1$ *and* λ_g, λ_d *both equal to zero.*

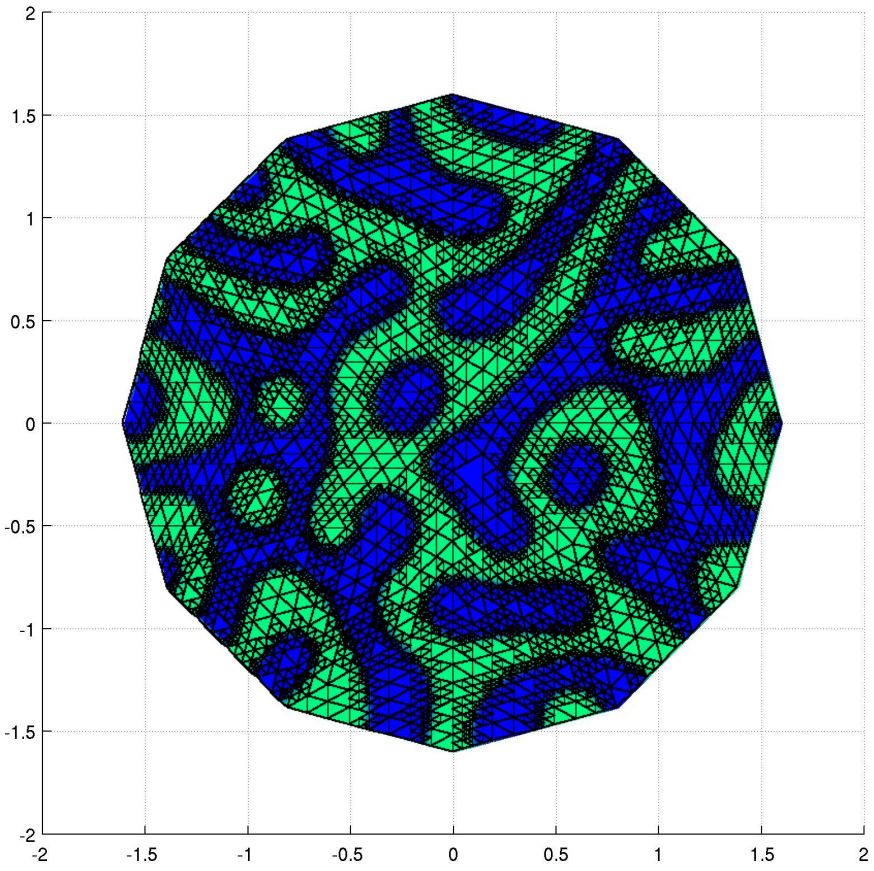

(a) Mesh superposed on solution

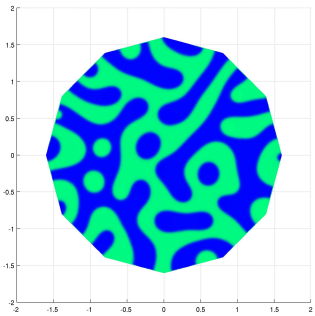

(b) Solution

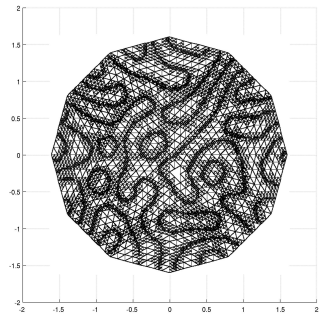

(c) Six level mesh

Figure 4.4: *Snapshot of the solution with the corresponding adaptive mesh from the spinodal decomposition simulation using* **(Pv1)** *and* $t_0 = 0$, $T = 0.15$, $n_{max} = 22500$, $\epsilon = 0.015$, $D = 1$ *and* λ_g, λ_d *both equal to zero. In Fig. 4.4a we superpose the solution Fig. 4.4b with the corresponding mesh Fig. 4.4c.*

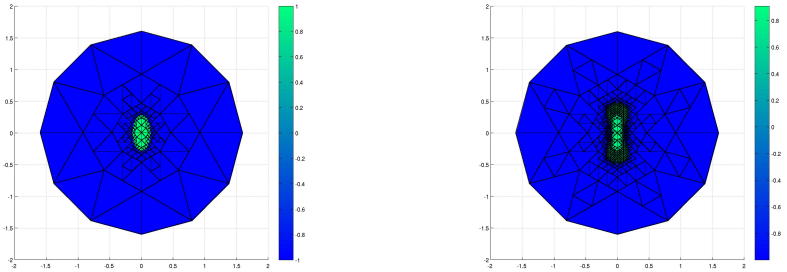

(a) N=0 **(b)** N=5328

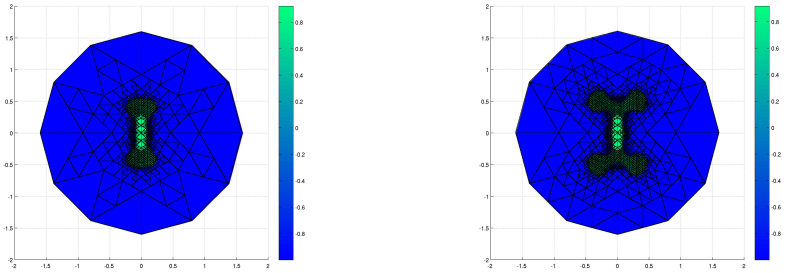

(c) N=9324 **(d)** N=15318

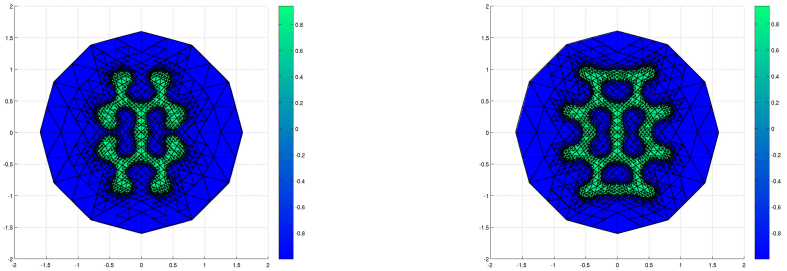

(e) N=23310 **(f)** N=27306

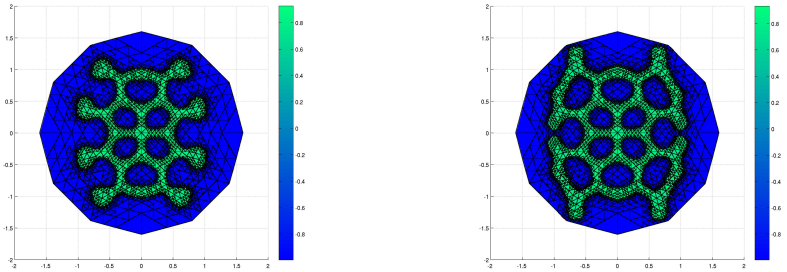

(g) N=31302 **(h)** N=35298

Figure 4.5: *Adaptive simulation snapshots with superposed corresponding adaptive mesh from the simulation of tumor growth using model* **(Pv1)**. *Green indicates a high density of tumor cells, while blue indicates a high density of healthy tissue cells. Here we have used* $t_0 = 0$, $T = 0.15$, $n_{max} = 40000$, $\epsilon = 0.0125$, $D = 0.25$, $\lambda_g = 70$ *and* $\lambda_d = 23$.

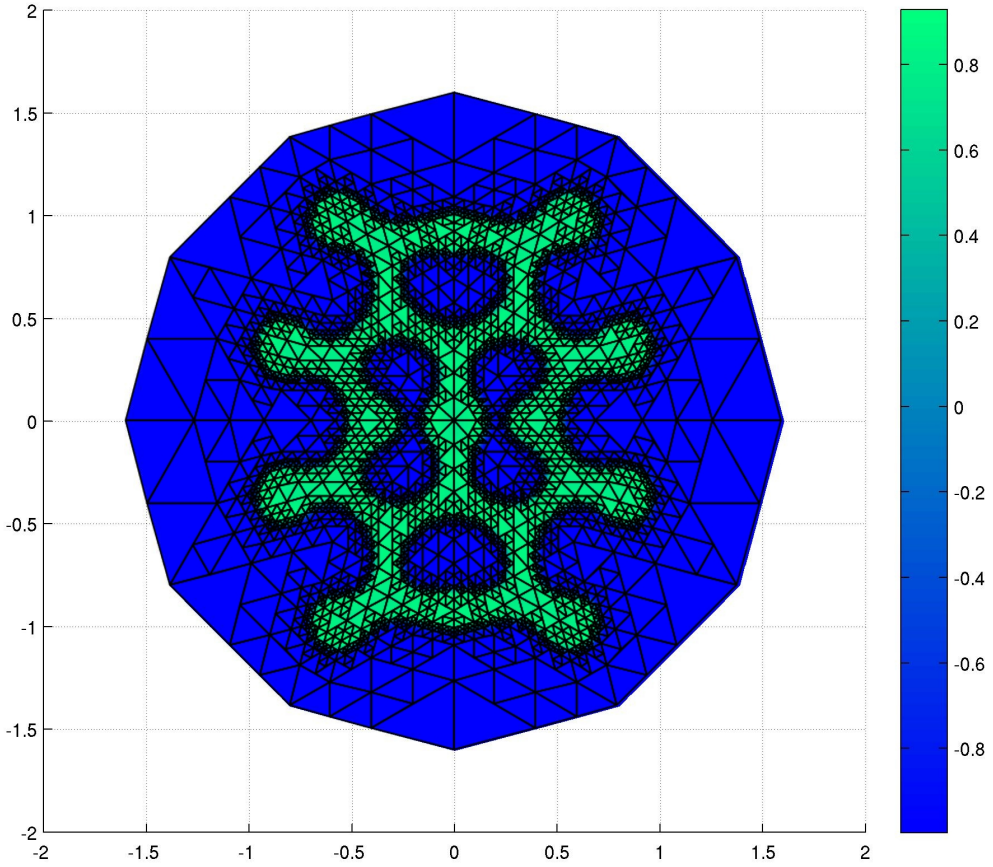

(a) Mesh superposed on solution

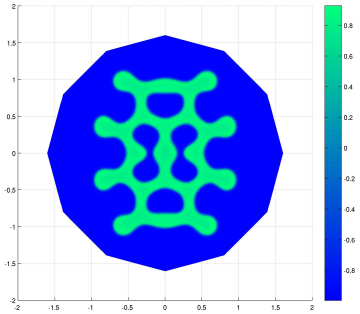

(b) Solution

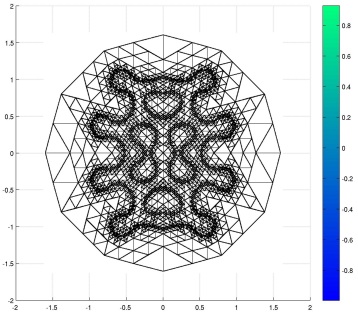

(c) Six level mesh

Figure 4.6: *Snapshot of the solution with the corresponding adaptive mesh from the simulation of tumor growth using model* **(Pv1)**. *In Fig. 4.6a we superpose the solution Fig. 4.6b with the corresponding mesh Fig. 4.6c. Here we have used* $t_0 = 0$, $T = 0.15$, $n_{max} = 40000$, $\epsilon = 0.0125$, $D = 0.25$, $\lambda_g = 70$ *and* $\lambda_d = 23$.

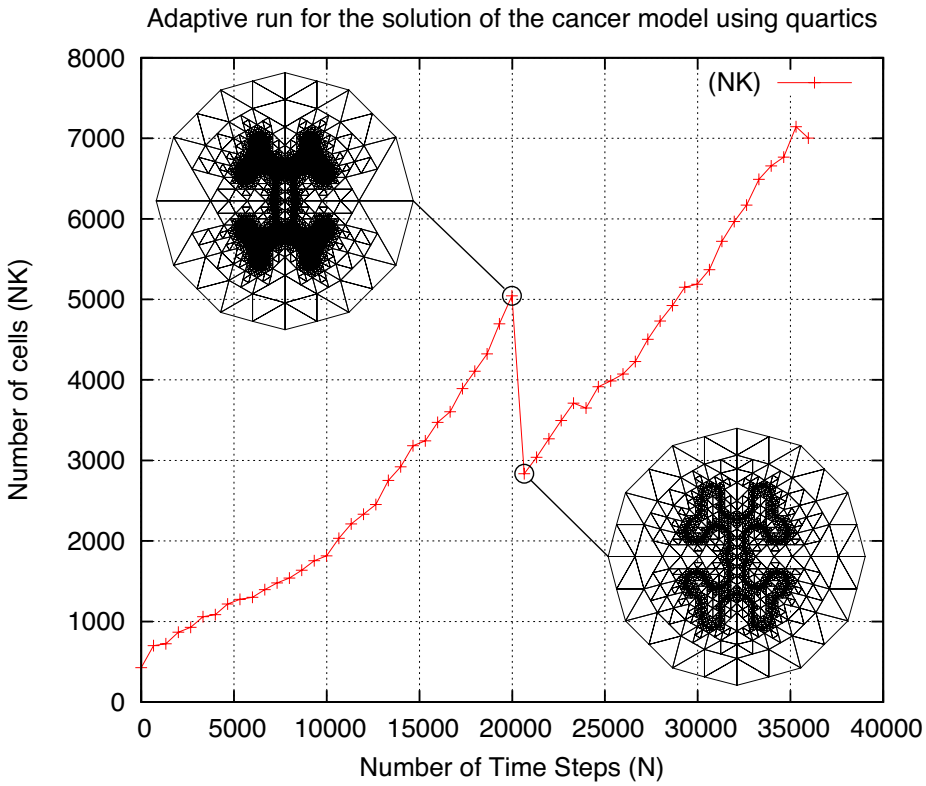

Figure 4.7: *Adaptive run for the cancer model* **(Pv1)**. *We observe that the increase of cells in the simulation is linear. We observe a drop of their number, due to coarsening, close to* $N = 20000$. *Then the number of cells continuous to grow linearly until the end of the simulation. Here we have used* $t_0 = 0$, $T = 0.15$, $n_{max} = 40000$, $\epsilon = 0.0125$, $D = 0.25$, $\lambda_g = 70$ *and* $\lambda_d = 23$.

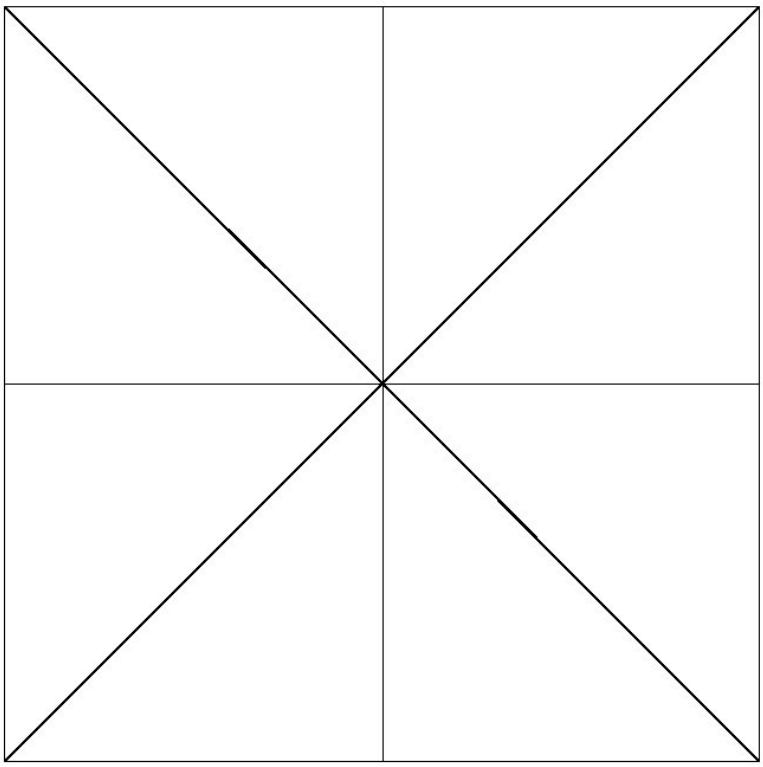

Figure 4.8: *Initial triangulation of the computational domains* $(0, 0.5)^2$, $(0, 1)^2$ *and* $(0, 2)^2$ *used in the solver test. We have uniformly refined the initial triangulations of the corresponding domains, three, four, and five times respectively, in order to generate the test meshes 1–3 shown in Fig. 4.9.*

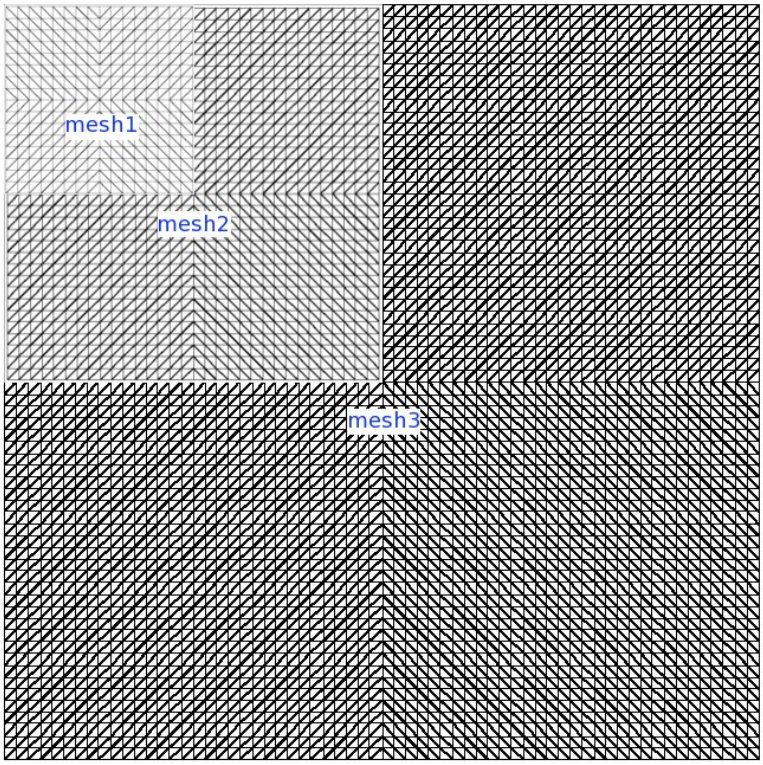

Figure 4.9: *Superposed meshes used in the solvers test. All the cells in the meshes 1–3 have the same size. To achieve this we have uniformly refined the initial triangulations Fig. 4.8 of our domains,* $(0, 0.5)^2$*,* $(0, 1)^2$ *and* $(0, 2)^2$*, three, four and five times respectively. Thus creating the hierarchy of meshes needed for our multilevel solvers, PCG and Multigrid.*

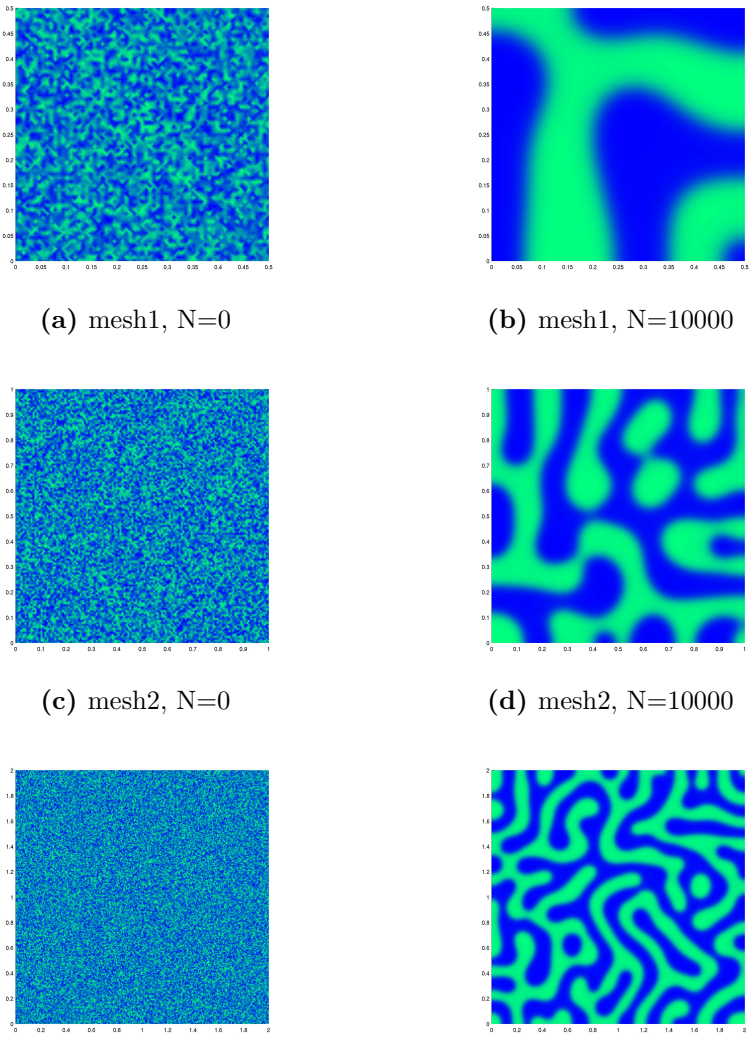

(a) mesh1, N=0 **(b)** mesh1, N=10000

(c) mesh2, N=0 **(d)** mesh2, N=10000

(e) mesh3, N=0 **(f)** mesh3, N=10000

Figure 4.10: *Initial profile,* $N = 0$*, and final profile,* $N = 10000$*, in the non-adaptive spinodal decomposition simulation using meshes 1–3 respectively. Here we have used the following parameters:* $D = 1$*,* $\epsilon = 0.015$*,* $t_0 = 0$*,* $T = 0.005$*,* $n_{max} = 10000$*,* $\lambda_g = \lambda_d = 0$*.*

Chapter 5

Energy Stable Schemes of Mixed-DG Type

5.1 Introduction

The goal of this chapter is to construct fully discrete energy stable schemes for the Cahn-Hilliard equation (2.15) and our diffuse interface tumor model **(MP1)**. Energy stability means that the discrete solutions dissipate some suitable energy in time, in analogy with the PDE model. In other words, the schemes preserve discrete versions of the continuous energy dissipation laws (2.14) and (2.27), respectively. It is generally accepted that schemes preserving discrete analogs of the energy dissipation laws lead to approximations that behave qualitatively more like their continuous counterparts.

In our endeavor we utilize mixed formulations of our IBVP's. As before, we use SIP-DG finite element methods to discretize space, though now mixed type. For the time discretization we use the convex-splitting (CS) approach popularized by David Eyre [24]. In the CS framework, one splits the energy into convex and concave pieces and treats the contribution from the convex part implicitly and the contribution from the concave part explicitly in the scheme. This methodology can lead to schemes that

are energy stable and are also uniquely solvable, both properties being, in the best case scenario, unconditional with respect to the time and space step sizes.

We first study a mixed formulation of the Cahn-Hilliard equation (2.15) to develop the methodology and gain insight on how to carry our results to the more complex Cahn-Hilliard tumor model **(MP1)**. For the Cahn-Hilliard equation we demonstrate unconditional energy stability and unique solvability. The energy stability leads to various unconditional uniform bounds on the sequence of numerical solutions. These bounds in turn will be utilized to establish *a priori* error estimates for the numerical solutions in a forthcoming paper (cf. [4]). Motivated by our work on the Cahn-Hilliard equation we then construct an energy stable scheme of mixed DG type for our Cahn-Hilliard tumor model. While this stability property will be unconditional with respect to time, it will, however, require a small restriction on the space step size.

It is worth noting that our results in this section will not consider mesh modification coming from adaptivity. Specifically, energy stability properties may not be guaranteed as the mesh is dynamically changed. We believe that an extension of our results to include this case is possible and thus it is a work in progress (cf. [3]).

5.2 Mixed Formulation of the Cahn-Hilliard Equation

Let $\Omega \subset R^d$, $d \geq 1$, be a convex polygonal domain. We consider the following mixed Cahn-Hilliard problem with natural boundary conditions and fast time scaling (cf. [15, 23]): **(P1)**

$$u_t = \triangle \mu, \qquad \text{in } \Omega_T, \tag{5.1a}$$

$$\mu = \frac{1}{\epsilon} f(u) - \epsilon \triangle u, \qquad \text{in } \Omega_T, \tag{5.1b}$$

$$\partial_n u = \partial_n \mu = 0, \qquad \text{on } \partial\Omega_T, \tag{5.1c}$$

$$u = u_0, \qquad \text{on } \partial\Omega \times \{t = 0\}, \tag{5.1d}$$

where $f(u) = F'(u)$, with $F(s) = \frac{1}{4}(s^2-1)^2$ and u_0 in $L^2(\Omega)$. We assume that a solution (u,μ) to problem **(P1)** exists in the space $L^2((0,T);H^2(\Omega)) \times L^2((0,T);H^2(\Omega))$. We proceed to derive an SIP-DG mixed formulation of **(P1)**.

5.2.1 Derivation of the SIP-DG Mixed Formulation

Let $(u,\mu) \in L^2((0,T);H^2(\Omega)) \times L^2((0,T);H^2(\Omega)) \subset L^2((0,T);E_h) \times L^2((0,T);E_h)$, where $E_h = H^2(\mathcal{T}_h)$, such that (u,μ) satisfies **(P1)**. Multiplying Eq. (5.1a) by a test function $v \in E_h$, using (3.24) and (3.25), and taking into consideration the homogeneous boundary conditions in (5.1c) we have

$$(u_t, v) = -\alpha_h(\mu, v), \quad \forall\ v \in E_h. \tag{5.2}$$

Treating Eq. (5.1b) similarly, we have

$$(\mu, v) = \frac{1}{\epsilon}(f(u), v) + \epsilon\alpha_h(u, v), \quad \forall\ v \in E_h. \tag{5.3}$$

Now from (5.2) and (5.3) we arrive at the following energy-space weak formulation of problem **(P1)**: **(VP1)** find $(u,\mu) \in L^2((0,T);E_h) \times L^2((0,T);E_h)$ such that

$$\begin{aligned}
(u_t, v) &= -\alpha_h(\mu, v), \quad \forall\ v \in E_h, && \text{(5.4a)}\\
(\mu, v) &= \frac{1}{\epsilon}(f(u), v) + \epsilon\alpha_h(u, v), \quad \forall\ v \in E_h, && \text{(5.4b)}\\
(u(\cdot,0), v) &= (u_0, v), \quad \forall\ v \in E_h. && \text{(5.4c)}
\end{aligned}$$

The role of the variational problem **(VP1)** is to aid in the definition of the semi- and fully-discrete mixed SIP-DG schemes. Next we define the following semi-discrete SIP-DG mixed formulation of problem **(P1)**: **(SDP1)** find $(u_h, \mu_h) \in L^2((0,T);V^h) \times$

$L^2((0,T);V^h)$ such that

$$\begin{aligned}
((u_h)_t, v_h) &= -\alpha_h(\mu_h, v_h), \quad \forall\ v_h \in V^h, && \text{(5.5a)}\\
(\mu_h, v_h) &= \frac{1}{\epsilon}(f(u_h), v_h) + \epsilon\alpha_h(u_h, v_h), \quad \forall\ v_h \in V^h, && \text{(5.5b)}\\
(u_h(\cdot,0), v_h) &= (u_0, v_h), \quad \forall\ v_h \in V^h. && \text{(5.5c)}
\end{aligned}$$

Before proceeding to the fully discrete scheme, let us define appropriate energy functionals, in both the spatially continuous and spatially discrete levels, and establish energy stability for each formulation.

5.2.2 Energy Stability of the Semi-Discrete SIP-DG Mixed Formulation

Let $u \in H^1(\Omega)$. Define

$$E(u) = \frac{1}{\epsilon}(F(u), 1) + \frac{\epsilon}{2}(\nabla u, \nabla u). \tag{5.6}$$

This is the same energy functional from Ch. 2 (cf. Eq. (2.3)) except for a rescaling by ϵ. Solutions of problem **(P1)** dissipate the energy E (5.6) at the rate

$$\frac{d}{dt}E(u) = \frac{d}{dt}\Big(\frac{1}{\epsilon}(F(u), 1) + \frac{\epsilon}{2}(\nabla u, \nabla u)\Big) = -\left\|\nabla\mu\right\|_\Omega^2 \leq 0. \tag{5.7}$$

The equation (5.7) describes a form of stability result called *energy stability*. By assuming that the initial energy, $E(u_0)$, is bounded by a constant, it can be shown that this form of stability implies the following stability bounds.

$$||u||_{L^\infty(0,T;H^1(\Omega))} \leq c, \tag{5.8}$$

and also,

$$||\nabla\mu||_{L^2(0,T;L^2(\Omega))} \leq c. \tag{5.9}$$

Now we proceed to derive an analogous energy dissipation result with (5.7) for our semi-discrete SIP-DG mixed formulation **(SDP1)**.

Derivation of the Discrete Energy Law

We introduce the discrete version of the Cahn-Hilliard energy functional (5.6) on E_h.

Definition 5.2.1. Let $v \in E_h$, then we define $E_{disc} : E_h \to R$ as,

$$E_{disc}(v) := \frac{1}{\epsilon}(F(v), 1) + \frac{\epsilon}{2}\alpha_h(v, v). \tag{5.10}$$

Remark. The above energy functional is positive on V^h. Also we have that for $v = u \in H^2(\Omega)$ satisfying problem **(P1)**, the discrete energy E_{disc} is consistent with the continuous energy E in the sense that $E(u) = E_{disc}(u)$ due to the consistency, given in (3.25), of the bilinear form using homogeneous Neumann boundary condition.

To show that the above energy functional E_{disc} satisfies an energy law in V^h we work as follow. Let (u_h, μ_h) be the solution pair of **(SDP1)**. Setting $v_h = \mu_h \in V^h$ in Eq. (5.5a) we have,

$$((u_h)_t, \mu_h) = -\alpha_h(\mu_h, \mu_h) \leq 0, \tag{5.11}$$

since $\alpha_h(\cdot, \cdot)$ is nonnegative definite in V^h. Similarly for $v = (u_h)_t \in V^h$ and using Eq. (5.5c) and (5.11) we have,

$$0 \geq (\mu_h, (u_h)_t) = \frac{1}{\epsilon}(f(u_h), (u_h)_t) + \epsilon\alpha_h(u_h, (u_h)_t),$$

which implies that

$$\frac{d}{dt}\Big(\frac{1}{\epsilon}(F(u_h), 1) + \frac{\epsilon}{2}\alpha_h(u_h, u_h)\Big) = -\alpha_h(\mu_h, \mu_h) \leq 0. \tag{5.12}$$

Therefore by using (5.12) we see that the discrete energy functional satisfies a discrete energy law.

Now we proceed to show an analogous discrete energy stability result, for the fully discrete scheme obtained from **(SDP1)**, by using the convex splitting of the energy technique for the time discretization (cf. [24]).

5.2.3 Convex Splitting Scheme

We define the following fully discrete scheme called the convex splitting: **(CSP1)** find $(u_h^n, \mu_h^n) \in V^h/R \times V^h$ for $n = 1, \ldots, N$ such that,

$$
\begin{aligned}
(\delta_{k_n} u_h^n, v_h) &= -\alpha_h(\mu_h^n, v_h), \quad \forall\ v_h \in V^h, && \text{(5.13a)}\\
(\mu_h^n, v_h) &= \frac{1}{\epsilon}(f_c(u_h^n) - f_e(u_h^{n-1}), v_h) + \epsilon\alpha_h(u_h^n, v_h), \quad \forall\ v_h \in V^h, && \text{(5.13b)}\\
(u_h^0, v_h) &= (u_0, v_h), \quad \forall\ v_h \in V^h, && \text{(5.13c)}
\end{aligned}
$$

where

$$\delta_{k_n} u_h^n = \frac{u_h^n - u_h^{n-1}}{k_n}, \quad \sum_{n=1}^{N} k_n = T.$$

Remark. In the convex splitting we rewrite the potential energy as a difference of two convex parts, $F := F_c - F_e$ (cf. [24]) where,

$$F_c(u) = \frac{1}{8}(u - \frac{1}{2})^4 \quad \text{and} \quad F_e(u) = \frac{1}{16}(u - \frac{1}{2})^2 - \frac{1}{128}. \tag{5.14}$$

The method is almost like an implicit Euler, but with the difference that the f_e part of f is treated explicitly. Existence and uniqueness of the solution can be established by following the steps in [26] done for the standard Galerkin FE, by replacing the continuous FE bilinear form with its discontinuous counterpart.

Before we prove the energy stability for the convex splitting scheme we establish a bound of the initial discrete energy functional showing that we start with an initial energy that is not infinite hence our formulations are well defined with respect to this matter. Also the same result will be needed later when we establish uniform bounds for the sequence of the numerical solutions of **(CSP1)**.

5.2.4 Initial Energy Bound

We can choose our PDE initial condition as $u_0 \in H^2(\Omega) \cap \{(u_0, 1) = 0\}$ for simplicity.

Lemma 5.2.4.1. *Let u_0 as above and $u_h^0 \in V^h/R$.*

$$\begin{aligned} E(u_h^0) &= \frac{1}{\epsilon}(F(u_h^0), 1) + \frac{\epsilon}{2}\alpha_h(u_h^0, u_h^0) \\ &\leq c||F(u_h^0)|| + c|||u_h^0|||^2 \\ &= c||\frac{1}{4}(1 - (u_h^0)^2)^2|| + c|||u_h^0|||^2. \end{aligned} \tag{5.15}$$

From the definition of $\alpha_h(\cdot, \cdot)$ (3.24) and the properties of L^2 projection (3.8) we have that,

$$E(u_h^0) \leq C, \tag{5.16}$$

where C independent of h and k_n.

Proof. Let $v_0 = u_h^0 - u_0 \in E^h/R$ then from (3.24) we have,

$$\begin{aligned} \alpha_h(v_0, v_0) = |||v_0|||_\alpha^2 &\leq \sum_{k \in \mathcal{T}_h} |v_0|_{1,K}^2 \\ &\quad + \sum_{e \in \mathcal{E}^I} \Big(2|\langle \{\partial_n v_0\}, [v_0] \rangle_e| + \gamma h_e^{-1} |[v_0]|_e^2 \Big), \ \gamma > 0, \\ \text{(using (3.8))} \qquad &\leq c \sum_{k \in \mathcal{T}_h} h_k^2 |u_0|_{2,K}^2 \\ \text{(using a.g.m.i.)} \qquad &\quad + \sum_{e \in \mathcal{E}^I} \Big(c h_e |\{\partial_n v_0\}|_e^2 + (c + \gamma) h_e^{-1} |[v_0]|_e^2 \Big), \end{aligned} \tag{5.17}$$

where a.g.m.i. stands for the arithmetic geometric mean inequality

$$ab \leq \frac{a^2}{2} + \frac{b^2}{2},$$

$a,\, b \geq 0$. Now using the trace inequality (3.2) and (3.8) we end up with

$$\begin{aligned} h_e^{-1}|[v_0]]|_e^2 &\leq ch_e^{-1}(||v_0||_{K'}|v_0|_{1,K'} + h_K^{-1}||v_0||_{K'}^2) \\ \text{(using } h_e \sim h_K\text{)} \qquad &\leq ch_k^{-1}(h_K^2|u_0|_{2,K'}h_K|u_0|_{2,K'} + h_K^{-1}h_K^4|u_0|_{2,K'}^2). \end{aligned}$$

Therefore we have,

$$h_e^{-1}|[v_0]]|_e^2 \leq ch_k^2|u_0|_{2,K'}^2, \tag{5.18}$$

where $K' = \{K^+, K^-\}$. In a similar way using (3.2),

$$\begin{aligned} h_e|\{\partial_n v_0\}|_e^2 &\leq ch_e|\{\nabla v_0\}|_e^2, \\ \text{(using } h_e \sim h_K\text{)} \qquad &\leq ch_k(||\nabla v_0||_{K'}|\nabla v_0|_{1,K'} + h_K^{-1}||\nabla v_0||_{K'}^2), \\ &\leq ch_k(|v_0|_{1,K'}|v_0|_{2,K'} + h_K^{-1}|v_0|_{1,K'}^2) \\ \text{(using (3.8))} \qquad &\leq c(1 + ||u_h^0||_{0,8}^8 + 2||u_h^0||_{0,4}^4), \end{aligned}$$

we arrive at

$$h_e|\{\partial_n v_0\}|_e^2 \leq ch_k^2|u_0|_{2,K'}^2. \tag{5.19}$$

Now using (5.18), (5.19) in (5.17) and the regularity of u_0 we have,

$$\begin{aligned} |||v_0|||_\alpha^2 = |||u_h^0 - u_0|||_\alpha^2 &\leq c\sum_{k\in\mathcal{T}_h} h_k^2|u_0|_{2,K}^2, \\ \text{(since } h \in (0,1]\text{)} \qquad &\leq c|u_0|_{2,\Omega}, \\ &\leq c|u_0|_{2,\Omega} + |||u_0|||_\alpha \\ &\leq c|u_0|_{2,\Omega} + c|u_0|_{1,\Omega}. \end{aligned}$$

By using the norm equivalence (3.27) we get,

$$|||u_h^0||| \leq c(|u_0|_{2,\Omega} + |u_0|_{1,\Omega}). \tag{5.20}$$

Now for the $(F(u_h^0), 1)$ term we are working as follow,

$$\begin{aligned}
(F(u_h^0), 1) &\leq c||F(u_h^0)||, \\
&= c||\frac{1}{4}(1-(u_h^0)^2)^2||, \\
&= c||1+(u_h^0)^4 - 2(u_h^0)^2||, \\
&\leq c(1+||u_h^0||_{0,8}^8 + 2||u_h^0||_{0,4}^4), \\
\text{(using (3.31))} \qquad &\leq c(1+|||u_h^0|||^8 + 2|||u_h^0|||^4). \qquad (5.21)
\end{aligned}$$

Finally using (5.20) and (5.21) in (5.15) we have the final bound on the initial discrete energy.

$$E_{dsic}(u_h^0) \leq C. \qquad (5.22)$$

□

We are now ready to show the energy stability of the fully discrete convex splitting scheme **(CSP1)**.

5.2.5 Derivation of the Discrete Energy Law for the Convex Splitting

Lemma 5.2.5.1. *Let $(u_h^{n+1}, \mu_h^{n+1}) \in V^h/R \times V^h$ be the solution pair of* **(CSP1)**. *We have the following energy law for* **(CSP1)**,

$$E_h(u_h^{n+1}) - E_h(u_h^n) \leq -k_n|||\mu_h^{n+1}|||_\alpha^2, \text{ for } n = 0, \ldots, N-1. \qquad (5.23)$$

Proof. Let $v_h = \mu_h^{n+1} \in V^h$, from Eq. (5.13a) we have,

$$(u_h^{n+1} - u_h^n, \mu_h^{n+1}) = -k_n\alpha_h(\mu_h^{n+1}, \mu_h^{n+1}) \leq 0. \qquad (5.24)$$

Now for $v_h = u_h^{n+1} - u_h^n \in V^h$ and using Eq. (5.13b) and (5.24) we have,

$$0 \geq (\mu_h^{n+1}, u_h^{n+1} - u_h^n) = \frac{1}{\epsilon}(f_c(u_h^{n+1}) - f_e(u_h^n), u_h^{n+1} - u_h^n) + \epsilon\alpha_h(u_h^{n+1}, u_h^{n+1} - u_h^n). \quad (5.25)$$

We proceed to bound from below the following term,

$$(f_c(u_h^{n+1}) - f_e(u_h^n), u_h^{n+1} - u_h^n).$$

Using the fact that $F_c'' \geq 0$ and $F_e'' \geq 0$ (since F_c, F_e are convex) and truncating the resulting Taylor series of F_c and F_e at the second derivative we arrive after some rearrangement of the terms to the following,

$$\begin{aligned} f_c(u_h^{n+1})(u_h^{n+1} - u_h^n) &= F_c(u_h^{n+1}) - F_c(u_h^n) + p_c(u_h^{n+1}, u_h^n), & (5.26) \\ -f_e(u_h^n)(u_h^{n+1} - u_h^n) &= F_e(u_h^n) - F_e(u_h^{n+1}) + p_e(u_h^{n+1}, u_h^n), & (5.27) \end{aligned}$$

where

$$p_c(u_h^{n+1}, u_h^n) = \frac{F_c''(\xi_{u_h^n, u_h^{n+1}})}{2}(u_h^n - u_h^{n+1})^2,$$

and

$$p_e(u_h^{n+1}, u_h^n) = \frac{F_e''(\zeta_{u_h^n, u_h^{n+1}})}{2}(u_h^{n+1} - u_h^n)^2,$$

are nonnegative, since F_c and F_e are convex. Hence taking L^2 inner product with $v_h = 1$ on all the terms in (5.26), (5.27) and adding them together we have,

$$\begin{aligned} (f_c(u_h^{n+1}), u_h^{n+1} - u_h^n) - (f_e(u_h^n), u_h^{n+1} - u_h^n) &= (F_c(u_h^{n+1}), 1) - (F_c(u_h^n), 1) \\ & (F_e(u_h^n), 1) - (F_e(u_h^{n+1}), 1) \\ & +(p, 1), \end{aligned}$$

where $p = p_c + p_e \geq 0$. This implies that,

$$\begin{aligned}(f_c(u_h^{n+1}), u_h^{n+1} - u_h^n) - (f_e(u_h^n), u_h^{n+1} - u_h^n) &= (F(u_h^{n+1}), 1) - (F(u_h^n), 1) \\ &\quad +(p, 1).\end{aligned}$$

Since $(p, 1) \geq 0$, we have,

$$(f_c(u_h^{n+1}) - f_e(u_h^n), u_h^{n+1} - u_h^n) \geq (F(u_h^{n+1}), 1) - (F(u_h^n), 1). \tag{5.28}$$

Also we need to bound from below this term $\alpha_h(u_h^{n+1}, u_h^{n+1} - u_h^n)$. By using lemma 3.24 we have that the bilinear form is nonnegative definite hence we can write,

$$\begin{aligned}0 &\leq \frac{1}{2}a_h(u_h^{n+1} - u_h^n, u_h^{n+1} - u_h^n), \\ &= \frac{1}{2}\alpha_h(u_h^{n+1}, u_h^{n+1}) - \alpha_h(u_h^{n+1}, u_h^n) + \frac{1}{2}\alpha_h(u_h^n, u_h^n).\end{aligned}$$

Adding and subtracting $\frac{1}{2}\alpha_h(u_h^{n+1}, u_h^{n+1})$ and grouping the terms together we have,

$$\begin{aligned}\frac{1}{2}a_h(u_h^{n+1} - u_h^n, u_h^{n+1} - u_h^n) &= \alpha_h(u_h^{n+1}, u_h^{n+1}) - \alpha_h(u_h^{n+1}, u_h^n) - \frac{1}{2}\alpha_h(u_h^{n+1}, u_h^{n+1}) \\ &\quad +\frac{1}{2}\alpha_h(u_h^n, u_h^n), \\ &= \alpha_h(u_h^{n+1}, u_h^{n+1} - u_h^n) - \frac{1}{2}\alpha_h(u_h^{n+1}, u_h^{n+1}) + \frac{1}{2}\alpha_h(u_h^n, u_h^n),\end{aligned}$$

which implies,

$$\begin{aligned}\alpha_h(u_h^{n+1}, u_h^{n+1} - u_h^n) &= \frac{1}{2}\alpha_h(u_h^{n+1}, u_h^{n+1}) - \frac{1}{2}\alpha_h(u_h^n, u_h^n) \\ &\quad +\frac{1}{2}a_h(u_h^{n+1} - u_h^n, u_h^{n+1} - u_h^n).\end{aligned}$$

Hence we obtain,

$$\alpha_h(u_h^{n+1}, u_h^{n+1} - u_h^n) \geq \frac{1}{2}\alpha_h(u_h^{n+1}, u_h^{n+1}) - \frac{1}{2}\alpha_h(u_h^n, u_h^n). \tag{5.29}$$

Thus by combining (5.25), (5.28) and (5.29) we get,

$$\begin{aligned} 0 \geq (\mu_h^{n+1}, u_h^{n+1} - u_h^n) &\geq \frac{1}{\epsilon}(F(u_h^{n+1}), 1) - \frac{1}{\epsilon}(F(u_h^n), 1) \\ &+ \frac{\epsilon}{2}\alpha_h(u_h^{n+1}, u_h^{n+1}) - \frac{\epsilon}{2}\alpha_h(u_h^n, u_h^n) \end{aligned}$$

which implies,

$$\frac{1}{\epsilon}(F(u_h^{n+1}), 1) + \frac{\epsilon}{2}\alpha_h(u_h^{n+1}, u_h^{n+1}) \leq \frac{1}{\epsilon}(F(u_h^n), 1) + \frac{\epsilon}{2}\alpha_h(u_h^n, u_h^n).$$

Thus we have our result

$$E_h(u_h^{n+1}) \leq E_h(u_h^n). \tag{5.30}$$

□

Next we establish uniform bounds on the sequence of numerical solutions of **(CSP1)**. The newly proved energy stability result (5.30) is being used in the proof of the bounds.

5.2.6 Uniform Bounds on the Sequence of Numerical Solutions

We continue to show the following bounds on the sequence of numerical solutions for the convex splitting scheme **(CSP1)** following the steps in [32] done for the Implicit Euler time desensitization method. The important difference here, besides the fact that we are using the CS as a time discretization scheme, is that our bounds are independent of the time step, k_n, and the space parameter h. We make note that the authors in [32] considered a slightly more general problem than **(P1)**. We believe that even for their formulation unconditional uniform bounds can be established by using our setting.

Lemma 5.2.6.1. *For any $h > 0$ and $k_n > 0$ there exists a unique solution $\{u_h^n, \mu_h^n\} \in V^h/R \times V^h$ to the n-th step of* **(CSP1)**, *$n = 1, \ldots, N$; in addition there exists a*

positive constant $C = C(\epsilon, \gamma_0, T)$ *independent of* h, k_n, *such that,*

$$\max_{n=1\to N}\Big(\epsilon|||u_h^n|||^2 + ||u_h^n||_\infty + \frac{1}{\epsilon}(F(u_h^n),1) \quad + \quad ||\mu_h^n||^2 + \epsilon k_n||\delta_{k_n}u_h^n||^2\Big) + \sum_{n=1}^{N} k_n|||\mu_h^n|||^2 \le C \tag{5.31}$$

$$\max_{n=1\to N}||\Delta_h u_h^n|| \quad \le \quad C \tag{5.32}$$

and

$$\sum_{n=1}^{N} k_n||u_h^n||_\infty^4 \quad \le \quad C \tag{5.33}$$

Proof. From (5.30) we have for $n = 1, \cdots, N$,

$$E_h(u_h^n) - E_h(u_h^{n-1}) \le -k_n|||\mu_h^n|||_\alpha^2$$

and using (3.27) we have,

$$E_h(u_h^n) - E_h(u_h^{n-1}) \le -ck_n|||\mu_h^n|||^2.$$

Summing up on n we get,

$$\sum_{n=1}^{l}\left(E_h(u_h^n) - E_h(u_h^{n-1}) + ck_n|||\mu_h^n|||^2\right) \le 0, \quad 1 \le n \le l \le N,$$

which implies,

$$E_h(u_h^l) + c\sum_{n=1}^{l}\left(k_n|||\mu_h^n|||^2\right) \le E_h(u_h^0), \quad 1 \le n \le l \le N.$$

Thus by taking maximum on both sides with respect to l we have,

$$\max_{l=1,\cdots,N}\left[E_h(u_h^l) + \sum_{n=1}^{l}\left(k_n|||\mu_h^n|||^2\right)\right] \le cE_h(u_h^0),$$

and by using (5.16) we get,

$$\max_{n=1,\cdots,N}\{E_h(u_h^n)\} + \sum_{n=1}^{N}\left(k_n|||\mu_h^n|||^2\right) \leq C.$$

Now by using (5.12), (3.27) on the previous we arrive at,

$$\max_{n=1,\cdots,N}\{\frac{1}{\epsilon}(F(u_h^n),1) + \frac{\epsilon}{2}|||u_h^n|||^2\} + \sum_{n=1}^{N}\left(k_n|||\mu_h^n|||^2\right) \leq C. \tag{5.34}$$

Hence we have shown the first, third and fifth bound of (5.31).

Now let $v = \triangle_h u_h^n$ in the equation (5.13b),

$$(\mu_h^n, \triangle_h u_h^n) = \epsilon\alpha_h(u_h^n, \triangle_h u_h^n) + \frac{1}{\epsilon}(f_c(u_h^n) - f_e(u_h^{n-1}), \triangle_h u_h^n). \tag{5.35}$$

Setting $w = u_h^n$ and $v = \triangle_h u_h^n$ in (3.28) and multiplying by ϵ we have,

$$-\epsilon||\triangle_h u_h^n||^2 = \epsilon\alpha_h(u_h^n, \triangle_h u_h^n). \tag{5.36}$$

Now combining (5.35) and (5.36) we have,

$$\begin{aligned}
\epsilon||\triangle_h u_h^n||^2 &= \frac{1}{\epsilon}(f_c(u_h^n) - f_e(u_h^{n-1}), \triangle_h u_h^n) - (\mu_h^n, \triangle_h u_h^n) \qquad (5.37)\\
\text{(using (3.28))} \qquad &\leq \frac{1}{\epsilon}(f_c(u_h^n) - f_e(u_h^{n-1}), \triangle_h u_h^n) + \alpha_h(\mu_h^n, u_h^n)\\
\text{(using a.g.m.i.)} \qquad &\leq \frac{c}{\epsilon^3}||(u_h^n)^3 - u_h^{n-1}||^2 + \frac{\epsilon}{2}||\triangle_h u_h^n||^2\\
&\quad +c|||\mu_h^n|||^2 + c|||u_h^n|||^2
\end{aligned}$$

Hence this implies,

$$\epsilon||\triangle_h u_h^n||^2 \leq c|||\mu_h^n|||^2 + c|||u_h^n|||^2 + \frac{c}{\epsilon^3}||(u_h^n)^3 - u_h^{n-1}||^2 \tag{5.38}$$

Now,

$$\begin{aligned} ||(u_h^n)^3 - u_h^{n-1}||^2 &= ((u_h^n)^3 - u_h^{n-1}, (u_h^n)^3 - u_h^{n-1}) \\ &= ||(u_h^n)^3||^2 + 2|((u_h^n)^3, u_h^{n-1})| + ||u_h^{n-1}||^2 \\ \text{(using a.g.m)} \qquad &\leq c||(u_h^n)^3||^2 + c||u_h^{n-1}||^2 \\ &\leq c||(u_h^n)||_{0,6}^6 + c||u_h^{n-1}||^2 \\ \text{(using (3.31))} \qquad &\leq c|||(u_h^n)|||^6 + c|||u_h^{n-1}|||^2 \\ \text{(using (5.34))} \qquad &\leq C. \end{aligned} \tag{5.39}$$

Hence using (5.38), (5.39) and (5.34),

$$\epsilon||\triangle_h u_h^n||^2 \leq c|||\mu_h^n|||^2 + C \tag{5.40}$$

where $C \sim O(\frac{1}{\epsilon^4})$ for $0 < \epsilon \ll 1$.

Now using (3.31) and (5.34) we have $||u_h^n|| \leq c|||u_h^n||| \leq C$ and using this in (5.40) and multiplying by k_n we have,

$$\epsilon k_n||u_h^n||^2||\triangle_h u_h^n||^2 \leq ck_n|||\mu_h^n|||^2 + Ck_n$$

By using (3.30) and that $u_h^n \in V^h/R$ we get,

$$\epsilon k_n||u_h^n||_\infty^4 \leq ck_n|||\mu_h^n|||^2 + Ck_n,$$

and this gives,

$$\epsilon \sum_{n=1}^{N} \left(k_n||u_h^n||_\infty^4\right) \leq c \sum_{n=1}^{N} \left(k_n|||\mu_h^n|||^2\right) + CT.$$

Hence after using (5.34) we have,

$$\sum_{n=1}^{N} \left(k_n||u_h^n||_\infty^4\right) \leq C. \tag{5.41}$$

Now for the remaining bounds of (5.31) we subtract the equation (5.13b) at n with itself at $n-1$ and setting $v = \mu_h^n$ we have,

$$\begin{aligned}
(\mu_h^n - \mu_h^{n-1}, \mu_h^n) &= \epsilon\alpha_h(u_h^n - u_h^{n-1}, \mu_h^n) \\
&\quad + \frac{1}{\epsilon}(f_c(u_h^n) - f_e(u_h^{n-1}) - f_c(u_h^{n-1}) + f_e(u_h^{n-2}), \mu_h^n). \\
(\mu_h^n - \mu_h^{n-1}, \mu_h^n) &= \epsilon k_n \alpha_h(\delta_{k_n} u_h^n, \mu_h^n) \\
&\quad + \frac{1}{\epsilon}(f_c(u_h^n) - f_e(u_h^{n-1}) - f_c(u_h^{n-1}) + f_e(u_h^{n-2}), \mu_h^n).
\end{aligned} \tag{5.42}$$

Also setting $v = k_n \epsilon \delta_{k_n} u_h^n$ in equation (5.13a) we have,

$$\epsilon k_n ||\delta_{k_n} u_h^n||^2 = -\epsilon k_n \alpha_h(\mu_h^n, \delta_{k_n} u_h^n). \tag{5.43}$$

Adding with (5.42),

$$(\mu_h^n - \mu_h^{n-1}, \mu_h^n) + \epsilon k_n ||\delta_{k_n} u_h^n||^2 = \frac{1}{\epsilon}(f_c(u_h^n) - f_e(u_h^{n-1}) - f_c(u_h^{n-1}) + f_e(u_h^{n-2}), \mu_h^n)$$

and after a little algebra we have,

$$\begin{aligned}
(\mu_h^n - \mu_h^{n-1}, \mu_h^n) + \epsilon k_n ||\delta_{k_n} u_h^n||^2 &= \frac{1}{\epsilon}(k_n \delta_{k_n} u_h^n [(u_h^n)^2 + u_h^n u_h^{n-1} + (u_h^{n-1})^2], \mu_h^n) \\
&\quad - \frac{1}{\epsilon}(k_n \delta_{k_n} u_h^{n-1}, \mu_h^n) \\
&= \frac{1}{\epsilon}(\sqrt{k_n}\delta_{k_n} u_h^n, \sqrt{k_n}[(u_h^n)^2 + u_h^n u_h^{n-1} + (u_h^{n-1})^2]\mu_h^n) \\
&\quad - \frac{1}{\epsilon}(\sqrt{k_n}\delta_{k_n} u_h^{n-1}, \sqrt{k_n}\mu_h^n).
\end{aligned}$$

Using Cauchy-Schwarz and a.g.m.i. we get,

$$\begin{aligned}(\mu_h^n - \mu_h^{n-1}, \mu_h^n) + \epsilon k_n ||\delta_{k_n} u_h^n||^2 \;\leq\; & \frac{\epsilon}{2} k_n ||\delta_{k_n} u_h^n||^2 \\ & + \frac{c}{2\epsilon^3} k_n ||[(u_h^n)^2 + u_h^n u_h^{n-1} + (u_h^{n-1})^2]\mu_h^n||^2 \\ & + \frac{\epsilon}{2} k_n ||\delta_{k_n} u_h^{n-1}||^2 + \frac{c}{2\epsilon^3} k_n ||\mu_h^n||^2 \end{aligned} \tag{5.44}$$

Observing,

$$\begin{aligned} 0 \;&\leq\; \frac{1}{2}(\mu_h^n - \mu_h^{n-1}, \mu_h^n - \mu_h^{n-1}) \\ &=\; \frac{1}{2}(\mu_h^n, \mu_h^n) - (\mu_h^n, \mu_h^{n-1}) + \frac{1}{2}(\mu_h^{n-1}, \mu_h^{n-1}) \\ &=\; (\mu_h^n, \mu_h^n) - (\mu_h^n, \mu_h^{n-1}) - \frac{1}{2}(\mu_h^n, \mu_h^n) + \frac{1}{2}(\mu_h^{n-1}, \mu_h^{n-1}) \\ &=\; (\mu_h^n, \mu_h^n - \mu_h^{n-1}) - \frac{1}{2}(\mu_h^n, \mu_h^n) + \frac{1}{2}(\mu_h^{n-1}, \mu_h^{n-1}). \end{aligned}$$

We have,

$$(\mu_h^n, \mu_h^n - \mu_h^{n-1}) = \frac{1}{2}(\mu_h^n, \mu_h^n) - \frac{1}{2}(\mu_h^{n-1}, \mu_h^{n-1}) + \frac{1}{2}(\mu_h^n - \mu_h^{n-1}, \mu_h^n - \mu_h^{n-1}),$$

and this means,

$$(\mu_h^n, \mu_h^n - \mu_h^{n-1}) \geq \frac{1}{2}||\mu_h^n||^2 - \frac{1}{2}||\mu_h^{n-1}||^2. \tag{5.45}$$

Also we have that,

$$||(u_h^n)^2 + u_h^n u_h^{n-1} + (u_h^{n-1})^2||_\infty^2 \leq (||u_h^n||_\infty^2 + ||u_h^n||_\infty ||u_h^{n-1}||_\infty + ||u_h^{n-1}||_\infty^2)^2,$$

and by using the known Young's inequality we get,

$$||(u_h^n)^2 + u_h^n u_h^{n-1} + (u_h^{n-1})^2||_\infty^2 \leq c(||u_h^n||_\infty^4 + ||u_h^{n-1}||_\infty^4). \tag{5.46}$$

Combining (5.45),(5.46) in (5.44) we get,

$$||\mu_h^n||^2 - ||\mu_h^{n-1}||^2 + \epsilon k_n ||\delta_{k_n} u_h^n||^2 - \epsilon k_n ||\delta_{k_n} u_h^{n-1}||^2 \quad \leq \quad \frac{c}{\epsilon^3} k_n (C_{h,k_n} + 1) ||\mu_h^n||^2 \tag{5.47}$$

where $C_{h,k_n} = c(||u_h^n||_\infty^4 + ||u_h^{n-1}||_\infty^4)$ and because of (5.33),

$$\sum_{n=1}^{N} k_n C_{h,k_n} < C, \text{ where } C \text{ independent of } h \text{ and } k_n \tag{5.48}$$

Now summing (5.47) from $n = 1, \cdots, l$ where $1 \leq n \leq l \leq N$
and assuming $\mu_h^0 = \delta_{k_n} u_h^0 = 0$ we get,

$$\begin{aligned} ||\mu_h^l||^2 + \epsilon k_l ||\delta_{k_n} u_h^l||^2 \quad &\leq \quad \sum_{n=1}^{l} \frac{c}{\epsilon^3} k_n (C_{h,k_n} + 1) ||\mu_h^n||^2 \\ \max_{n=1,\cdots,N} \{||\mu_h^n||^2 + \epsilon k_n ||\delta_{k_n} u_h^n||^2\} \quad &\leq \quad \sum_{n=1}^{N} \frac{c}{\epsilon^3} k_n (C_{h,k_n} + 1) ||\mu_h^n||^2 \end{aligned} \tag{5.49}$$

From (5.49) we can deduct,

$$||\mu_h^n||^2 \leq 1 + \sum_{n=1}^{N} (\frac{c}{\epsilon^3} k_n (C_{h,k_n} + 1) ||\mu_h^n||^2)$$

and by applying to it a Gronwall inequality and by using (5.48) we have that,

$$||\mu_h^n||^2 \leq C \tag{5.50}$$

where C independent of h and k_n.
Combining (5.50) and (5.48) in (5.49) we have the following bounds of (5.31),

$$\max_{n=1,\cdots,N} \{||\mu_h^n||^2 + \epsilon k_n ||\delta_{k_n} u_h^n||^2\} \leq C \tag{5.51}$$

Now from (5.37) we have that,

$$\begin{aligned} \epsilon||\triangle_h u_h^n||^2 &= \frac{1}{\epsilon}(f_c(u_h^n) - f_e(u_h^{n-1}), \triangle_h u_h^n) - (\mu_h^n, \triangle_h u_h^n) \\ \text{(using a.g.m.i.)} \qquad &\leq \frac{c}{\epsilon^3}||(u_h^n)^3 - u_h^{n-1}||^2 + \frac{\epsilon}{4}||\triangle_h u_h^n||^2 \\ &\quad + \frac{c}{\epsilon}||\mu_h^n||^2 + \frac{\epsilon}{4}||\triangle_h u_h^n||^2. \end{aligned}$$

Thus by using (5.39) and (5.51) we get,

$$\frac{\epsilon}{2}||\triangle_h u_h^n||^2 \leq \frac{c}{\epsilon^3}||(u_h^n)^3 - u_h^{n-1}||^2 + \frac{c}{\epsilon}||\mu_h^n||^2 \leq C, \tag{5.52}$$

and by taking maximum on both sides we have (5.31).

Now to show the final bound of (5.31) we have from (5.52),

$$||\triangle_h u_h^n|| \leq C, \ \forall n$$

and this implies,

$$\begin{aligned} ||u_h^n||\ ||\triangle_h u_h^n|| &\leq C||u_h^n|| \\ \text{(using (3.31))} \qquad &\leq C|||u_h^n||| \\ \text{(using (5.31))} \qquad &\leq C. \end{aligned} \tag{5.53}$$

Lastly by using (3.30) and the previous bound (5.53) we have our last bound.

$$||u_h^n||_\infty^2 \leq C, \ \forall n$$

which gives,

$$\max_{n=1,\cdots,N}\{||u_h^n||_\infty\} \leq C. \tag{5.54}$$

□

It is worth mentioning that the above bounds are important in the proof of the convergence of the convex splitting scheme. The proof is work in progress (cf. [4]) and we follow the ideas that can be found in [32].

Motivated by our work for the Cahn-Hilliard equation problem **(P1)** we are extending our energy stability results to the tumor model with Dirichlet boundary conditions.

5.3 Cahn-Hilliard Equation with Nonlinear Growth and Linear Death

We define the mixed formulation, (**P2**), with fast time scaling, similarly as in (**PM1**).

$$\begin{aligned}
\partial_t u &= \triangle \bar{\mu} \quad \text{in } \Omega_T, && (5.55a)\\
\bar{\mu} &:= \frac{1}{\epsilon} f(u) - \epsilon \triangle u + \frac{1}{\epsilon} w \quad \text{in } \Omega_T, && (5.55b)\\
-\triangle w &= g'(u), \quad \text{in } \Omega_T, && (5.55c)\\
u = \mu &= 0, \quad \text{on } \partial\Omega_T, && (5.55d)\\
u &= u_0, \quad \text{on } \Omega \times \{0\}. && (5.55e)
\end{aligned}$$

Working analogously as in section 2.6. We define for $u \in H^2(\Omega)$ the energy functional E,

$$E(u) = \frac{1}{\epsilon}(F(u), 1) + \frac{\epsilon}{2}(\nabla u, \nabla u) + \frac{1}{\epsilon}(g(u), 1)_{H^{-1}} \tag{5.56}$$

where the H^{-1} inner product is defined in (2.24). As in section 2.6 we have the following energy law at the PDE level for (**P2**),

$$\partial_t E = \frac{1}{\epsilon}(f(u), u_t) + \epsilon(\nabla u, \nabla u_t) + \frac{1}{\epsilon}(g'(u), u_t)_{H^{-1}} = -||\nabla \bar{\mu}||_\Omega^2 \tag{5.57}$$

The following technical lemma will be proved useful later on in our discussion, thus we mention it next.

Lemma 5.3.0.2. *Let g be a C^m, $m \geq 2$, real valued function on R, and h_d, h_g be C^m also such that $g = h_d - h_g$. Then given a compact interval $I = [a, b]$ on R, there exists $\tilde{g} \in C^2(R)$ such that $\tilde{g} = g$ on I and $\tilde{g}$ is quadratic function on I^c. Also $\tilde{g}$ has a convex splitting, that is there are convex functions g_c, $g_e \in C^2(R)$, such that $\tilde{g} = g_c - g_e$. Additionally g_c'', g_e'' can be chosen to be bounded on R.*

Proof. We proceed to prove the above lemma by construction. Let $m_1 = \min_I h_d''$ and $m_2 = \min_I h_g''$. By adding $c_1 := |m_1 + 1| + |m_2 + 1|$ on h_d'', and h_g'' we guarantee that the resulting functions are positive on I. Thus we define the following continuous functions $g_e|_I'' := h_g|_I'' + c_1$, $g_c|_I'' := h_d|_I'' + c_1$ on I and continuously extend them by a constant on I^c, that is preserving their continuity on R by extending them on $R \backslash I$ using their constant values $g_e''(a) = h_g''(a) + c_1$, $g_e''(b) = h_g''(b) + c1$ and $g_c''(a) = h_d''(a) + c_1$, $g_c''(b) = h_d''(b) + c_1$ at the endpoints of I. Hence we have that g_c'', g_e'' are positive and bounded on R by construction. Now by integrating them twice and choosing appropriately the integration constants we have the following twice continuously differentiable functions on R, that is easy to verify that they satisfy the required properties.

$$g_e(x) = \begin{cases} h_g(x) + c_1 \dfrac{x^2}{2}, & \text{on } I, \\ (h_g'(a) + c_1)\dfrac{x^2}{2} + (h_g'(a) - h_g''(a))x + h_g(a) - h_g'(a)\dfrac{a^2}{2} & \\ \qquad -(h_g'(a) - h_g''(a))a, & \text{on } \{x \leq a\}, \\ (h_g'(b) + c_1)\dfrac{x^2}{2} + (h_g'(b) - h_g''(b))x + h_g(b) - h_g'(b)\dfrac{b^2}{2} & \\ \qquad -(h_g'(b) - h_g''(b))b, & \text{on } \{x \geq b\}. \end{cases}$$

and

$$g_c(x) = \begin{cases} h_d(x) + c_1\dfrac{x^2}{2}, & \text{on } I, \\ (h_d'(a) + c_1)\dfrac{x^2}{2} + (h_d'(a) - h_d''(a))x + h_d(a) - h_d'(a)\dfrac{a^2}{2} & \\ \qquad -(h_d'(a) - h_d''(a))a, & \text{on } \{x \le a\}, \\ (h_d'(b) + c_1)\dfrac{x^2}{2} + (h_d'(b) - h_d''(b))x + h_d(b) - h_d'(b)\dfrac{b^2}{2} & \\ \qquad -(h_d'(b) - h_d''(b))b, & \text{on } \{x \ge b\}. \end{cases}$$

□

From now on we will assume that g represents the source term $\tilde{g}$ described in lemma 5.3.0.2. Also the compact interval I in practice is chosen large enough such that it contains the expected range of values of u. In our case for the aforementioned source term described in section 2.6, I can be chosen to be $[-1, 2]$. We are stressing the fact that the assumption of the lemma 5.3.0.2 is not restrictive, since in practice the solution never exceeds the interval $[-1, 2]$.

Now equipped with the result of the previous lemma we can continue our discussion on the energy stability. First we will consider the case of time discretization only. This case will give us the inside to develop the ideas that will be needed later when showing the analogous result in the semi-discrete and fully discrete schemes.

5.3.1 Stability Analysis of a Time-Discrete, Space-Continuous Scheme

First we rewrite $F = F_c - F_e$ using (5.14) and $g = g_c - g_e$ as in lemma 5.3.0.2, where the letter c stands for contractive and e for expansive. Then we write the following

time discretization of (**P2**), called the convex splitting (**SDTP2**).

$$\begin{aligned} u^{n+1} - u^n &= s\triangle\bar{\mu}^{n+1} && (5.58a)\\ \bar{\mu}^{n+1} &:= \frac{1}{\epsilon}f_c(u^{n+1}) - \frac{1}{\epsilon}f_e(u^n) - \epsilon\triangle u^{n+1} + \frac{1}{\epsilon}w^{n+1} && (5.58b)\\ -\triangle w^{n+1} &= g_c'(u^{n+1}) - g_e'(u^n) && (5.58c) \end{aligned}$$

Our Goal is to show that $E(u^{n+1}) \leq E(u^n)$.

Proof. Multiplying equation (5.58a) with $\bar{\mu}^{n+1}$ and integrating once by parts we have,

$$\begin{aligned} (u^{n+1} - u^n, \bar{\mu}^{n+1}) &= s(\triangle\bar{\mu}^{n+1}, \bar{\mu}^{n+1})\\ &= -s(\nabla\bar{\mu}^{n+1}, \nabla\bar{\mu}^{n+1}) = -s||\nabla\bar{\mu}^{n+1}||^2 \end{aligned} \tag{5.59}$$

where,

$$\begin{aligned} (\bar{\mu}^{n+1}, u^{n+1} - u^n) &= \frac{1}{\epsilon}(f_c(u^{n+1}), u^{n+1} - u^n) - \frac{1}{\epsilon}(f_e(u^n), u^{n+1} - u^n)\\ &\quad -\epsilon(\triangle u^{n+1}, u^{n+1} - u^n) + \frac{1}{\epsilon}(w^{n+1}, u^{n+1} - u^n) \end{aligned} \tag{5.60}$$

Thus our goal is to show that

$E(u^{n+1}) - E(u^n) \leq -s||\nabla\bar{\mu}^{n+1}||^2 = (\bar{\mu}^{n+1}, u^{n+1} - u^n)$

Hence,

$$(g_c'(u^{n+1}) - g_e'(u^n), u^{n+1} - u^n)_{H^{-1}} = (\nabla w^{n+1}, \nabla\Psi_{u^{n+1}-u^n}) = (w^{n+1}, -\triangle\Psi_{u^{n+1}-u^n})$$

where $-\triangle\Psi_{u^{n+1}-u^n} = u^{n+1} - u^n$ then

$$\begin{aligned}(w^{n+1}, u^{n+1} - u^n) &= (g_c'(u^{n+1}) - g_e'(u^n), u^{n+1} - u^n)_{H^{-1}} \\ &= (g_c'(u^{n+1}), u^{n+1} - u^n)_{H^{-1}} - (g_e'(u^n), u^{n+1} - u^n)_{H^{-1}}.\end{aligned} \tag{5.61}$$

We use the fact that $g_c'' \geq 0$ and $g_e'' \geq 0$ and by truncating the Taylor series at the second derivative we have,

$$g_c'(u^{n+1})(u^{n+1} - u^n) = g_c(u^{n+1}) - g_c(u^n) + p_c(u^{n+1}, u^n) \tag{5.62}$$

$$-g_e'(u^n)(u^{n+1} - u^n) = g_e(u^n) - g_e(u^{n+1}) + p_e(u^{n+1}, u^n), \tag{5.63}$$

where $p_c, p_e \geq 0$ are the terms containing the second derivative. Thus taking H^{-1} inner product with the function $v = 1$ on all the terms in (5.62), (5.63) and adding them together we have,

$$\begin{aligned}(g_c'(u^{n+1}), u^{n+1} - u^n)_{H^{-1}} - (g_e'(u^n), u^{n+1} - u^n)_{H^{-1}} &= (g_c(u^{n+1}), 1)_{H^{-1}} - (g_c(u^n), 1)_{H^{-1}} \\ &\quad (g_e(u^n), 1)_{H^{-1}} - (g_e(u^{n+1}), 1)_{H^{-1}} \\ &\quad +(p, 1)_{H^{-1}}\end{aligned}$$

Which becomes,

$$\begin{aligned}(g_c'(u^{n+1}), u^{n+1} - u^n)_{H^{-1}} - (g_e'(u^n), u^{n+1} - u^n)_{H^{-1}} &= (g(u^{n+1}), 1)_{H^{-1}} \\ &\quad -(g(u^n), 1)_{H^{-1}} \\ &\quad +(p, 1)_{H^{-1}},\end{aligned} \tag{5.64}$$

Now let $\Psi_1,\ \Psi_p \in H_0^1$ be the unique solution of,

$$-\triangle\Psi_1 = 1, -\triangle\Psi_p = p$$

and by using weak maximum principle (cf. [29]) we have that $\Psi_1 \geq 0$. Hence,

$$\begin{aligned}(p,1)_{H^{-1}} &= (\nabla\Psi_p, \nabla\Psi_1) \\ &= (p, \Psi_1) \qquad \text{(by (2.24))},\end{aligned}$$

so

$$(p,1)_{H^{-1}} = (p,\Psi_1) \geq 0, \qquad \text{(since } p, \Psi_1 \geq 0). \tag{5.65}$$

Thus from (5.61), (5.64) and (5.65) we have,

$$(w^{n+1}, u^{n+1} - u^n) \geq (g(u^{n+1}),1)_{H^{-1}} - (g(u^n),1)_{H^{-1}} \tag{5.66}$$

Now we need to bound from below this term $(-\triangle u^{n+1}, u^{n+1} - u^n)$. We integrating once by parts and apply the boundary conditions (2.22d),

$$(-\triangle u^{n+1}, u^{n+1} - u^n) = (\nabla u^{n+1}, \nabla u^{n+1} - \nabla u^n) \tag{5.67}$$

Also can write,

$$\begin{aligned}0 &\leq \frac{1}{2}(\nabla u^{n+1} - \nabla u^n, \nabla u^{n+1} - \nabla u^n) \\ &= \frac{1}{2}||\nabla u^{n+1}||^2 - (\nabla u^{n+1}, \nabla u^n) + \frac{1}{2}||\nabla u^n||^2 \\ &= ||\nabla u^{n+1}||^2 - (\nabla u^{n+1}, \nabla u^n) - \frac{1}{2}||\nabla u^{n+1}||^2 + \frac{1}{2}||\nabla u^n||^2 \\ &= (\nabla u^{n+1}, \nabla u^{n+1} - \nabla u^n) - \frac{1}{2}||\nabla u^{n+1}||^2 + \frac{1}{2}||\nabla u^n||^2\end{aligned}$$

and this gives,

$$(\nabla u^{n+1}, \nabla u^{n+1} - \nabla u^n) \geq \frac{1}{2}||\nabla u^{n+1}||^2 - \frac{1}{2}||\nabla u^n||^2. \tag{5.68}$$

So from (5.67) and (5.68) we have,

$$(-\triangle u^{n+1}, u^{n+1} - u^n) \geq \frac{1}{2}||\nabla u^{n+1}||^2 - \frac{1}{2}||\nabla u^n||^2. \tag{5.69}$$

Finally we need to bound from below the following term $(f_c(u^{n+1}), u^{n+1} - u^n) - (f_e(u^n), u^{n+1} - u^n)$. In order to do that we work similarly as before.
We use the fact that $F_c'' \geq 0$ and $F_e'' \geq 0$ and truncating the Taylor series at the second derivative we have,

$$\begin{aligned} f_c(u^{n+1})(u^{n+1} - u^n) &= F_c(u^{n+1}) - F_c(u^n) + p_c(u^{n+1}, u^n), & (5.70)\\ -f_e(u^n)(u^{n+1} - u^n) &= F_e(u^n) - F_e(u^{n+1}) + p_e(u^{n+1}, u^n), & (5.71) \end{aligned}$$

where $p_c, p_e \geq 0$ are the terms containing the second derivative. Thus taking L^2 inner product with the function $v = 1$ on all the terms in (5.70), (5.71) and adding them together we have,

$$\begin{aligned} (f_c(u^{n+1}), u^{n+1} - u^n)_{L^2} - (f_e(u^n), u^{n+1} - u^n)_{L^2} &= (F_c(u^{n+1}), 1)_{L^2} - (F_c(u^n), 1)_{L^2} \\ &\quad (F_e(u^n), 1)_{L^2} - (F_e(u^{n+1}), 1)_{L^2} \\ &\quad +(p, 1)_{L^2}, \end{aligned}$$

which implies,

$$\begin{aligned} (f_c(u^{n+1}), u^{n+1} - u^n)_{L^2} - (f_e(u^n), u^{n+1} - u^n)_{L^2} &= (F(u^{n+1}), 1)_{L^2} - (F(u^n), 1)_{L^2} \\ &\quad +(p, 1)_{L^2}. \end{aligned}$$

Since $(p,1)_{L^2} \geq 0$, we have,

$$(f_c(u^{n+1}), u^{n+1}-u^n)_{L^2} - (f_e(u^n), u^{n+1}-u^n)_{L^2} \quad \geq \quad (F(u^{n+1}),1)_{L^2} - (F(u^n),1)_{L^2}. \tag{5.72}$$

Therefore using (5.59), (5.60), (5.66), (5.69) and (5.72) we have the following,

$$\begin{aligned} 0 \geq -s||\nabla\bar{\mu}^{n+1}|| \quad &\geq \quad (F(u^{n+1}),1)_{L^2} - (F(u^n),1)_{L^2} \\ &\quad + \frac{\epsilon^2}{2}||\nabla u^{n+1}||^2 - \frac{\epsilon^2}{2}||\nabla u^n||^2 \\ &\quad + \frac{1}{\epsilon}(g(u^{n+1}),1)_{H^{-1}} - \frac{1}{\epsilon}(g(u^n),1)_{H^{-1}} \\ &= \quad E(u^{n+1}) - E(u^n) \end{aligned}$$

Hence we have that our energy functional E satisfies

$$E(u^{n+1}) \leq E(u^n).$$

□

Next we use DG to discretise the formulation **(P2)**.

5.3.2 Derivation of the Weak and DG Mixed Formulation

Let $(u,\bar{\mu},w) \in (H_0^1(\Omega)\cap H^2(\Omega))\times(H_0^1(\Omega)\cap H^2(\Omega))\times(H_0^1(\Omega)\cap H^2(\Omega)) \subset E_h \times E_h \times E_h$ such that $(u,\bar{\mu},w)$ satisfies **(P2)** and $v \in E_h$ a test function, then by multiplying equation (5.55a), integrating the right hand side by parts and using (3.17) we have,

$$(u_t, v) = -\alpha_h^D(\bar{\mu}, v), \ \forall \ v \in E_h \tag{5.73}$$

Similarly from equation (5.55b) we have,

$$(\bar{\mu}, v) = \frac{1}{\epsilon}(f(u), v) + \epsilon\alpha_h^D(u, v) + \frac{1}{\epsilon}(w, v), \ \forall\ v \in E_h \tag{5.74}$$

Working in a similar way on equation (5.55c) and combining (5.73), (3.17) and (5.74) we arrive at the following weak formulation of **(P2)** in $L^2(E_h; [0, T])$: **(VP2)**, find $(u, \bar{\mu}, w) \in L^2(E_h; [0, T]) \times L^2(E_h; [0, T]) \times L^2(E_h; [0, T])$ such that,

$$\begin{aligned}
(u_t, v) &= -\alpha_h^D(\bar{\mu}, v), \ \forall\ v \in E_h, && (5.75a)\\
(\bar{\mu}, v) &= \frac{1}{\epsilon}(f(u), v) + \epsilon\alpha_h^D(u, v) + \frac{1}{\epsilon}(w, v), \ \forall\ v \in E_h, && (5.75b)\\
\alpha_h^D(w, v) &= (g'(u), v), \ \forall\ v \in E_h, && (5.75c)\\
(u(\cdot, t), v) &= (u_0, v), \ \forall\ v \in E_h. && (5.75d)
\end{aligned}$$

The weak formulation **(VP2)** is consistent with the mixed formulation at the PDE level **(P2)**, due to the consistency of the bilinear form $\alpha_h^D(\cdot, \cdot)$ given by (3.18). The energy space formulation motivates us to define the following time continuous DG mixed formulation: **(SDP2)**, find $(u_h, \bar{\mu_h}, w_h) \in L^2(V^h; [0, T]) \times L^2(V^h; [0, T]) \times L^2(V^h; [0, T])$ such that,

$$\begin{aligned}
((u_h)_t, v) &= -\alpha_h^D(\bar{\mu_h}, v), \ \forall\ v \in V^h, && (5.76a)\\
(\bar{\mu_h}, v) &= \frac{1}{\epsilon}(f(u_h), v) + \epsilon\alpha_h^D(u_h, v) + \frac{1}{\epsilon}(w_h, v), \ \forall\ v \in V^h, && (5.76b)\\
\alpha_h^D(w_h, v) &= (g'(u_h), v), \ \forall\ v \in V^h, && (5.76c)\\
(u_h(\cdot, t), v) &= (u_0, v), \ \forall\ v \in V^h. && (5.76d)
\end{aligned}$$

Now we proceed to derive the energy law for the semi-discrete and fully discrete formulations of **(SDP2)**.

5.3.3 Energy Stability of the Semi-Discrete DG Mixed Formulation

The goal here is to derive an analogous discrete result for our DG formulation **(SDP2)** with (5.57) done at the PDE level. Before we proceed to do this we first need the following definition of the discrete version of H^{-1} inner product introduced in section 2.6 at the PDE level.

Definition 5.3.1. Let $f,\ g \in L^2$ then,

$$(f,g)_{H_h^{-1}} := \alpha_h^D(\Psi_f, \Psi_g) \tag{5.77}$$

and $\Psi_f,\ \Psi_g \in V^h$ unique and satisfy,

$$\alpha_h^D(\Psi_f, v) \ = \ (f,v),\ \forall v \in V^h$$

and

$$\alpha_h^D(\Psi_g, v) \ = \ (g,v),\ \forall v \in V^h.$$

Now for $f,\ g \in L^2$ and by multiplying the above two relations by test functions $v_1 = \Psi_g,\ v_2 = \Psi_f \in V^h$ respectively we have that,

$$(f,g)_{H_h^{-1}} := \alpha_h^D(\Psi_f, \Psi_g) = (\Psi_f, g) = (f, \Psi_g) \tag{5.78}$$

Remark. The H_h^{-1} inner product is well defined in L^2 because of the positive definiteness of the bilinear $\alpha_h^D(\cdot,\cdot)$ in V^h given by lemma 3.3.1.1.

Now we are ready to derive the energy stability for **(SDP2)**.

Derivation of the Discrete Energy Law

Definition 5.3.2. Let $v \in E_h$. We define $E_{disc} : E_h \to R$, the discrete version of the energy functional E as,

$$E_{disc}(u_h) := \frac{1}{\epsilon}(F(u_h), 1) + \frac{\epsilon}{2}\alpha_h^D(u_h, u_h) + \frac{1}{\epsilon}(g(u_h), 1)_{H_h^{-1}} \geq 0. \tag{5.79}$$

Remark. We have that for $u_h \in H_0^2(\Omega)$ satisfying **(P2)** the discrete energy E_{disc} is consistent with the continuous energy E because of the consistency of the bilinear given by (3.18).

To show the energy law we work as follow. We set $v = \bar{\mu_h} \in V^h$ in equation (5.76a), thus we have,

$$((u_h)_t, \bar{\mu_h}) = -\alpha_h^D(\bar{\mu_h}, \bar{\mu_h}) \leq 0, \tag{5.80}$$

since the bilinear form is positive definite. Using $v = (u_h)_t \in V^h$ in (5.76b), (5.76c), and combining it with (5.80) and using (5.78) we have our result,

$$0 \geq (\bar{\mu_h}, (u_h)_t) \quad = \quad \frac{1}{\epsilon}(f(u_h), (u_h)_t) + \epsilon\alpha_h^D(u_h, (u_h)_t) + \frac{1}{\epsilon}(g'(u_h), (u_h)_t)_{H_h^{-1}},$$

which implies,

$$\frac{d}{dt}E_{disc}(u_h) \leq 0. \tag{5.81}$$

5.3.4 Energy Stability of the Fully Discrete CS-DG Mixed Formulation

Convex Splitting Scheme

We define next the following fully discrete scheme called the convex splitting: **(CSP2)** find $({u_h}^{n+1}, {\bar{\mu}_h}^{n+1}, {w_h}^{n+1}) \in V^h \times V^h \times V^h$ for $n = 0, \ldots, N-1$ such that,

$$
\begin{aligned}
({u_h}^{n+1} - {u_h}^{n}, v) &= -k_n \alpha_h^D({\bar{\mu}_h}^{n+1}, v), && \text{(5.82a)}\\
({\bar{\mu}_h}^{n+1}, v) &= \frac{1}{\epsilon}(f_c({u_h}^{n+1}) - f_e({u_h}^{n}), v) + \epsilon \alpha_h^D({u_h}^{n+1}, v) \\
&\quad + \frac{1}{\epsilon}({w_h}^{n+1}, v), && \text{(5.82b)}\\
\alpha_h^D({w_h}^{n+1}, v) &= (g_c'({u_h}^{n+1}) - g_e'({u_h}^{n}), v), && \text{(5.82c)}\\
({u_h}^{0}, v) &= (u_0, v), && \text{(5.82d)}
\end{aligned}
$$

for all $v \in V^h$. Now we are ready to show the final result for this chapter which is the energy stability of **(CSP2)** under the discrete energy functional defined in (5.79).

Derivation of the Discrete Energy Law for the Convex Splitting

Theorem 5.3.4.1. *Let $({u_h}^{n+1}, {\bar{\mu}_h}^{n+1}, {w_h}^{n+1}) \in V^h \times V^h \times V^h$ be the solution triplet of* **(CSP2)**, *for $n = 0, \ldots, N-1$. Then we have an energy law satisfied for* **(CSP2)** *under the energy functional E_{disc} defined in (5.79) for any k_n and for h sufficiently small. That is,*

$$E_{disc}(u_h^{n+1}) \leq E_{disc}(u_h^{n+1}).$$

Proof. Let $v = {\bar{\mu}_h}^{n+1} \in V^h$, from equation (5.82a) we have,

$$({u_h}^{n+1} - {u_h}^{n}, {\bar{\mu}_h}^{n+1}) = -k_n \alpha_h^D({\bar{\mu}_h}^{n+1}, {\bar{\mu}_h}^{n+1}) \leq 0, \tag{5.83}$$

Now for $v = {u_h}^{n+1} - {u_h}^{n} \in V^h$ and using equation (5.82b) and (5.83) we have,

$$0 \geq (\bar{\mu_h}^{n+1}, {u_h}^{n+1} - {u_h}^n) = \frac{1}{\epsilon}(f_c({u_h}^{n+1}) - f_e({u_h}^n), {u_h}^{n+1} - {u_h}^n) + \epsilon\alpha_h^D({u_h}^{n+1}, {u_h}^{n+1} - {u_h}^n) + \frac{1}{\epsilon}({w_h}^{n+1}, {u_h}^{n+1} - {u_h}^n). \tag{5.84}$$

We need to bound from below the following term,

$$(f_c({u_h}^{n+1}) - f_e({u_h}^n), {u_h}^{n+1} - {u_h}^n).$$

We use the fact that $F_c'' \geq 0$ and $F_e'' \geq 0$ (since F_c, F_e are convex), truncating the Taylor series at the second derivative and by rewriting we get,

$$f_c({u_h}^{n+1})({u_h}^{n+1} - {u_h}^n) = F_c({u_h}^{n+1}) - F_c({u_h}^n) + p_c({u_h}^{n+1}, {u_h}^n) \tag{5.85}$$

$$-f_e({u_h}^n)({u_h}^{n+1} - {u_h}^n) = F_e({u_h}^n) - F_e({u_h}^{n+1}) + p_e({u_h}^{n+1}, {u_h}^n) \tag{5.86}$$

where
$p_c({u_h}^{n+1}, {u_h}^n) = \frac{F_c''(\xi_{{u_h}^n, {u_h}^{n+1}})}{2}({u_h}^n - {u_h}^{n+1})^2$
and
$p_e({u_h}^{n+1}, {u_h}^n) = \frac{F_e''(\zeta_{{u_h}^n, {u_h}^{n+1}})}{2}({u_h}^{n+1} - {u_h}^n)^2$ are nonnegative, and

$$p_F := p_c + p_e \geq 0 \tag{5.87}$$

Taking L^2 inner product with $v = 1$ on all the terms in (5.85), (5.86) and adding them together we have,

$$(f_c({u_h}^{n+1}), {u_h}^{n+1} - {u_h}^n) - (f_e({u_h}^n), {u_h}^{n+1} - {u_h}^n) = (F_c({u_h}^{n+1}), 1) - (F_c({u_h}^n), 1) + (F_e({u_h}^n), 1) - (F_e({u_h}^{n+1}), 1), + (p_F, 1).$$

This implies,

$$\begin{aligned}(f_c({u_h}^{n+1}), {u_h}^{n+1} - {u_h}^n) - (f_e({u_h}^n), {u_h}^{n+1} - {u_h}^n) &= (F({u_h}^{n+1}), 1) - (F({u_h}^n), 1) \\ &\quad +(p_F, 1).\end{aligned}$$

Since $(p_F, 1) \geq 0$, we have,

$$(f_c({u_h}^{n+1}) - f_e({u_h}^n), {u_h}^{n+1} - {u_h}^n) \geq (F({u_h}^{n+1}), 1) - (F({u_h}^n), 1). \tag{5.88}$$

Also we need to bound from below $\alpha_h^D({u_h}^{n+1}, {u_h}^{n+1} - {u_h}^n)$. From lemma 3.3.1.1 we have that the bilinear form is positive definite hence,

$$\begin{aligned}0 &\leq \frac{1}{2}a_h({u_h}^{n+1} - {u_h}^n, {u_h}^{n+1} - {u_h}^n), \\ &= \frac{1}{2}\alpha_h^D({u_h}^{n+1}, {u_h}^{n+1}) - \alpha_h^D({u_h}^{n+1}, {u_h}^n) \\ &\quad +\frac{1}{2}\alpha_h^D({u_h}^n, {u_h}^n), \\ &= \alpha_h^D({u_h}^{n+1}, {u_h}^{n+1}) - \alpha_h^D({u_h}^{n+1}, {u_h}^n) - \frac{1}{2}\alpha_h^D({u_h}^{n+1}, {u_h}^{n+1}) \\ &\quad +\frac{1}{2}\alpha_h^D({u_h}^n, {u_h}^n), \\ &= \alpha_h^D({u_h}^{n+1}, {u_h}^{n+1} - {u_h}^n) - \frac{1}{2}\alpha_h^D({u_h}^{n+1}, {u_h}^{n+1}) + \frac{1}{2}\alpha_h^D({u_h}^n, {u_h}^n).\end{aligned}$$

which implies,

$$\begin{aligned}\alpha_h^D({u_h}^{n+1}, {u_h}^{n+1} - {u_h}^n) &= \frac{1}{2}\alpha_h^D({u_h}^{n+1}, {u_h}^{n+1}) \\ &\quad -\frac{1}{2}\alpha_h^D({u_h}^n, {u_h}^n) + \frac{1}{2}a_h({u_h}^{n+1} - {u_h}^n, {u_h}^{n+1} - {u_h}^n),\end{aligned}$$

and thus,

$$\alpha_h^D({u_h}^{n+1}, {u_h}^{n+1} - {u_h}^n) \geq \frac{1}{2}\alpha_h^D({u_h}^{n+1}, {u_h}^{n+1}) - \frac{1}{2}\alpha_h^D({u_h}^n, {u_h}^n). \tag{5.89}$$

Finally we need to bound from below the following term,

$$(g_c'({u_h}^{n+1}) - g_e'({u_h}^n), {u_h}^{n+1} - {u_h}^n)_{H_h^{-1}} = ({w_h}^{n+1}, {u_h}^{n+1} - {u_h}^n).$$

We use the fact that $g_c'' \geq 0$ and $g_e'' \geq 0$ (since g_c, g_e are convex) and truncating the Taylor series at the second derivative and by rewriting we get,

$$g_c'({u_h}^{n+1})({u_h}^{n+1} - {u_h}^n) = g_c({u_h}^{n+1}) - g_c({u_h}^n) + p_c({u_h}^{n+1}, {u_h}^n), \tag{5.90}$$

$$-g_e'({u_h}^n)({u_h}^{n+1} - {u_h}^n) = g_e({u_h}^n) - g_e({u_h}^{n+1}) + p_e({u_h}^{n+1}, {u_h}^n), \tag{5.91}$$

where
$p_c({u_h}^{n+1}, {u_h}^n) = \frac{g_c''(\xi_{{u_h}^n, {u_h}^{n+1}})}{2}({u_h}^n - {u_h}^{n+1})^2$
and
$p_e({u_h}^{n+1}, {u_h}^n) = \frac{g_e''(\zeta_{{u_h}^n, {u_h}^{n+1}})}{2}({u_h}^{n+1} - {u_h}^n)^2$ are nonnegative, and

$$P_G := p_c + p_e. \tag{5.92}$$

Hence by taking H_h^{-1} inner product with $v = 1$ on all the terms in (5.90), (5.91) and adding them together we have,

$$\begin{aligned}(g_c'({u_h}^{n+1}), {u_h}^{n+1} - {u_h}^n)_{H_h^{-1}} &- (g_e'({u_h}^n), {u_h}^{n+1} - {u_h}^n)_{H_h^{-1}}, \\ &= (g_c({u_h}^{n+1}), 1)_{H_h^{-1}} - (g_c({u_h}^n), 1)_{H_h^{-1}} + (g_e({u_h}^n), 1)_{H_h^{-1}} \\ &\quad -(g_e({u_h}^{n+1}), 1)_{H_h^{-1}} + (p_G, 1)_{H_h^{-1}}.\end{aligned}$$

Therefore we have,

$$\begin{aligned}(g_c'({u_h}^{n+1}), {u_h}^{n+1} - {u_h}^n)_{H_h^{-1}} &- (g_e'({u_h}^n), {u_h}^{n+1} - {u_h}^n)_{H_h^{-1}}, \\ &= (g({u_h}^{n+1}), 1)_{H_h^{-1}} - (g({u_h}^n), 1)_{H_h^{-1}} + (p_G, 1)_{H_h^{-1}},\end{aligned}$$

which implies,

$$(g_c'({u_h}^{n+1}) - g_e'({u_h}^n), {u_h}^{n+1} - {u_h}^n) = (g({u_h}^{n+1}), 1) - (g({u_h}^n), 1) + (p_G, 1)_{H_h^{-1}}. \quad (5.93)$$

Thus by combining (5.84), (5.88), (5.89) and (5.93) we get,

$$\begin{aligned}0 \geq (\bar{\mu_h}^{n+1}, {u_h}^{n+1} - {u_h}^n) &= \frac{1}{\epsilon}(F({u_h}^{n+1}), 1) - \frac{1}{\epsilon}(F({u_h}^n), 1), \\ \text{unknown sign term} &+ \frac{1}{\epsilon}\Big((p_F, 1) + (p_G, 1)_{H_h^{-1}}\Big), \\ &+ \frac{\epsilon}{2}\alpha_h^D({u_h}^{n+1}, {u_h}^{n+1}) - \frac{\epsilon}{2}\alpha_h^D({u_h}^n, {u_h}^n), \\ \text{positive term} &+ \frac{\epsilon}{2}\alpha_h^D({u_h}^{n+1} - {u_h}^n, {u_h}^{n+1} - {u_h}^n), \\ &+ \frac{1}{\epsilon}(g({u_h}^{n+1}), 1)_{H_h^{-1}} - \frac{1}{\epsilon}(g({u_h}^n), 1)_{H_h^{-1}}.\end{aligned} \quad (5.94)$$

Hence by assuming that $(p_F, 1) + (p_G, 1)_{H_h^{-1}} \geq 0$ (we are showing it right after this proof), we have by combining (5.96) and (5.94) our result.

$$\begin{aligned}\frac{1}{\epsilon}(F({u_h}^{n+1}), 1) + \frac{\epsilon}{2}\alpha_h^D({u_h}^{n+1}, {u_h}^{n+1}) &+ \frac{1}{\epsilon}(g({u_h}^{n+1}), 1)_{H_h^{-1}} \leq \frac{1}{\epsilon}(F({u_h}^n), 1) \\ &+ \frac{\epsilon}{2}\alpha_h^D({u_h}^n, {u_h}^n) + \frac{1}{\epsilon}(g({u_h}^n), 1)_{H_h^{-1}}.\end{aligned}$$

Therefore we have shown that,

$$E_{disc}({u_h}^{n+1}) \leq E_{disc}({u_h}^n). \quad (5.95)$$

□

Thus to complete the previous proof we need to show the following,

Lemma 5.3.4.2. *Let P_F and P_G as in (5.87) and (5.92) respectively then,*

$$(p_G, 1)_{H_h^{-1}} + (p_F, 1) \geq 0. \tag{5.96}$$

Proof. Let Ψ_1^h be the SIP-DG solution of $\alpha_h^D(\Psi_1^h, v) = (1, v)\ \forall v \in V^h$. Then according to our definition of the H_h^{-1} inner product we have from (5.78),

$$(p_G, 1)_{H_h^{-1}} = (\Psi_1^h, p_G). \tag{5.97}$$

Let also $\Psi_1 \geq 0$, (from max principle [29]), to be the PDE solution of,

$$\begin{aligned} -\triangle\Psi_1 &= 1, \text{ in } \Omega, \\ \Psi_1 &= 0, \text{ on } \partial\Omega. \end{aligned}$$

By adding and subtracting Ψ_1 in (5.97) we have,

$$\begin{aligned} (p_G, 1)_{H_h^{-1}} = (\Psi_1^h, p_G) &= (\Psi_1^h - \Psi_1, p_G) + (\Psi_1, p_G), \\ \text{(use Cauchy-Schwartz)} \qquad &\geq -||\Psi_1^h - \Psi_1||_\Omega ||p_G||_\Omega + (\Psi_1, p_G), \\ \text{(use (3.6) for } r := q+1) \qquad &\geq -ch^r |\Psi_1|_{H^r} ||p_G||_\Omega + (\Psi_1, p_G) \end{aligned}$$

and this implies,

$$(p_G, 1)_{H_h^{-1}} \geq -ch^r ||\Psi_1||_{H^r} ||p_G||_\Omega + (\Psi_1, p_G). \tag{5.98}$$

Next we make use of the following elliptic regularity result (cf. [29]) for the Poisson's equation.

$$||\Psi_1||_{H^{m+2}} \leq ||f||_{H^m},\ m = 0, 1, \cdots \tag{5.99}$$

where $f \in H^m$ is the source term and Ψ_1 is the PDE solution.

Thus by using (5.99), for $f \equiv 1$, we have that $||1||_{H^m} = ||1||_\Omega = (vol(\Omega))^{1/2}$ and for $m = r - 2$, since $r \geq 2$, we have from (5.98),

$$(p_G, 1)_{H_h^{-1}} \geq -ch^r (vol(\Omega))^{1/2} ||p_G||_\Omega + (\Psi_1, p_G). \tag{5.100}$$

Now we have that,

$$\begin{aligned} ||p_G||_\Omega &= \left|\left| \frac{g_c''(\xi_{{u_h}^n, {u_h}^{n+1}}) + g_e''(\zeta_{{u_h}^n, {u_h}^{n+1}})}{2} ({u_h}^{n+1} - {u_h}^n)^2 \right|\right|_\Omega \leq \frac{C_1}{2} ||({u_h}^{n+1} - {u_h}^n)^2||_\Omega, \\ &= \frac{C_1}{2} ||({u_h}^{n+1} - {u_h}^n)||^2_{L^4(\Omega)} \leq \frac{C_1}{2} C_{inv}^2 h^{-1} ||({u_h}^{n+1} - {u_h}^n)||^2_\Omega \end{aligned} \tag{5.101}$$

and also,

$$(p_F, 1) = \left(\frac{F_c''(\Upsilon_{{u_h}^n, {u_h}^{n+1}}) + F_e''(\Psi_{{u_h}^n, {u_h}^{n+1}})}{2} ({u_h}^{n+1} - {u_h}^n)^2, 1 \right) \geq \frac{C_2}{2} ||{u_h}^{n+1} - {u_h}^n||^2_\Omega, \tag{5.102}$$

where g_e'' and g_c'' are bounded functions from lemma 5.3.0.2 thus,

$$\infty > C_1 = \max_R (g_c'' + g_e'') > 0$$

and

$$C_2 = \min_R (F_c'' + F_e'') \geq 1 > 0,$$

for the F defined above.

Now by using (5.101) in (5.100) we get,

$$(p_G, 1)_{H_h^{-1}} \geq -ch^{r-1} (vol(\Omega))^{1/2} \frac{C_1}{2} C_{inv}^2 ||{u_h}^{n+1} - {u_h}^n||^2_\Omega + (\Psi_1, p_G). \tag{5.103}$$

Adding (5.102) and (5.103) we have,

$$\begin{aligned}(p_G,1)_{H_h^{-1}}+(p_F,1) \quad &\geq \quad -ch^{r-1}(vol(\Omega))^{1/2}\frac{C_1}{2}C_{inv}^2||{u_h}^{n+1}-{u_h}^n||_\Omega^2+(\Psi_1,p_G)\\ &\quad +\frac{C_2}{2}||{u_h}^{n+1}-{u_h}^n||_\Omega^2,\end{aligned}$$

which implies,

$$(p_G,1)_{H_h^{-1}}+(p_F,1) \quad \geq \quad \big(\frac{C_2}{2}-ch^{r-1}(vol(\Omega))^{1/2}\frac{C_1}{2}C_{inv}^2\big)||{u_h}^{n+1}-{u_h}^n||_\Omega^2+(\Psi_1,p_G). \tag{5.104}$$

Thus by choosing in (5.104) h "sufficiently" small,

$$h\leq \sqrt[r-1]{\frac{C_2}{c(vol(\Omega))^{1/2}C_1C_{inv}^2}}$$

the relation (5.96) follows. □

Chapter 6

Conclusion

We would like to finish our discussion with some concluding remarks and future plans.

6.1 Concluding Remarks

In this dissertation we have introduced a novel simplified diffuse interface model of tumor growth. This model features essentially the Cahn-Hilliard equation with an added reaction term that is specialized for the context of cancerous tumor progression. Although our model is mathematically simpler, by having less equations and using less variables, than other similar models discussed in the literature, we have shown that it produces simulations that are comparable to those obtained by those models. This is a very attractive feature because it allows us to use our simpler model as a basis to develop the theoretical and practical framework for the introduction of other more realistic and possibly more complicated models.

We presented in our work the first primitive-variable, completely discontinuous numerical implementation of a 2D scheme for a diffuse interface model of cancer growth. As a special case (by switching off the reaction term of the diffuse interface model) we have implemented in 2D the first primitive-variable, completely discontinuous, scheme for the Cahn-Hilliard equation and we have demonstrated the expected convergence rate for the scheme introduced by Feng and Karakashian in

[27], thus verifying their theoretical convergence rate result. Also we have provided evidence that the more general diffuse interface model is also convergent with the optimal error order, as the time and space step sizes are reduced toward zero. This motivates us to pursue a theoretical proof of the convergence rate of that scheme, by following the steps in [27].

In our work we have implemented a practical spatially adaptive meshing algorithm for the numerical schemes just mentioned. We have demonstrated that substantial computational savings can be achieved when using a 2D spatially adaptive mesh for our models, rather than a uniform, static mesh. This fact demonstrated the effectiveness of a very simple, but powerful, marking strategy based on an inverse estimate. This serves as an inspiration for a future work that will investigate and establish a more theoretical framework for the aforementioned marking strategy. Also from our numerous numerical experiments we have observed that the solutions of our models might progress with different speeds throughout their evolution. This fact motivates the use of time adaptive techniques along with our spatial ones.

The efficiency of our numerical algorithms depended on the implementation of fast solvers for the systems of equations resulting from the DG-FE discretizations. We have developed solvers based on *multigrid* and *sparse direct solver* techniques. We observed that although our solvers have performed satisfactorily a margin for improvement exists. In the case of multigrid solvers the need to use a variable V-cycle –by increasing the number of smoothing steps in lower levels – might be wasteful and hints to us that a better solver might be obtained based on domain decomposition techniques by following the ideas in [25].

Finally we have devised and analyzed a mixed DG-FE scheme of convex splitting (CS) type for the Cahn-Hilliard equation and our diffuse interface cancer model in any space dimension. For our mixed schemes we have proved unconditional energy stability in the case of the Cahn-Hilliard equation scheme and a conditional energy stability in the case of the diffuse interface cancer model scheme, with respect to a broken analog of their continuous energy. Also in the case of the Cahn-Hilliard

equation we have proved unconditional uniform bounds on the sequence of numerical solutions, a result that is crucial in the pursue of a convergence proof of our scheme (cf. [4]). It is a very interesting problem to show that the same results remain valid under spatial and time adaptivity. Also for the Chan-Hilliard case we have shown unconditional unique solvability, something that for the cancer model remains an open question even at the PDE level.

6.2 Future Plans

Our immediate plan is the implementation of our mixed formulation schemes and the comparison with our existing primitive variable formulation schemes. We plan to demonstrate the flexibility and effectiveness of our algorithms by solving a more realistic brain tumor model. A model that will contain complex domain geometries (resembling the human brain), involve advective velocity, nutrient diffusion, pressure effects and will take into consideration spatial heterogeneity (by modifying the diffusion coefficient in (2.20a) to account for the different properties of the gray and white brain mater). The following cancer growth model with *nutrient diffusion* and *advective velocity* encapsulates some of the aforementioned properties.

$$
\begin{aligned}
\partial_t u &= \triangle \mu + S - \nabla \cdot (u\vec{U}), \quad \text{in } \Omega_T, \\
S &= \eta \lambda_g u - \lambda_d u, \quad \text{in } \Omega_T, \\
\mu &= f(u) - \epsilon^2 \triangle u, \quad \text{in } \Omega_T, \\
\triangle \eta &= \lambda_\eta u \eta, \ \text{ with } \ \eta = 1 \ \text{ on } \ \partial\Omega, \\
\vec{U} + \nabla \Pi &= -\lambda u \nabla \mu, \ \Pi\text{: pressure} = 0 \text{ on } \partial\Omega \text{ Darcy equation} \\
\nabla \cdot \vec{U} &= S, \ \text{ Mass conservation} \\
u &= u_0, \ \text{ on } \Omega \times \{0\}, \\
\partial_n u = \partial_n \mu &= 0, \ \text{ on } \partial\Omega_T.
\end{aligned}
$$

To validate our methods, a comparison of the simulated results with CT-scan data must be performed. Also the development and implementation of an adaptive code in three dimensions, by extending our existing work in two dimensions, is a plan that follows naturally. Finally, the derivation and numerical solution of a Cahn-Hilliard-type tumor growth model with a stochastic source term, in two and three dimensions, using our existing machinery should be a realistic goal.

Bibliography

Bibliography

[1] R. Adams. *Sobolev Spaces*. Academic Press, New York, NY, 1975. 20, 24

[2] N. D. Alikakos, P. W. Bates, and X. Chen. Convergence of the Cahn-Hilliard equation to the Hele-Shaw model. *Arch. Rational Mech. Anal.*, 128:165–205, 1994. 15

[3] A. Aristotelous, O. Karakashian, and S. M. Wise. Adaptive Discontinuous Galerkin Finite Element Methods for a Diffuse Interface Model of Biological Growth. 2011. in preparation. 82

[4] A. Aristotelous, O. Karakashian, and S. M. Wise. A mixed discontinuous galerkin, convex splitting scheme for a modified Cahn-Hilliard equation. 2011. in preparation. 82, 100, 121

[5] D. N. Arnold. An interior penalty finite element method with discontinuous elements. *SIAM J. Numer. Anal.*, 19:742–760, 1982. 29, 31

[6] G. A. Baker. Finite element methods for elliptic equations using nonconforming elements. *Math. Comp.*, 31:44–59, 1977. 34, 38, 40

[7] G. A. Baker, W. N. Jureidini, and O. A. Karakashian. Piecewise solenoidal vector fields and the Stokes problems. *SIAM J. Numer. Anal.*, 27:1466–1485, 1990. 27, 32

[8] J. L. Bona, V. A. Dougalis, O. A. Karakashian, and W. R. McKinney. Fully discrete methods with grid refinement for the generalized Korteweg-de Vries

equation. *Proceedings of the workshop on viscous and numerical approximations of shock waves, N.C. State University*, pages 117–124, 1990. 43

[9] J. L. Bona, V. A. Dougalis, O. A. Karakashian, and W. R. McKinney. Conservative high order schemes for the Generalized Korteweg-de Vries equation. *Philos. Trans. Royal Soc. London, Ser.*, pages 107–164, 1995. 43

[10] J. H. Bramble and J. E. Pasciak. The analysis of smoothers for multigrid algorithms. *Math. Comp.*, 58:467–488, 1992. 63

[11] S. Brenner and R. Scott. *The Mathematical Theory of Finite Element Methods.* Springer-Verlag, New York, NY, 1994. 26, 27

[12] S. C. Brenner. An optimal-order nonconforming multigrid method for the biharmonic equation. *SIAM J. Numer. Anal.*, 76(5):1124–1138, 1989. 63

[13] S. C. Brenner. Poincaré–Friedrichs inequalities for H^1 functions. *SIAM J. Numer. Anal.*, 41(1):306–324 (electronic), 2003. 34

[14] Susanne Brenner and Li-Yeng Sung. Multigrid algorithms for C^0 interior penalty methods. *SIAM J. Numer. Anal.*, 44(1):199–223, 2006. 63

[15] J. W. Cahn. On spinodal decomposition. *Acta Metall.*, 9:795, 1961. 9, 12, 13, 15, 82

[16] P. G. Ciarlet. *The Finite Element Method for Elliptic Problems.* North-Holland, Amsterdam, 1978. 25, 28

[17] D. S. Cohen and J. D. Murray. A generalized diffusion model for growth and dispersal in a population. *J. Math. Biol.*, 12:237–249, 1981. 3, 7, 9, 15, 16

[18] V. Cristini, X. Li, J. S. Lowengrub, and S. M. Wise. Nonlinear simulations of solid tumor growth using a mixture model: Invasion and branching. *J. Theor. Biol.*, 58:723–763, 2009. 4, 7, 10, 17, 18

[19] Timothy Davis. *Direct Methods for Sparse Linear Systems*. SIAM, 2006. 56

[20] W. Döfler. Aconvergent adaptive algorithm for poisson's equation. *SIAM J. Numer. Anal.*, 33:1106–1124, 1986. xiii, 43

[21] C. M. Elliott and D. A. French. A nonconforming finite-element method for the two-dimensional Cahn-Hilliard equation. *SIAM J. Numer. Anal.*, 26:884–903, 1989. 12, 15

[22] C. M. Elliott, D. A. French, and F. A. Miller. A second order splitting method for the Cahn-Hilliard equation. *Numer. Math.*, 54:575–590, 1989. 15

[23] C. M. Elliott and S. Zheng. On the Cahn-Hilliard equation. *Arch. Rational Mech. Anal.*, 96:339–357, 1986. 13, 15, 82

[24] David J. Eyre. Unconditionally gradient stable time marching the Cahn-Hilliard equation. In *Computational and mathematical models of microstructural evolution (San Francisco, CA, 1998)*, volume 529, pages 39–46. MRS, Warrendale, PA, 1998. 81, 86

[25] X. Feng and O. A. Karakashian. Two-level nonoverlapping additive Schwarz methods for a discontinuous Galerkin approximation of the biharmonic problem. *J. Scient. Comput.*, 22:299–324, 2005. 34, 38, 120

[26] X. Feng and S. M. Wise. Analysis of a Darcy-Cahn-Hilliard diffuse interface model for the Hele-Shaw flow and its fully discrete finite element approximation. *SIAM J. Numer. Anal.*, 2011. in review. 86

[27] Xiaobing Feng and Ohannes A. Karakashian. Fully discrete dynamic mesh discontinuous Galerkin methods for the Cahn-Hilliard equation of phase transition. *Math. Comp.*, 76(259):1093–1117 (electronic), 2007. 1, 3, 4, 34, 39, 41, 49, 50, 65, 120

[28] Emmanuil H. Giorgoulis, Paul Houston, and Juha Virtanen. An a posteriori error indicator for discontinuous Galerkin approximations of fourth order elliptic problems. *IMA J. Numer. Anal.*, page (electronic), 2009. 43

[29] P. Grisvard. *Singularities in Boundary Value Problems.* Research Notes in Applied Mathematics. MASSON and Springer–Verlag, 1992. 35, 105, 116

[30] Ohannes A. Karakashian and Frederic Pascal. A posteriori error estimates for a discontinuous Galerkin approximation of second-order elliptic problems. *SIAM J. Numer. Anal.*, 41(6):2374–2399 (electronic), 2003. 31, 43, 47

[31] Ohannes A. Karakashian and Frederic Pascal. Convergence of adaptive discontinuous Galerkin approximations of second-order elliptic problems. *SIAM J. Numer. Anal.*, 41(6):2374–2399 (electronic), 2007. 43

[32] David Kay, Vanessa Styles, and Endre Süli. Discontinuous Galerkin finite element approximation of the Cahn-Hilliard equation with convection. *SIAM J. Numer. Anal.*, 47(4):2660–2685, 2009. 1, 3, 33, 34, 92, 100

[33] David Kay and Richard Welford. A multigrid finite element solver for the Cahn-Hilliard equation. *J. Comput. Phys.*, 212(1):288–304, 2006. 61

[34] Evgeniy Khain and Leonard M. Sander. Generalized Cahn-Hilliard equation for biological applications. *Phys. Rev. E*, 77(5):51129, 2008. 4, 7, 16

[35] J. S. Kim, K. Kang, and J. S. Lowengrub. Conservative multigrid methods for Cahn-Hilliard fluids. *J. Comput. Phys.*, 193:511–543, 2003. 61

[36] I. Mozolevski and E. Süli. A priori error analysis for the *hp*-version of the discontinuous Galerkin finite element method for the biharmonic equation. *Comput. Meth. Appl. Math.*, 3:596–607, 2003. 34, 38

[37] F. Lara Ochoa and A. Montalvo Robles. A reaction-diffusion model describing the phenomenon of cellular confluence. *Kinam Rev. Fís.*, 5(4):297–322, 1983. 4, 7, 15

[38] Rob Stevenson. An analysis of non conforming methods, leading to an improved method for the morley element. *Math. Comp.*, 72(241):55–81 (electronic), 2002. 63

[39] U. Trottenberg, C. W. Oosterlee, and A. Schüller. *Multigrid*. Academic Press, New York, 2005. 62

[40] G. N. Wells, E. Kuhl, and K. Garikipati. A discontinuous galerkin method for the Cahn-Hilliard equation. *J. Comput. Phys.*, 218:860–877, 2006. 3

[41] S. M. Wise, J. S. Lowengrub, H. B. Frieboes, and V. Cristini. Three-dimensional multispecies nonlinear tumor growth–I Model and numerical method. *J. Theor. Biol.*, 253:524–543, 2008. 4, 7, 9, 10, 18

[42] Y. Xia, Y. Xu, and C. W. Shu. Local discontinuous galerkin methods for the Cahn-Hilliard type equations. *J. Comput. Phys.*, 227:472–491, 2007. 3

Vita

Andreas Costa Aristotelous was born in Larnaca, Cyprus on May 26, 1977. He graduated from St. George Lyceum in Larnaca, Cyprus in 1995, having followed the science concentration. Upon his high school graduation he served in the Cyprus military, in the artillery corps, having the rank of second lieutenant, discharged in 1997.

He attended the University of Cyprus in Nicosia, Cyprus, where he studied mathematics with emphasis in applied mathematics, and obtained his Bachelor of Science degree in mathematics in 2001. Upon his graduation he moved to the United States to pursue graduate studies.

He received his Master of Science degree in applied mathematics from Florida Institute of Technology, in Melbourne, Florida in 2003 and remained as a PhD student at the same institution until his transfer to the University of Tennessee, Knoxville, in August, 2004.

He received his PhD degree in mathematics from the University of Tennessee, Knoxville, in August, 2011. Upon his graduation he accepted a joint Postdoctoral and Visiting Assistant Professor position at the Statistical and Applied Mathematical Science Institute (SAMSI) in the research triangle park, North Carolina, and the Duke University in Durham, North Carolina.